

https://dspace.org/

A linear vibration isolator integrating a non-linear energy sink (nes)

Waite, Clinton

2024
University of the Witwatersrand, Johannesburg
https://hdl.handle.net/10539/45325
Waite, Clinton.(2024). A linear vibration isolator integrating a non-linear energy sink (nes) [Masters dissertation, University of the Witwatersrand, Johannesburg]. WIReDSpace. https://hdl.handle.net/10539/45325

Downloaded from a DSpace repository. https://dspace.org/

A LINEAR VIBRATION ISOLATOR INTEGRATING A NON-LINEAR ENERGY SINK (NES)

Research Project – CIVN7019A

Clinton Waite

Student number: 1430921

E-mail address: 1430921@students.wits.ac.za

Supervisor: Dr Kuinian Li

School of Civil and Environmental Engineering
University of Witwatersrand
Johannesburg
6 December 2024

ABSTRACT

This report investigates the integration of traditional linear vibration isolators with non-linear energy sinks (NES) to enhance vibration control in structures subjected to dynamic loading. Structures often respond to dynamic loads—such as machinery vibrations, seismic activity, and environmental factors—by vibrating at their natural frequencies, potentially leading to resonance and structural failure. Vibration isolation and damping systems, such as linear isolators and NES, mitigate these effects. Linear isolators are effective at higher frequencies but have limited performance at lower frequencies, while NES systems offer broader frequency-range effectiveness. This study explores the effectiveness of combining these systems to optimize vibration control. Through simulation of both simple and complex setups, the research compares the vibration response of traditional linear isolators, NES-integrated isolators, and NES systems combined with additional damping elements. Key findings demonstrate that integrating NES with linear isolators significantly reduces peak transmissibility and improves vibration reduction under harmonic and seismic loading. However, the integration's effectiveness varies depending on system configuration and specific loading conditions, highlighting the need for further optimization. The study also presents a parametric analysis for designing vibration control systems tailored to diverse applications, offering valuable insights for engineering practice in reducing structural vibrations.

DECLARATION

I declare that this research proposal is my own unaided work. It is being submitted to the Degree of Master of Science to the University of the Witwatersrand, Johannesburg. It has not been submitted before for any degree or examination to any other University.



……

6 day of December 2024

TABLE OF CONTENTS

ABSTRACT i
DECLARATION ii

1 THE CONTEXT OF THE STUDY 1
1.1 Introduction 1
1.2 The problem statement 2
1.3 Objectives 2
1.4 Research Questions 3

2 LITERATURE REVIEW 4
2.1 Background 4
2.1.1 Natural Frequency Theory 4
2.1.2 Transmissibility Theory 5
2.1.3 Linear Isolator Theory 6
2.1.4 Non-linear energy sink (NES) Theory 7
2.2 Literature on related works 9
2.2.1 Types of NES systems 9
2.2.2 Comparison and combination with linear systems 10
2.2.3 Seismic Application 14
2.3 Gaps in the study 19

3 THE RESEARCH METHODOLOGY 20
3.1 Data collection and analysis methods 20
3.2 Calculation methods and details 20

4 TRADITIONAL LINEAR ISOLATOR 22
4.1 Introduction 22
4.2 The setup 22
4.3 Force Transmissibility of Configuration 1 23
4.4 Displacement Transmissibility of Configuration 1 24

4.5 Conclusion **25**

5 NON-LINEAR ENERGY SINK (NES) **26**
5.1 Introduction **26**
5.2 The setup **26**
5.3 Study of the parameters **26**
5.4 Conclusion **28**

6 LINEAR ISOLATOR INTEGRATED NES **29**
6.1 Introduction **29**
6.2 The setup **29**
6.3 Configuration 2A **32**
6.3.1 Force Transmissibility of Configuration 2A 32
6.3.2 Displacement Transmissibility of Configuration 2A 33
6.4 Configuration 2B **35**
6.4.1 Force Transmissibility of Configuration 2B 35
6.4.2 Displacement Transmissibility of Configuration 2B 36
6.5 Conclusion **37**

7 LINEAR ISOLATOR INTEGRATED A SKYHOOK DAMPER AND A NES SYSTEM **38**
7.1 Introduction **38**
7.2 The setup **38**
7.3 Force Transmissibility of Configuration 3 ..... **40**
7.4 Displacement Transmissibility of Configuration 3 ..... **42**
7.5 Conclusion **44**

8 TRANSMISSIBILITY DISCUSSION **45**
8.1 Traditional Linear Isolator **45**
8.2 Linear isolator integrated NES **47**
8.2.1 Configuration 2A 48
8.2.2 Configuration 2B 56

8.3 Linear isolator integrated skyhook damper and NES 57
8.4 Comparison of Transmissibility Results 63

9 APPLICATION TO EARTHQUAKES 66
9.1 The applied loads 66
9.2 SDOF Structure 68
9.2.1 Traditional Linear Isolator 68
9.2.2 Linear isolator integrated NES 71
9.3 MDOF Structure 75
9.3.1 Traditional Linear Isolator 75
9.3.2 Linear isolator integrated NES 80
9.4 Earthquake behaviour discussion 85

10 CONCLUSION 92
10.1 General discussion 92
10.2 Limitations and recommendations for further study 94

11 REFERENCES 96

TABLE OF FIGURES

Figure 2-1: Graph showing the relationship between transmissibility and frequency ratio for various damping ratios in a SDOF system (Zou et al., 2014) 6
Figure 2-2: Types of idealised vibration isolators (Crede and Ruzicka, 2002) 6
Figure 2-3: Diagrams showing: (a) type-I NES, (b) type II NES, and (c) type-III NES. All springs and dampers shown are uncompressed when horizontal (Sapsis et al., 2012)..... 8
Figure 2-4: Configuration of the modified NES system (AL-Shudeifat, 2014) 9
Figure 2-5: A linear system with an NES system using an ideal cubic non-linear stiffness (Xue et al., 2020) 10
Figure 2-6: Model of a traditional linear vibration isolator (Li, 2020) 11
Figure 2-7: a) Model of a traditional linear vibration isolator integrated with a skyhook damper, b) Model of a traditional linear vibration isolator integrated with a groundhook damper (Li, 2020) 12
Figure 2-8: Non-linear stiffness modelled using a) inclined springs, and non-linear damping modelled using b) inclined damper (Qiu et al., 2021) 13
Figure 2-9: Non-linear isolation systems formed using a) non-linear stiffness and non-linear damping, b) non-linear damping, and c) non-linear stiffness (Qiu et al., 2021) 13
Figure 2-10: Transmissibility graphs for systems (a), (b), (c) and (d) (Qiu et al., 2021) 14
Figure 2-11: Depiction of large-scale model testing setup (Luo et al., 2014) 15
Figure 2-12: Output results for all NES systems locked versus unlocked for the El Centro earthquake (Luo et al., 2014) 16
Figure 2-13: Output results for all NES systems locked versus Type I NES unlocked for the El Centro earthquake (Luo et al., 2014) 17
Figure 2-14: Output results for all NES systems locked versus SSVI NES unlocked for the El Centro earthquake (Luo et al., 2014) 18
Figure 4-1: Setup of a traditional linear isolator – Configuration 1..... 22
Figure 4-2: Single degree of freedom model of the traditional linear isolator..... 23
Figure 5-1: NES system at rest 26
Figure 5-2: NES system with relative displacement..... 27

Figure 5-3: Force and position components of the NES system 27
Figure 6-1: Setup of a linear isolator integrated a NES system (damper to base) - Configuration 2A 29
Figure 6-2: Setup of a linear isolator integrated a NES system (spring to base) - Configuration 2B 30
Figure 6-3: Two DOF model of a linear isolator integrated a NES system (damper to base)–Configuration 2A 30
Figure 6-4: Two DOF model of a linear isolator integrated a NES system (spring to base) - Configuration 2B 31
Figure 6-5: Configuration 2A shown with effective linear stiffness component .. 31
Figure 6-6: Configuration 2B shown with effective linear stiffness component .. 32
Figure 7-1: Setup of a linear isolator integrated a skyhook damper and NES system - Configuration 3 38
Figure 7-2: Three DOF model of a linear isolator integrated a skyhook damper and NES system - Configuration 3 39
Figure 7-3: Configuration 3 shown with effective linear stiffness component 40
Figure 8-1: Traditional linear isolator transmissibility plotted against frequency ratio for various damping ratios 45
Figure 8-2: Damping ratio values for various heights of (a) steel buildings, (b) steel reinforced concrete buildings, (c) reinforced concrete buildings and (d) reinforced concrete chimneys 46
Figure 8-3: Peak force transmissibility for varying values of k_2 in Configuration 2A 49
Figure 8-4: Peak force transmissibility for varying values of m_2 in Configuration 2A 49
Figure 8-5: Peak force transmissibility for varying values of c_3 in Configuration 2A 50
Figure 8-6: Peak force transmissibility for varying values of L_0 in Configuration 2A 50
Figure 8-7: Peak force transmissibility for varying values of x_i in Configuration 2A 51
Figure 8-8: Configuration 2A transmissibility graphs for various m_2 values 53

Figure 8-9: Configuration 2A transmissibility graphs for various c_3 values 54
Figure 8-10: Configuration 2A transmissibility graphs for various L_0 values..... 54
Figure 8-11: Configuration 2A transmissibility graphs for various x_i values..... 55
Figure 8-12: Optimised transmissibility graph of Configuration 2A..... 55
Figure 8-13: Optimised transmissibility graph of Configuration 2B..... 56
Figure 8-14: Force transmissibility graph of a linear isolated integrated a skyhook damper (Li, 2020)..... 57
Figure 8-15: Peak force transmissibility for varying values of k_3 in Configuration 3 59
Figure 8-16: Peak force transmissibility for varying values of m_3 in Configuration 3..... 59
Figure 8-17: Peak force transmissibility for varying values of L_0 in Configuration 3 60
Figure 8-18: Peak force transmissibility for varying values of x_i in Configuration 3 60
Figure 8-19: Optimised force transmissibility graph of Configuration 3 without c_1 62
Figure 8-20: Optimised force transmissibility graph of Configuration 3 with c_1 . 63
Figure 8-21: Optimised Configuration 1, 2A, 2B and 3 Transmissibility Results 64
Figure 8-22: Optimised Configuration 1, 2A, 2B and 3 Transmissibility Results at Loading Frequency Ratio=10..... 65
Figure 8-23: Optimised Configuration 1, 2A, 2B and 3 Transmissibility Results at Loading Frequency Ratio=20..... 65
Figure 9-1: Measured acceleration of the El Centro Earthquake..... 67
Figure 9-2: Measured acceleration of the Northridge Earthquake..... 67
Figure 9-3: Setup of a SDOF structure with a linear isolator for application of seismic loading..... 68
Figure 9-4: Setup of a SDOF structure with a linear isolator for application of seismic loading for analysis 68
Figure 9-5: Displacement-Time graph of the response of a SDOF structure with a linear isolator to the El Centro Earthquake..... 69

Figure 9-6: Base shear-Time graph of the response of a SDOF structure with a linear isolator to the El Centro Earthquake 70
Figure 9-7: Displacement-Time graph of the response of a SDOF structure with a linear isolator to the Northridge Earthquake 70
Figure 9-8: Base shear-Time graph of the response of a SDOF structure with a linear isolator to the Northridge Earthquake 71
Figure 9-9: Setup of a SDOF structure with a linear isolator integrated NES for application of seismic loading 71
Figure 9-10: Setup of a SDOF structure with a linear isolator integrated NES for application of seismic loading for analysis 72
Figure 9-11: Displacement-Time graph of the response of a SDOF structure with a linear isolator integrated NES to the El Centro Earthquake 73
Figure 9-12: Base Shear-Time graph of the response of a SDOF structure with a linear isolator integrated NES to the El Centro Earthquake 74
Figure 9-13: Displacement-Time graph of the response of a SDOF structure with a linear isolator integrated NES to the Northridge Earthquake 74
Figure 9-14: Base Shear-Time graph of the response of a SDOF structure with a linear isolator integrated NES to the Northridge Earthquake 75
Figure 9-15: Setup of a MDOF structure with a linear isolator for application of seismic loading 75
Figure 9-16: Setup of a MDOF structure with a linear isolator for application of seismic loading for analysis 76
Figure 9-17: Displacement-Time graph of the response of a MDOF structure with a linear isolator to the El Centro Earthquake 77
Figure 9-18: Base shear-Time graph of the response of a MDOF structure with a linear isolator to the El Centro Earthquake 78
Figure 9-19: Displacement-Time graph of the response of a MDOF structure with a linear isolator to the Northridge Earthquake 78
Figure 9-20: Base shear-Time graph of the response of a MDOF structure with a linear isolator to the Northridge Earthquake 79
Figure 9-21: Setup of a MDOF structure with a linear isolator integrated NES for application of seismic loading 80

Figure 9-22: Setup of a MDOF structure with a linear isolator integrated NES for application of seismic loading for analysis 81
Figure 9-23: Setup of a MDOF structure with a linear isolator integrated NES for application of seismic loading for analysis with effective stiffness..... 81
Figure 9-24: Displacement-Time graph of the response of a MDOF structure with a linear isolator integrated NES to the El Centro Earthquake..... 83
Figure 9-25: Base shear-Time graph of the response of a MDOF structure with a linear isolator integrated NES to the El Centro Earthquake 83
Figure 9-26: Displacement-Time graph of the response of a MDOF structure with a linear isolator integrated NES to the Northridge Earthquake..... 84
Figure 9-27: Base shear-Time graph of the response of a MDOF structure with a linear isolator integrated NES to the Northridge Earthquake 84
Figure 9-28: Displacement-Time graph of the response of a SDOF structure to the El Centro Earthquake 85
Figure 9-29: Base shear-Time graph of the response of a SDOF structure to the El Centro Earthquake..... 85
Figure 9-30: Displacement-Time graph of the response of a SDOF structure to the Northridge Earthquake 86
Figure 9-31: Base shear-Time graph of the response of a SDOF structure to the Northridge Earthquake 86
Figure 9-32: Displacement-Time graph of the response of a MDOF structure's third floor to the El Centro Earthquake 87
Figure 9-33: Shear-Time graph of the response of a MDOF structure's third floor to the El Centro Earthquake 88
Figure 9-34: Displacement-Time graph of the response of a MDOF structure's third floor to the Northridge Earthquake 88
Figure 9-35: Shear-Time graph of the response of a MDOF structure's third floor to the Northridge Earthquake 89

1 THE CONTEXT OF THE STUDY

1.1 Introduction

Upon loading a structure, either by exciting it's support (or foundation) or by applying load to the structure itself, the structure often responds by vibrating. The load in this case would be a dynamic load, which is a load that changes in magnitude and/or direction with time. A few examples of a dynamic loads include: vibrating machinery; earthquakes; wind; crowds moving in synchronisation; explosions.

A natural frequency is the frequency that a system will naturally tend to vibrate at under free vibration (vibration after applying an initial displacement or velocity), and this frequency is a function of the properties of the system itself, completely independent of the loading applied to it (Lim, 2018). If the applied loading causes a system to vibrate at a frequency close to one of it's natural frequencies, this could induce vigorous vibrations known as resonance, and may result in sever consequences such as injury or even complete structural failure of the system, as often seen as a result of earthquakes (Lim, 2018). The lowest natural frequency of a system is termed the 'fundamental natural frequency'.

There are two main measures of vibration control, namely isolating vibrations through the use of isolators, and absorbing or damping vibrations through the use of dampers. While vibration isolation aims to reduce vibrations transmitting to other parts of the system by simply preventing vibration energy from passing through it, vibration damping absorbs vibration energy into itself thus reducing the vibration energy transmitting into the rest of the system (Ruzicka and Derby, 1971; Countervail, 2019). Isolators can be either linear or non-linear in nature, and are generally used to isolate the source of vibration (often machinery) in order to protect the structure supporting it, however, isolators can also be used to protect a payload from vibrations in it's support structure. Similarly, dampers can also be either linear or non-linear in nature, however, dampers are used to absorb vibration energy in order to reduce vibrations transferring into the system to be protected.

The effectiveness of the vibration isolation can be measured through transmissibility, which is a ratio of the response of the system being protected to

that of the source of vibration (where a transmissibility of less than one indicates an effective reduction in vibration). The transmissibility of linear isolators is only less than one for frequencies above the root of two (approximately 1.41) times the fundamental natural frequency of a system. This is not ideal as it leaves the system to be protected vulnerable to vibrations at lower frequencies. Ideally one would want the vibration control to be effective at any frequency. A further disadvantage of linear isolators is that it typically has a narrow frequency range of effectiveness. A non-linear energy sink (NES) is a type of non-linear damper that has been researched within the industry, and has benefits such as being effective at lower frequencies while also having a wider range of effective frequencies.

1.2 The problem statement

Means of reducing vibrations in structures have come a long way. Studies have been done on linear isolators as well as NESs as vibration controlling systems. Many studies have been conducted to compare the effectiveness of the two types of systems as well as by combining different types of NESs for isolating vibrations. The effectiveness of combining linear isolators with non-linear energy sinks, however, is unknown.

This study aims to investigate the effect of using these two categories of vibration control systems together through simulating the vibration response in a simple model, after which the combined system can be calibrated and optimised such that it can be tested in a multi-storey building simulation against equipment vibration as well as seismic loading. The ultimate purpose of the investigation is to improve vibration control performance of linear isolators and broaden the knowledge basis of the research field in order to more effectively protect structures against vibrations in practice.

1.3 Objectives

In order to achieve this aim, the following objectives are outlined for this study:

1. To accurately model the behaviour of linear isolators;
2. To accurately model the behaviour of non-linear energy sinks;
3. To obtain a comprehensive understanding of how linear isolators and non-linear energy sinks work when integrated;

- This includes creating a simulation of a setup and performing a parametric study to evaluate how the integration works.
- A simple setup of a linear isolator and a NES will be used to start off with, after which more complex setups may be considered.
- The possibility of optimising the setup must also be investigated. This would ultimately contribute to a guideline for designers to use to reduce vibrations.

4. Test the combined vibration control system in a multi-storey building simulation against both machine vibrations and seismic loading.

1.4 Research Questions

The objectives listed above can be translated into research questions which are answerable in the discussion and conclusion chapters of this report:

1. How does the traditional linear isolator model behave when subjected to harmonic loading?
2. How does the linear isolator integrated NES system behave when subjected to harmonic loading, and how does this compare to the traditional linear isolator acting alone?
3. How does the linear isolator integrated skyhook damper and NES system behave when subjected to harmonic loading, and how does this compare to the other configurations?
4. How does the linear isolator integrated NES system behave at a higher loading frequency ratio?
5. How does the traditional linear isolator model behave when subjected to seismic loading?
6. How does the linear isolator integrated NES system behave when subjected to seismic loading, and how does this compare to the traditional linear isolator acting alone?

2 LITERATURE REVIEW

2.1 Background

2.1.1 Natural Frequency Theory

A system is said to be in free vibration when it is naturally vibrating due to it being subjected to an initial displacement or velocity (Yang, 2001). The frequency of this vibration is termed “natural frequency”, and is a property of the system itself and completely independent of the loads subjected to it (Ewins, 2001).

The formula for determining the natural frequency (ω) of a single degree of freedom (SDOF) system theoretically is (Yang, 2001):

$$\omega = \sqrt{k/m}$$

The natural frequency of a SDOF system can therefore be increased by increasing the system’s stiffness or decreasing the system’s mass. While this formula is only valid for a SDOF system, the trend between natural frequency, mass and stiffness still stands for multi-degree of freedom (MDOF) systems, where there are various masses requiring multiple variables to describe the system’s position. The number of degrees of freedom correlates with the number of natural frequencies the system has, the numerically lowest of which is termed the ‘fundamental natural frequency’.

In practice, there are many cases where a complex MDOF system can be reduced and simplified into a SDOF system. While some may interpret this approach as an oversimplification with limited application as the accuracy of solutions are questionable, in many cases this approach provides an idea of the fundamental behaviour of the system as a whole.

Loading can also be applied at a given frequency, termed the ‘loading frequency’, and the system will tend to vibrate at this frequency upon loading. The closer the loading frequency is to a natural frequency, the larger the displacements due to vibration. When the loading frequency is very close to a natural frequency, the system could go into resonance where the system can vibrate vigorously with amplified displacements. Typically, the displacements that occur during resonance

at the fundamental natural frequency are larger than that of resonance displacements at higher natural frequencies.

2.1.2 Transmissibility Theory

Absolute transmissibility is a ratio measuring the response amplitude to the excitation amplitude of a system due to an isolator (Crede and Ruzicka, 2002). It can be a measure of velocity, force, acceleration or displacement (Harris, 2002).

In a system under consideration, there are two main possible problems to be addressed regarding vibration isolation. The one possibility is that the foundation of the structure is excited, and the goal is to protect the equipment supported by the structure from vibrations. Typically, motion (or displacement) transmissibility (a ratio of the response vibration amplitude of the equipment to the induced vibration amplitude of the foundation) is used for this case (Blake, 2002). The other possibility is that the equipment supported by the structure is the source of vibrations, and the goal is to protect the foundation of the structure from feeling the resulting forces. Typically, force transmissibility (a ratio of the response force experienced by the foundation to the induced force transmitted by the equipment) is used in this case (Blake, 2002). For vibration isolation purposes, it is always the goal to achieve a small transmissibility ratio such that the section being protected vibrates minimally.

When a single degree of freedom (SDOF) system is acted on by a continuous load, typically the displacement transmissibility and force transmissibility of the system are identical, whereas similar loading applied to a multi-degree of freedom (MDOF) system does not show similar behaviour by default (Lage *et al.*, 2014).

Given the damping seen in a system, the transmissibility varies depending on the frequency ratio, that is, the ratio of the vibration frequency exciting the system to the natural frequency of the system, as seen in Figure 2-1. For a traditional and simple SDOF system, it can be seen that a transmissibility of less than one (where the response amplitude is smaller than the excitation amplitude) is only possibly for frequency ratios above the square root of two.

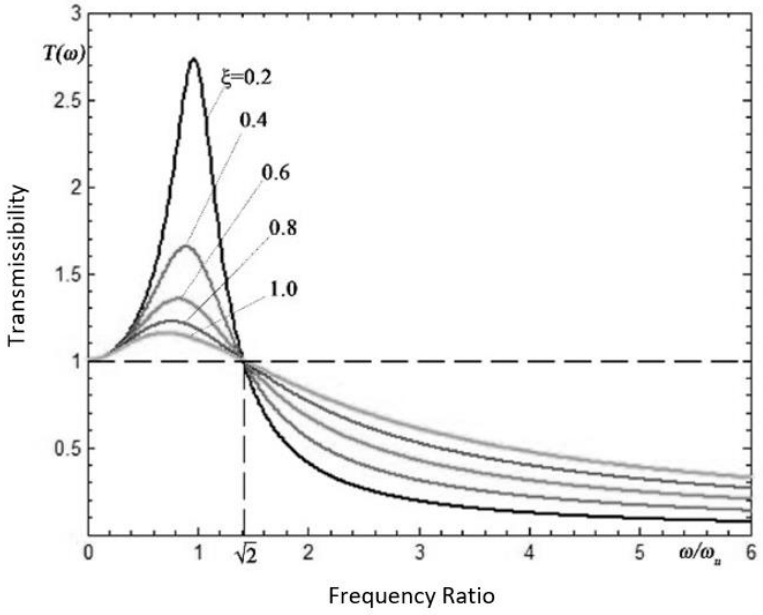


Figure 2-1: Graph showing the relationship between transmissibility and frequency ratio for various damping ratios in a SDOF system (Zou *et al.*, 2014)

2.1.3 Linear Isolator Theory

Isolators are used to restrict vibrations travelling from one system to another, thereby reducing the response of a system due to excitation (Harris, 2002). An isolator must be able to support the relevant load as well as dissipate vibrations or energy (Crede and Ruzicka, 2002). Linear isolators are distinct in that the stiffness of the isolator remains constant and the motion transmissibility and force transmissibility are equal (Crede and Ruzicka, 2002). Figure 2-2 shows diagrams of the types of idealised linear vibration isolators, where various damper setups are used with an ideal spring.

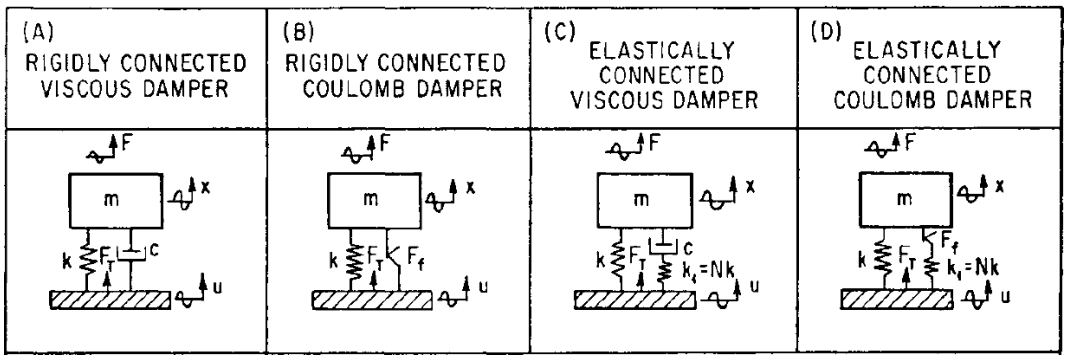


Figure 2-2: Types of idealised vibration isolators (Crede and Ruzicka, 2002)

There are many different types of isolators, each with variations of their own. An elastomeric isolator is one made of a polymer with elastic properties. The polymer is typically rubber, can be formed into a great variety of shapes and acts as both the elastic (load supporting) and damping (energy dissipating) components of the isolator (Crede and Ruzicka, 2002). For a linear isolator, the isolator cross section should remain symmetrical and uniform. An elastomeric isolator is an attractive option as for a given weight and space it provides extremely good elastic, deflection, energy storage and dissipating action (Racca and Harris, 2002). Elastomeric isolators are useful in damping aggressive vibrations at resonance as the amplitude of vibrations are much lower than with metal springs (Racca and Harris, 2002).

Plastic isolators have two components, a structural component made of rigid thermoplastic material (polystyrene is commonly used), and a resilient component made of a thermoplastic elastomer (butadiene styrene is commonly used) (Racca and Harris, 2002). While this solution is cost effective and the isolator can be formed to be very uniform and stable, plastic isolators often have a limited temperature range, larger than average creep and is limited by the strength of the material (Racca and Harris, 2002).

Metal springs can also act as linear vibration isolators, often used where large static deflections are a key factor and in cases where extreme temperatures make other solutions unfeasible (Racca and Harris, 2002). In cases where the metal spring primarily provides the elastic load-supporting component with minimal damping, a damper must be added (Crede and Ruzicka, 2002).

In general, the disadvantages of linear isolators are their narrow range of frequencies at which they are effective, and that they are only effective (where the transmissibility is lower than one) at frequencies above the square root of two times the fundamental natural frequency, as shown in Figure 2-1.

2.1.4 Non-linear energy sink (NES) Theory

The stiffness of a NES increases with an increase in force and deflection. This relationship is often seen in conical springs and rubber acting in compression (Crede and Ruzicka, 2002). This can also be achieved by using linear springs

positioned either perpendicularly or at an angle such that the lateral forces that develop due to deflection always cancel each other out but the in-plane forces build up with increasing deflection, as shown in Figure 2-3.

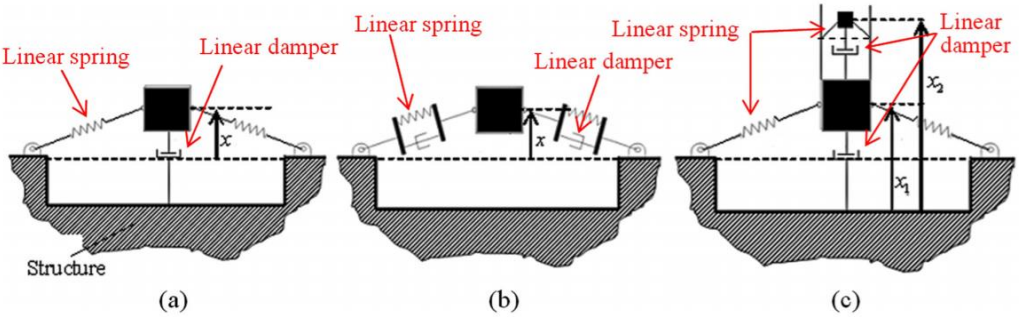


Figure 2-3: Diagrams showing: (a) type-I NES, (b) type II NES, and (c) type-III NES. All springs and dampers shown are uncompressed when horizontal (Sapsis *et al.*, 2012)

While linear isolators generally have a narrow effective frequency range, NESs (which are essentially non-linear systems) are effective at reducing vibrations over a broader range (Ding and Chen, 2020). Further details of NESs are expanded on in Section 2.2: Literature on related works.

2.2 Literature on related works

2.2.1 Types of NES systems

The article, "Highly efficient nonlinear energy sink" (AL-Shudeifat, 2014) investigates a modified Type 1 NES system (also called a Type VII NES), where the transverse linear springs are in compression when in the vertical position, meaning that the system has two positions where the springs are not stressed and are in equilibrium, one to the right and one to the left of the vertical, as shown in Figure 2-4.

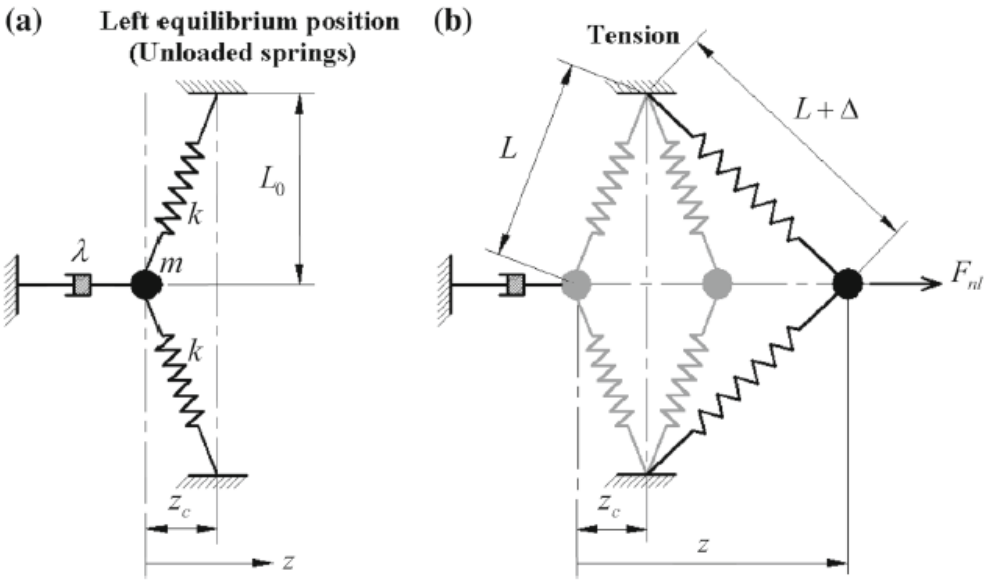


Figure 2-4: Configuration of the modified NES system (AL-Shudeifat, 2014)

This configuration produces "negative linear and nonlinear stiffness components". The performance of this modified NES system is compared to a simple Type 1 NES system. It was found that the Type 1 NES system is highly effective at transferring and dissipating forces when a linear structure is subjected to lower initial velocities (0 to 0.25 m/s approximately), however, at higher initial velocities the effectiveness is reduced. When calibrated correctly, the modified NES system is highly effective for a much broader range of initial velocities (0 to 1 m/s). It was also found that the modified NES system is less sensitive in terms of effectiveness when the damping and stiffness of the system is adjusted. Not only was it found that the modified NES system is more effective at rapid energy dissipation, but also that the system is

effective in “shock mitigation for multi external energy inputs at different impulse times”.

2.2.2 Comparison and combination with linear systems

The study, “Comparison of linear and nonlinear vibration isolation system under random excitation” (Smirnov and Mondrus, 2016) found that when considering low-frequency base excitations, that the nonlinear vibration isolation system is much more efficient at protecting equipment than the linear vibration isolation system while also being more compact and lightweight than the linear system.

The study, “Vibration reduction evaluation of a linear system with a nonlinear energy sink under a harmonic and random excitation” (Xue *et al.*, 2020) revolved around a numerical calculation of the response of a linear system with an NES that used a spring with an ideal cubic nonlinear stiffness. A representation of the model is shown in Figure 2-5.

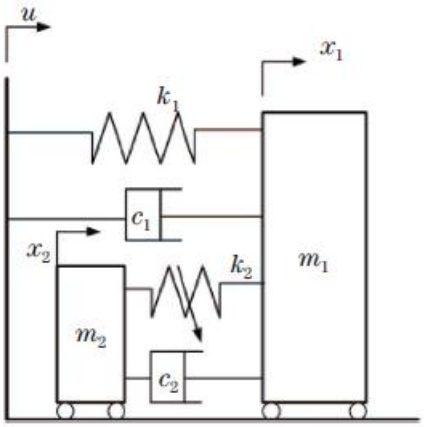


Figure 2-5: A linear system with an NES system using an ideal cubic non-linear stiffness (Xue et al.*, 2020)*

The findings were that the NES is effective in reducing vibrations, however, that a random jump in the response may occur at any frequency during harmonic excitation, which is detrimental to the linear system. It is however expected that an increase in the nonlinear stiffness and decrease in damping ratio could improve performance while also improving the stability of the linear system.

The study, “A passive vibration isolator integrated a skyhook damper or a groundhook damper” (Li, 2020) compares a traditional linear vibration isolator acting on its own (a single degree of freedom (SDOF) system as shown in Figure

2-6) to one integrated with either a skyhook damper or a groundhook damper (a two degree of freedom (2DOF) system as shown in Figure 2-7) in terms of its effectiveness in isolating vibrations. The integrated systems were found to still be linear systems.

In order for a traditional linear vibration isolator to be effective at low frequencies, it must lower the system's natural frequency. However, in order to do this, the system's stiffness must substantially decrease without compromising the system's ability to resist it's loads. This is not possible when using a traditional isolator. By considering the force and displacement transmissibility as well as the numerical models of the systems, it was found that the integrated systems are effective in a broader range of frequencies. This allows the system to cater for vibration isolation at lower frequencies without compromising on it's ability to resist loads.

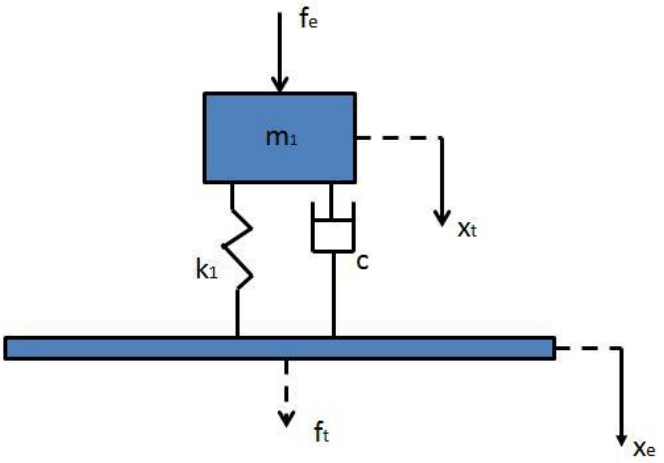


Figure 2-6: Model of a traditional linear vibration isolator (Li, 2020)

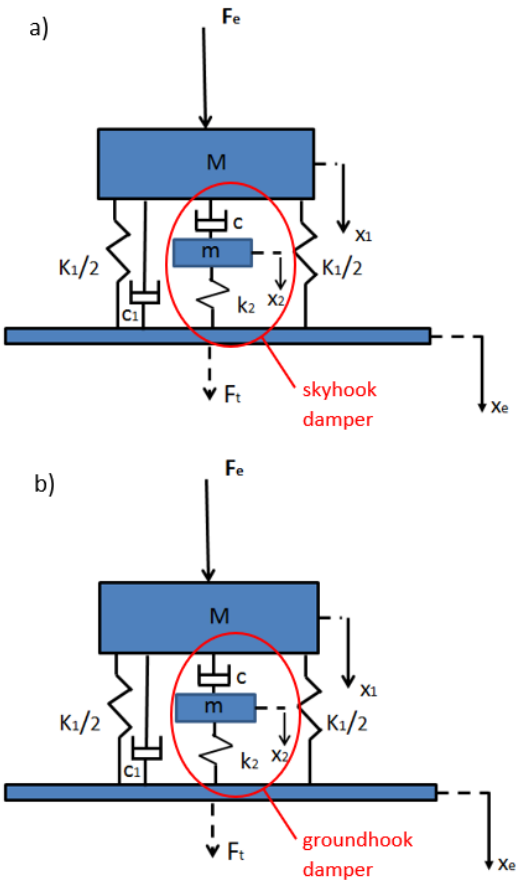


Figure 2-7: a) Model of a traditional linear vibration isolator integrated with a skyhook damper, b) Model of a traditional linear vibration isolator integrated with a groundhook damper (Li, 2020)

Adjusting the various parameters effecting the force transmissibility, it was found that increasing the mass ratio, damping ratio and ν (ω_2/ω_1) reduces the force transmissibility compared to the traditional system. It was also seen that that the force transmissibility at higher frequencies is slightly higher for larger values of ν and damping ratio. Overall, it was concluded that the integrated system can achieve good vibration isolation even with low damping elements.

The article, "The analysis and design of nonlinear vibration isolators under both displacement and force excitations" (Qiu *et al.*, 2021) considers the use of non-linear isolators and compares the transmissibility performance to a traditional linear isolator.

Non-linear stiffness and damping are modelled by using inclined springs and dampers as shown in Figure 2-8.

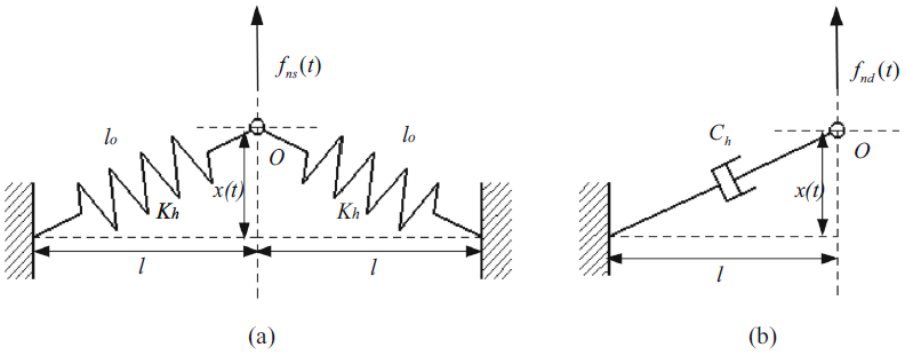


Figure 2-8: Non-linear stiffness modelled using a) inclined springs, and non-linear damping modelled using b) inclined damper (Qiu et al.*, 2021)*

These modelling techniques are used to create non-linear systems (a), (b) and (c) as shown in Figure 2-9.

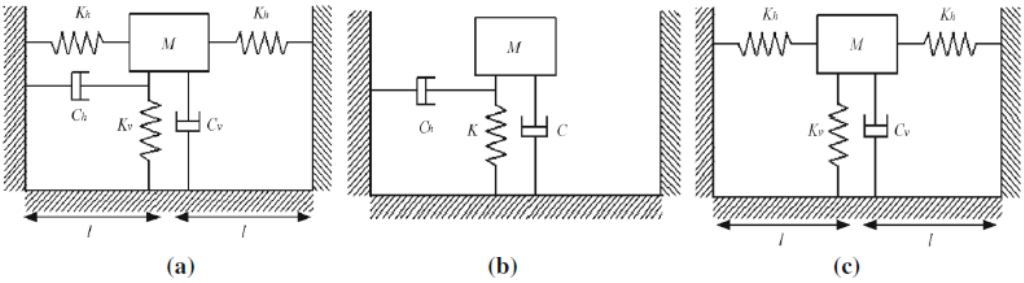


Figure 2-9: Non-linear isolation systems formed using a) non-linear stiffness and non-linear damping, b) non-linear damping, and c) non-linear stiffness (Qiu et al.*, 2021)*

The transmissibility of systems (a), (b) and (c) are compared with a traditional linear isolator system (termed system (d)) using comparative input parameters. From the graph in Figure 2-10, it is found that compared to system (d), systems (a) and (c) are effective over a larger frequency range and achieve a lower transmissibility for frequency ratios greater than 1 including a lower peak transmissibility, and that system (b) achieves a lower peak transmissibility while closely matching transmissibility either side of the peak.

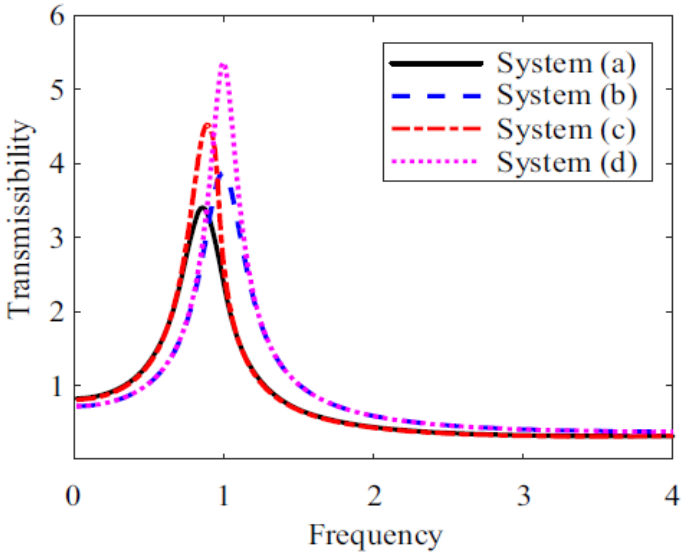


Figure 2-10: Transmissibility graphs for systems (a), (b), (c) and (d) (Qiu et al.*, 2021)*

Therefore, overall the non-linear isolation systems are considered to have achieved positive isolation results (Qiu *et al.*, 2021).

2.2.3 Seismic Application

The article, "Large-scale experimental evaluation and numerical simulation of a system of nonlinear energy sinks for seismic mitigation" (Luo *et al.*, 2014) outlines an experiment conducted on a model of a nine-storey steel structure intended to represent a mid-rise building. The model had six NES devices attached to the top two storeys. Of these 6 devices, 4 of them were simple devices (Type 1 NES as shown in Figure 2-11 on the outside of the top two floors) which have a single degree of freedom (SDOF) with an essentially nonlinear spring and linear damping. The mass of each of these devices were approximately 1.5% of the total building mass. The other 2 devices were single-sided vibro-impact devices (SSVI NES as shown in Figure 2-11 on the middle section of the top two floors) that have a moving mass, a linear spring and a stop plate to facilitate non-smooth impact movements. The mass of each of these devices were approximately 3.4% of the total building mass.

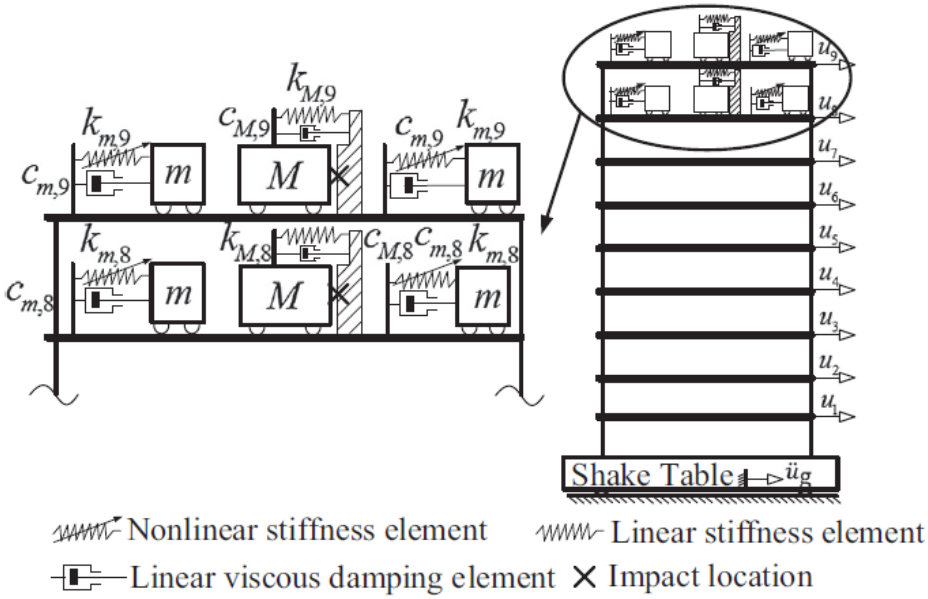


Figure 2-11: Depiction of large-scale model testing setup (Luo *et al.*, 2014)

The structure was loaded on a shaking table by simulating ground motion of three historic earthquakes namely the Kobe earthquake of 1995, the Northridge earthquake of 1994 as well as the Imperial Valley (or El Centro) earthquake of 1940.

Four sets of experiments were conducted, first with all NES devices locked to get a baseline response, second and third with either type of NES device active at a time and lastly with both types of NES devices active simultaneously. Results of the seventh-storey acceleration and displacement, first-storey strain and base shear were compared. It was found that the seventh-storey acceleration increased when all NES devices were unlocked due to the impact of the SSVI NES devices, while the seventh storey displacement, first-storey strain and base shear all notably decreased (Luo *et al.*, 2014). The results from the El Centro earthquake are shown in Figure 2-12 to demonstrate the results found.

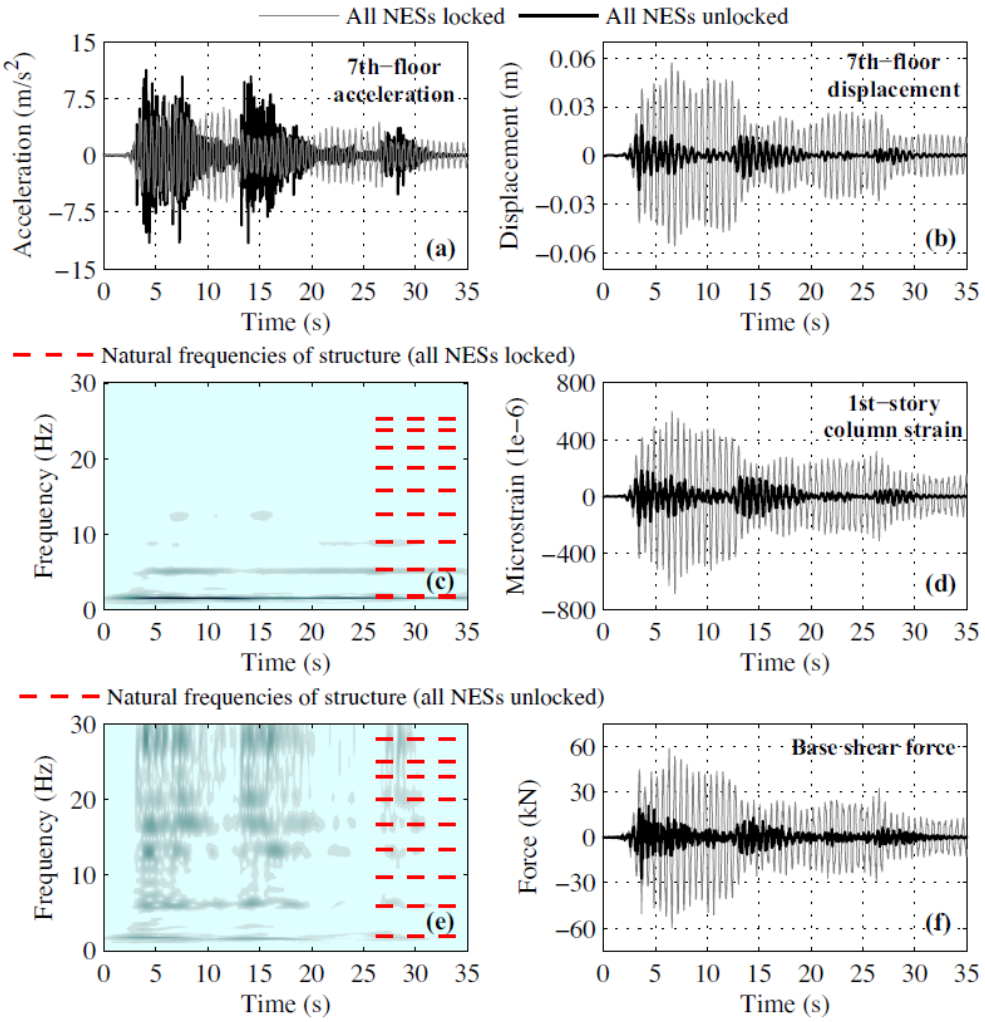


Figure 2-12: Output results for all NES systems locked versus unlocked for the El Centro earthquake (Luo et al., *2014)*

The average results reduced by approximately 40% and the peak results reduced by approximately 60%. It was proposed that the reduction in response was mainly due to the SSVI NES devices that rapidly redistributes and dissipates energy, and that the Type 1 NES devices then become effective in dissipating the residual energy (Luo *et al.*, 2014).

When only one type of NES device was active at a time, they were also found to be effective in dissipating energy and decreasing responses. Using the Type 1 NES devices alone avoids increasing the floor acceleration (as shown in Figure 2-13), however, it is not as effective in decreasing displacement as using the SSVI NES devices alone (as shown in Figure 2-14).

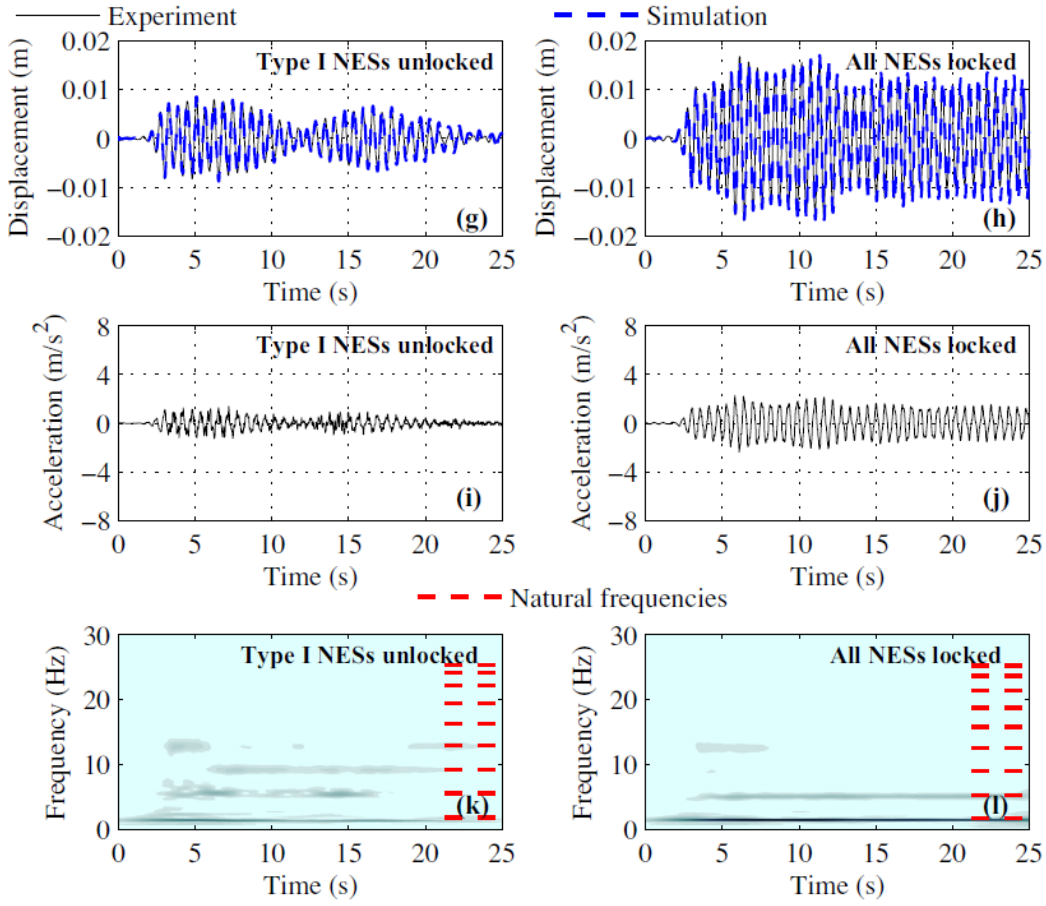


Figure 2-13: Output results for all NES systems locked versus Type I NES unlocked for the El Centro earthquake (Luo et al.*, 2014)*

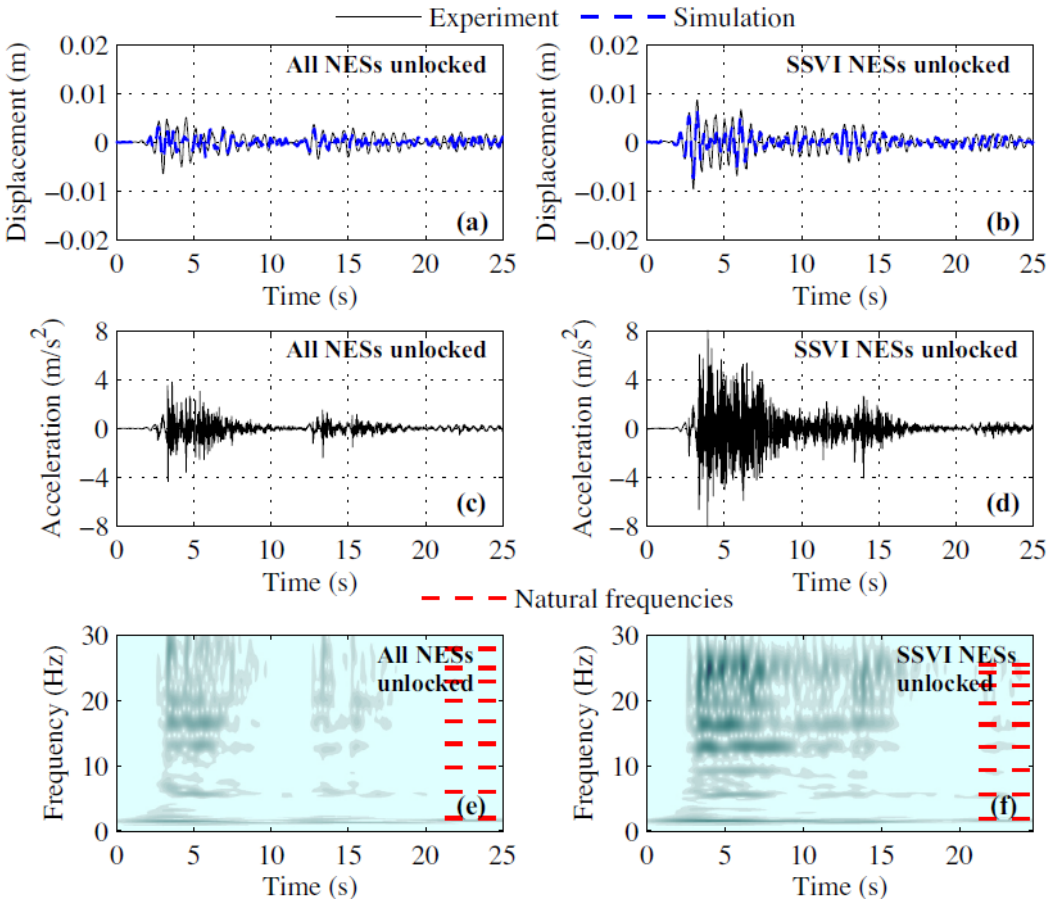


Figure 2-14: Output results for all NES systems locked versus SSVI NES unlocked for the El Centro earthquake (Luo et al.*, 2014)*

Overall, using the different types of NES devises in isolation was not as effective in reducing responses as having both types of NES working together, and using the Type 1 NES in conjunction with the SSVI NES decreases the acceleration peaks caused by the SSVI NES as compared to when it is used alone (Luo *et al.*, 2014). A numerical model was also developed and calibrated to expand on results for a wider variety of ground motion. The main intention of the experiment was to study the effectiveness of using NES to protect large civil structures from seismic events. It was concluded that NES devices are effective in mitigating the response of structures for the ground motions considered.

2.3 Gaps in the study

Studies have been done around the effectiveness of traditional linear isolators and dealing with vibration control in structures, comparing this to the effectiveness of various types and combinations of NES systems as well as setups combining the traditional vibration isolator and various damping systems.

While these studies provided great insight into the behaviour of these various means of vibration control, there is a gap in the research whereby the effectiveness of traditional linear isolators integrated NES systems are investigated and compared to the performance of the systems in isolation.

3 THE RESEARCH METHODOLOGY

3.1 Data collection and analysis methods

This study is a desktop study. Various linear isolator and NES setups are considered and modelled using software. Simulations are performed where loading is applied. The response of the setups to the loading will be captured from the software; outputs of interest are deflections, velocities, accelerations and vibration frequencies. From these recorded responses, transmissibility graphs and time history graphs are produced and compared to one another for detailed analysis. A parametric study is performed whereby all variables are altered to investigate the effect of each.

The software program, MATLAB, is used for the modelling and loading of structures for analysis. MATLAB, produced by MathWorks, is a programming software designed for use by engineers and scientists to run complex mathematical calculations (MathWorks, 2021).

It is possible to use MATLAB together with numerical integration techniques to model and load systems and record the simulated response. This allows one to compare the predicted responses of each isolator setup to evaluate the effectiveness of combining linear isolators and NES.

3.2 Calculation methods and details

First the force transmissibility and displacement transmissibility equations are determined for each of the following setups:

1. Configuration 1 – A traditional linear isolator
2. Configuration 2A – A linear isolator integrated a NES system (damper to base)
3. Configuration 2B – A linear isolator integrated a NES system (spring to base)
4. Configuration 3 – A linear isolator integrated a skyhook damper and a NES system

Next the transmissibility equations must be plotted against the loading frequency ration on a graph. While this is easy to do for the traditional linear isolator since the

equations are not as a function of any additional variables, for Configurations 2A, 2B and C where there is a NES system attached, these transmissibility equations are as a function of the relative longitudinal stiffness of the non-linear stiffness component since this varies based on the relative position vector of the NES mass, which continuously changes and is not easy to predict.

In order to determine the relative position of the NES mass at all times such that the effective linear stiffness and therefore the system response can be correctly represented, a MATLAB code is developed which simulates the system's response calculated using the 4^{th} order Runge-Kutta numerical analysis method. This numerical analysis method is considered reasonably accurate compared to others when performing dynamic analyses, particularly when the calculations are set to repeat at small enough time intervals.

This calculation involves the repetitive process of using the numerical analysis method code to determine the relative position-time, velocity-time and acceleration-time graphs for of each of the masses within the system being analysed, determining the maximum transmissibility value from these graphs and repeating the process for a range of loading frequency values such that the transmissibility vs loading frequency graph can be plotted given the chosen variable parameters.

This process is again repeated while adjusting each of the system's adjustable variables, including the masses, spring stiffnesses, dampers as well as the NES non-linear spring original and stretched lengths in order to find the optimised value for each parameter given the system being considered. This process is done for each of the configurations and the results compared.

A similar process is again followed for application to earthquakes, however here, the response of the setup needs to be determined based on the input loading from the historical earthquakes considered rather than a continuous load input from machinery. The transmissibility for this application is determined from the displacement-time graphs which must be studied closely since the loading frequency is not as consistent as with equipment.

4 TRADITIONAL LINEAR ISOLATOR

4.1 Introduction

In this chapter the traditional linear isolator will be considered and analysed. The objective is to decide on the setup to be analysed and determine the force transmissibility and displacement transmissibility equations which is further discussed in Section 8.1.

4.2 The setup

The traditional linear isolator is a very basic system which uses springs (with total stiffness k_1) to support the payload (mass m_1) together with a dashpot acting as a damper (c_1) which work together to isolate vibrations as shown in the setup in Figure 4-1.

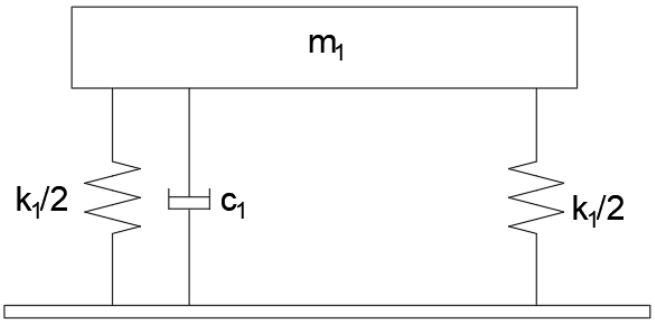


Figure 4-1: Setup of a traditional linear isolator – Configuration 1

In Figure 4-2, force applied by the payload (m_1) itself is shown as F_1, and when determining the force transmissibility, the force experienced by the base as a result is equal to F_0. The displacement of the payload is represented by x_1, and

when determining the displacement transmissibility, the displacement of the base is considered as x_0.

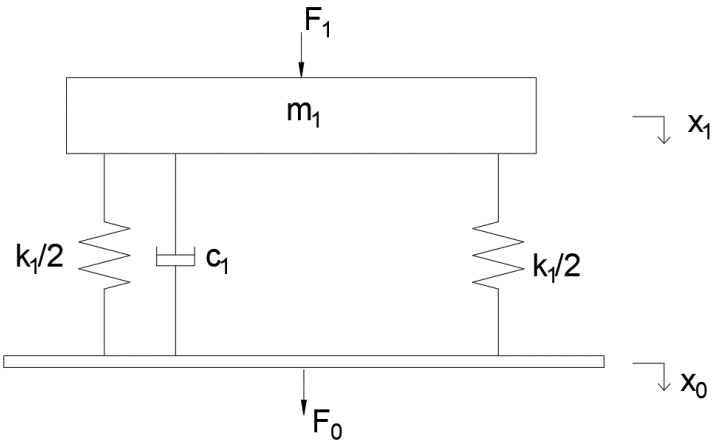


Figure 4-2: Single degree of freedom model of the traditional linear isolator

4.3 Force Transmissibility of Configuration 1

Force transmissibility is typically used to measure the effectiveness of the system in reducing vibrations from transmitting from the payload to the base.

For this investigation, F_1 which is shown as being applied to m_1 will be considered as a harmonic force with a loading frequency of ω. From this model, while considering x_0 = 0 for the force transmissibility response, the equations of motion can be determined as:

$$m_1\ddot{x_1} + c_1\dot{x_1} + k_1x_1 = F_1\cos(\omega t) \quad (1)$$

$$F_0 = k_1x_1 + c_1\dot{x_1} \quad (2)$$

where $\dot{x_1}$ and $\ddot{x_1}$ represent the velocity (first derivative) and acceleration (second derivative) of m_1 respectively.

Performing Fourier Transformation on equation 1 gives:

$$F_1 = (-m_1\omega^2 + k_1 + i\omega c_1)X_1 \quad (3)$$

Performing Fourier Transformation on equation 2 gives:

$$F_0 = (k_1 + i\omega c_1)\,X_1 \quad (4)$$

The force transmissibility equation for this system can therefore be shown as:

$$T_f = \frac{F_0}{F_1} = \frac{k_1 + i\omega c_1}{-m_1\omega^2 + k_1 + i\omega c_1} \quad (5)$$

Using $P = \frac{A + jB}{C + jD} = \sqrt{\frac{A^2 + B^2}{C^2 + D^2}}$ where A and C are the real parts of the numerator and denominator of an equation respectively, and B and D are the imaginary parts of the numerator and denominator of an equation respectively, the force transmissibility equation gives:

$$T_f = \sqrt{\frac{{k_1}^2 + \omega^2 {c_1}^2}{(k_1 - m_1\omega^2)^2 + \omega^2 {c_1}^2}} \quad (6)$$

The following relationships associated with a single-degree-of-freedom (SDOF) system can be used to simplify the force transmissibility equation:

$$\lambda = \frac{\omega}{\omega_1} \qquad \omega_1 = \sqrt{\frac{k_1}{m_1}} \qquad \xi = \frac{c_1}{2m_1\omega_1}$$

where λ is the frequency ratio and ω_1 is the first natural frequency of the system.

From this, the force transmissibility equation gives:

$$T_f = \sqrt{\frac{{w_1}^4 {m_1}^2 + 4\,{w_1}^4 {m_1}^2 \xi^2 \lambda^2}{({w_1}^2 m_1 - {w_1}^2 m_1 \lambda^2)^2 + 4\,{w_1}^4 {m_1}^2 \xi^2 \lambda^2}} \quad (7)$$

Equation 7 can be simplified to determine the final force transmissibility equation:

$$T_f = \sqrt{\frac{1 + 4\xi^2\lambda^2}{(1 - \lambda^2)^2 + 4\xi^2\lambda^2}} \quad (8)$$

4.4 Displacement Transmissibility of Configuration 1

Displacement transmissibility is typically used to measure the effectiveness of the system in reducing vibrations from transmitting from the base to the payload.

Here we do not consider the forces applied to the payload and base (as represented by F_1 and F_0 respectively), however, we do consider both displacements represented by x_1 and x_0 respectively. From this model the equations of motion can be determined as:

$$m_1\ddot{x_1} + c_1(\dot{x_1} - \dot{x_0}) + k_1(x_1 - x_0) = 0 \quad (9)$$

Performing Fourier Transformation on equation 9 results in the following relationship:

$$(-m_1\omega^2 + k_1 + i\omega c_1)X_1 = (k_1 + i\omega c_1)\, X_0 \quad (10)$$

The displacement transmissibility equation for this system can therefore be shown as:

$$T_d = \frac{X_1}{X_0} = \frac{k_1 + i\omega c_1}{-m_1\omega^2 + k_1 + i\omega c_1} \quad (11)$$

As before, the displacement transmissibility equation can be solved and simplified to give:

$$T_d = \sqrt{\frac{1 + 4\xi^2\lambda^2}{(1-\lambda^2)^2 + 4\xi^2\lambda^2}} \quad (12)$$

4.5 Conclusion

The force transmissibility and displacement transmissibility equations for the traditional linear isolator setup analysed are shown in Equation 8 and Equation 12 respectively.

Comparing the equations, it can be seen that they are identical, meaning that this is a linear system. Further discussion and analysis can be found in Section 8.1.

5 NON-LINEAR ENERGY SINK (NES)

5.1 Introduction

For this investigation, a typical Type 1 NES system is being studied. In order for this system to be used, a clear understanding of how the system's stiffness varies with time and displacement is required. This understanding must be definable in measurable parameters in order to simulate it's behaviour when integrated with other systems in later chapters.

5.2 The setup

Figure 5-1 shows the system at rest where it is composed of central mass (m_1), two springs (each with stiffness k_1) orientated at 90-degrees from the direction of motion being considered, and a damper c_1 connecting the NES mass to the payload. The springs have an original length of L_0, and can be pre-tensioned by stretching the springs by a distance x_i when connecting them to the NES mass m_1. At rest, the springs are level and the lateral load from each end completely cancel each other out resulting in a zero effective longitudinal stiffness in the direction of motion, the NES system can be shown as:

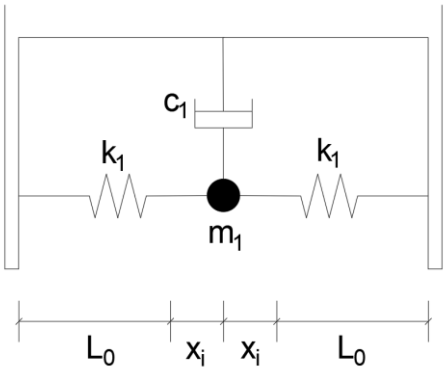


Figure 5-1: NES system at rest

5.3 Study of the parameters

When the system is loaded and the NES mass moves, the relative longitudinal displacement of the mass from the payload mass is represented by x_m. A typical example of this can be seen in Figure 5-2.

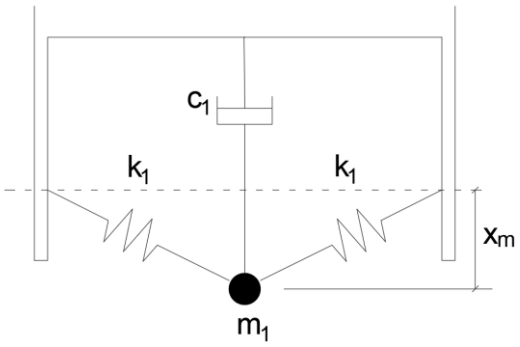


Figure 5-2: NES system with relative displacement

The force and position components for each spring is shown in Figure 5-3:



Figure 5-3: Force and position components of the NES system

Where F represents the tension in the system, F_x the linear force in the direction of motion and F_y the perpendicular force which gets cancelled out by the opposite spring's F_y.

From this we can determine that:

$$F = \left[\sqrt{(L_0 + x_i)^2 + {x_m}^2} - L_0\right]k_1 \tag{14}$$

$$\sin\theta = \frac{x_m}{\sqrt{(L_0+x_i)^2+{x_m}^2}} \tag{15}$$

$$\sin\theta = \frac{F_x}{F} \tag{16}$$

Manipulating equation 16, we find:

$$F_x = F \sin\theta$$

$$= \left[\sqrt{(L_0 + x_i)^2 + {x_m}^2} - L_0\right] k_1 \,.\, \frac{x_m}{\sqrt{(L_0 + x_i)^2 + {x_m}^2}}$$

$$= k_1 x_m - \frac{L_0 k_1 x_m}{\sqrt{(L_0 + x_i)^2 + {x_m}^2}} \tag{17}$$

Since the force in a spring is equal to it's stiffness multiplied by the change in length from the original length, k'_1 is introduced as the effective longitudinal stiffness of each spring k_1 in the direction of motion and the equivalent force in the direction of motion can be shown as:

$$F_x = x_m k'_1 \tag{18}$$

Therefore, for each perpendicular spring:

$$k'_1 = \frac{F_x}{x_m}$$

$$k'_1 = \left| k_1 - \frac{L_0 k_1}{\sqrt{(L_0 + x_i)^2 + {x_m}^2}} \right| \tag{19}$$

Since the direction of the force will be determined by the relative displacement variable, the relative longitudinal stiffness can be taken as an absolute value.

5.4 Conclusion

The linear force (F_x) as well as the effective longitudinal stiffness (k'_1) in the direction of motion of NES mass (m_1) has been determined in Equation 17 and Equation 19 respectively.

This relative longitudinal stiffness equation is used in all computations where the NES system is considered going forward in this study.

6 LINEAR ISOLATOR INTEGRATED NES

6.1 Introduction

In this chapter a traditional linear isolator integrated NES will be considered and analysed. The objective is to decide on the setups to be analysed and determine the force transmissibility and displacement transmissibility equations for each setup which is further discussed in Section 8.2.

6.2 The setup

A traditional linear isolator (composed of spring stiffness k_1 and damping c_1) is coupled together with an NES system formed of a central mass (m_2), two springs (each with stiffness k_2) orientated at 90-degrees from the direction of motion being considered and connected to the payload mass m_1, a damper connecting the NES mass m_2 to the payload mass m_1, as well as a connection means from the NES mass m_2 to the base in the form of either an additional damper (c_3 as shown in Figure 6-1 for Configuration 2A) or a spring (k_3 as shown in Figure 6-2 for Configuration 2B) .

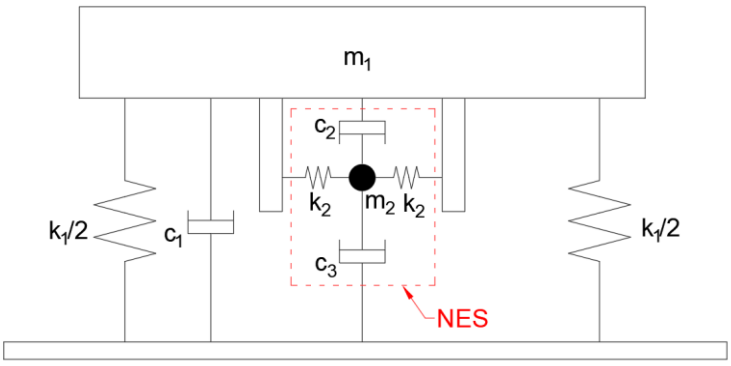


Figure 6-1: Setup of a linear isolator integrated a NES system (damper to base) - Configuration 2A

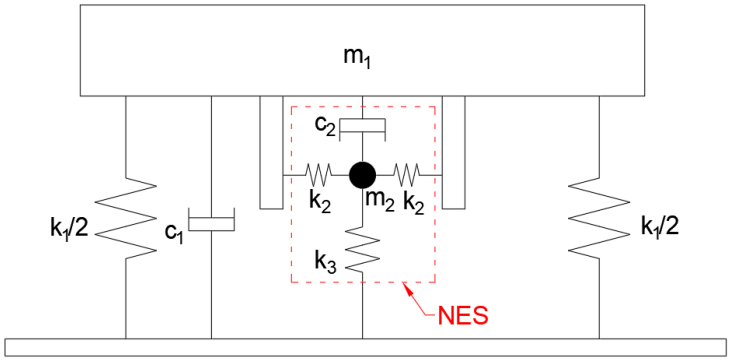


Figure 6-2: Setup of a linear isolator integrated a NES system (spring to base) - Configuration 2B

As before, the force applied by the payload (m_1) and the force experienced as a result by the base is represented by F_1 and F_0 respectively when determining the force transmissibility (as shown in Figure 6-3 and Figure 6-4 for Configuration 2A and 2B respectively). The displacement of the payload and the NES mass is represented by x_1 and x_2 respectively, and when determining the displacement transmissibility, the displacement of the base is considered as x_0.

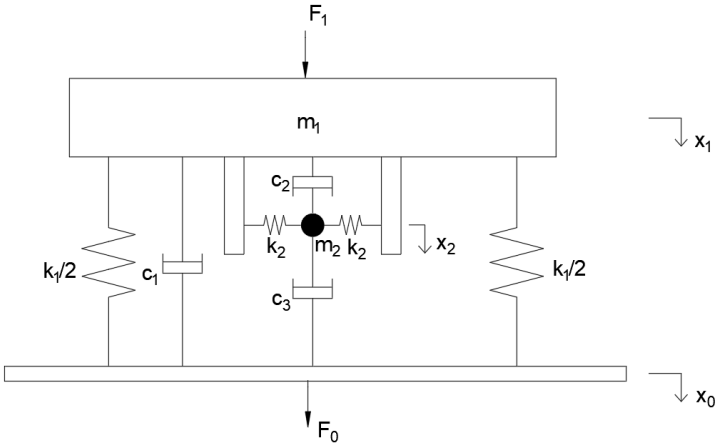


Figure 6-3: Two DOF model of a linear isolator integrated a NES system (damper to base)–Configuration 2A

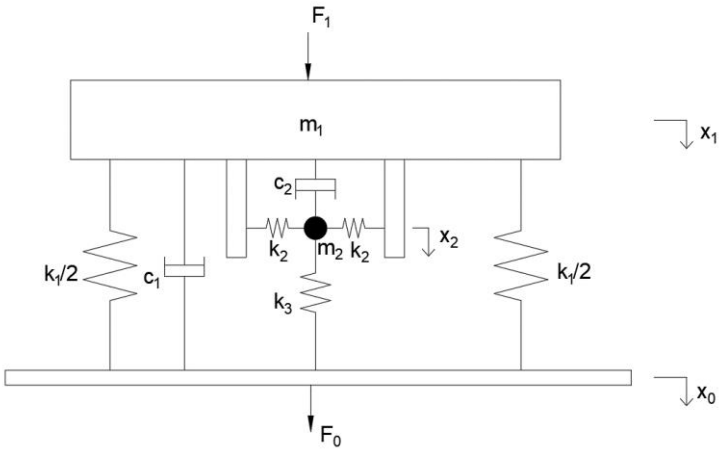


Figure 6-4: Two DOF model of a linear isolator integrated a NES system (spring to base) - Configuration 2B

These models can be adjusted to display the two k_2 non-linear springs as $2k'_2$ representing the effective linear stiffness in the direction of motion being considered. This simplifies the process of working with the models, and is visually shown in Figure 6-5 and Figure 6-6 as an arrow through the spring symbol as follows:

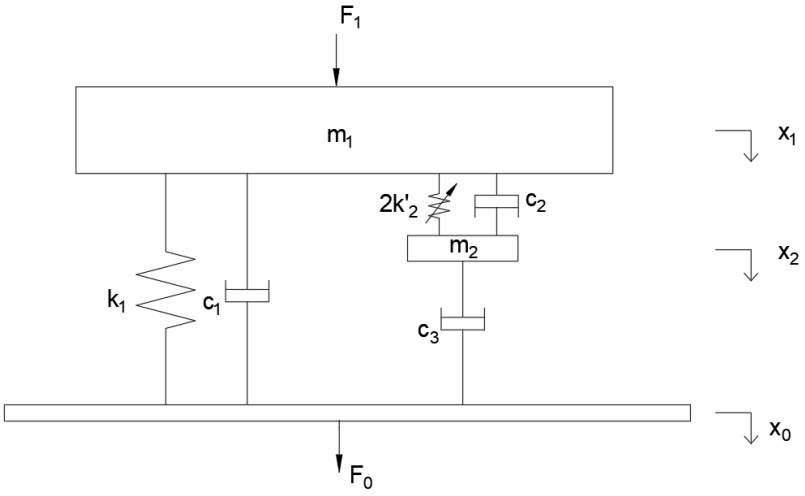


Figure 6-5: Configuration 2A shown with effective linear stiffness component

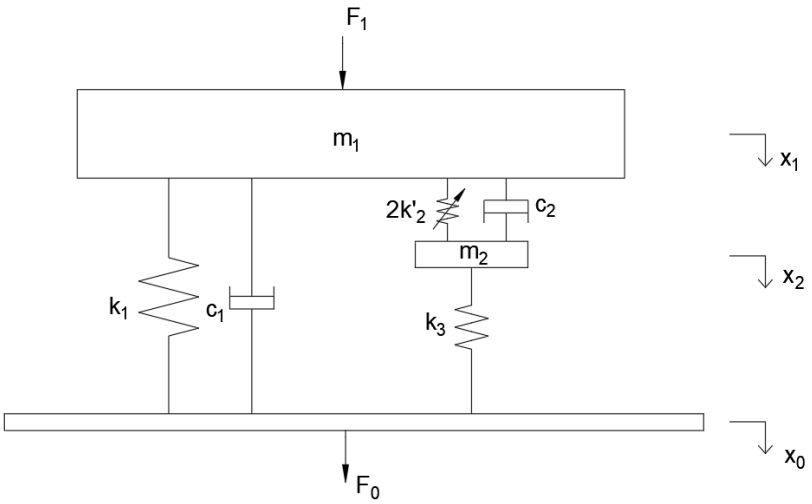


Figure 6-6: Configuration 2B shown with effective linear stiffness component

6.3 Configuration 2A

6.3.1 Force Transmissibility of Configuration 2A

As before, F_1 applied to m_1 will be considered as a harmonic force with a loading frequency of ω. From this model, while considering x_0 = 0 for the force transmissibility response, the equations of motion can be determined as:

$$m_1\ddot{x_1} + c_1\dot{x_1} + c_2(\dot{x_1} - \dot{x_2}) + k_1x_1 + 2k'_2(x_1 - x_2) = F_1\cos(\omega t) \quad (20)$$

$$m_2\ddot{x_2} + c_2(\dot{x_2} - \dot{x_1}) + c_3\dot{x_2} + 2k'_2(x_2 - x_1) = 0 \quad (21)$$

$$F_0 = k_1x_1 + c_1\dot{x_1} + c_3\dot{x_2} \quad (22)$$

Performing Fourier Transformation on equation 20 gives:

$$F_1 = (-m_1\omega^2 + k_1 + 2k'_2 + i\omega c_1 + i\omega c_2)X_1 + (-2k'_2 - i\omega c_2)X_2 \quad (23)$$

Performing Fourier Transformation on equation 21 gives:

$$(-m_2\omega^2 + 2k'_2 + i\omega c_3 + i\omega c_2)X_2 = (-2k'_2 - i\omega c_2)X_1$$

Making X_1 the subject of the formula gives:

$$X_1 = \frac{(-m_2\omega^2 + 2k'_2 + i\omega c_3 + i\omega c_2)}{(-2k'_2 - i\omega c_2)}X_2 \quad (24)$$

Performing Fourier Transformation on equation 22 gives:

$$F_0 = (k_1 + i\omega c_1)X_1 - (i\omega c_3)X_2 \tag{25}$$

Substituting equation 24 into equation 23 gives:

$$F_1 = \frac{(-m_1\omega^2 + k_1 + 2k'_2 + i\omega c_1 + i\omega c_2)(-m_2\omega^2 + 2k'_2 + i\omega c_3 + i\omega c_2)}{(-2k'_2 - i\omega c_2)} X_2$$

$$+(-2k'_2 - i\omega c_2)X_2 \tag{26}$$

Substituting equation 24 into equation 25 gives:

$$F_0 = (k_1 + i\omega c_1)\frac{(-m_2\omega^2 + 2k'_2 + i\omega c_3 + i\omega c_2)}{(-2k'_2 - i\omega c_2)} X_2 - (i\omega c_3)X_2 \tag{27}$$

Solving for T_f using equations 26 and 27 and cancelling the common X_2, the force transmissibility equation can be shown as:

$$T_f = \frac{F_0}{F_1} =$$

$$\frac{(iwc_1 + k_1)(iwc_2 + iwc_3 - m_2w^2 + 2k_2) + wc_3(2ik_2 - wc_2)}{(iwc_2 + iwc_3 - m_2w^2 + 2k_2)(iwc_1 + iwc_2 - m_1w^2 + k_1 + 2k_2) + wc_2(wc_2 - 2ik_2) - k_2(2iwc_2 + 4k_2)} \tag{28}$$

where for the purposes of this formula k'_2 is being represented as k_2.

Due to the non-linear stiffness parameter as well as the complex nature of the equation, it is being left in this format for now. The equation is further discussed in Chapter 8 – Transmissibility Discussion.

6.3.2 Displacement Transmissibility of Configuration 2A

Determining the displacement transmissibility of the system, where the forces F_1 and F_0 are not considered, however, we do consider the displacements of the payload, NES mass and the base represented by x_1, x_2 and x_0 respectively. From this model the equations of motion can be determined as:

$$m_1\ddot{x_1} + c_1(\dot{x_1} - \dot{x_0}) + c_2(\dot{x_1} - \dot{x_2}) + k_1(x_1 - x_0) + 2k'_2(x_1 - x_2) = 0 \tag{29}$$

$$m_2\ddot{x_2} + c_2(\dot{x_2} - \dot{x_1}) + c_3(\dot{x_2} - \dot{x_0}) + 2k'_2(x_2 - x_1) = 0 \tag{30}$$

Performing Fourier Transformation on equation 29 gives:

$$(-m_1\omega^2 + k_1 + 2k'_2 + i\omega c_1 + i\omega c_2)X_1 - (k_1 - i\omega c_1)X_0 - (2k'_2 + i\omega c_2)X_2 = 0$$

Making X_2 the subject of the formula gives:

$$X_2 = \frac{(-m_1\omega^2+k_1+2k'_2+i\omega c_1+i\omega c_2)}{(2k'_2+i\omega c_2)}X_1 - \frac{(k_1-i\omega c_1)}{(2k'_2+i\omega c_2)}X_0 \quad (31)$$

Performing Fourier Transformation on equation 30 gives:

$$(-m_2\omega^2 + 2k'_2 + i\omega c_3 + i\omega c_2)X_2 + (i\omega c_3)X_0 - (2k'_2 + i\omega c_2)X_1 = 0 \quad (32)$$

Substituting equation 31 into equation 32 gives:

$$\frac{(-m_2\omega^2 + k_3 + 2k'_2 + i\omega c_3 + i\omega c_2)(-m_1\omega^2 + k_1 + 2k'_2 + i\omega c_1 + i\omega c_2)}{(2k'_2 + i\omega c_2)}X_1$$

$$-\frac{(-m_2\omega^2 + 2k'_2 + i\omega c_3 + i\omega c_2)(k_1 - i\omega c_1)}{(2k'_2 + i\omega c_2)}X_0 + (i\omega c_3)X_0 - (2k'_2 + i\omega c_2)X_1 = 0$$

Solving for T_d, the force transmissibility equation can be shown as:

$$T_d = \frac{X_1}{X_0} =$$

$$\frac{(iwc_1 + k_1)(iwc_2 + iwc_3 - m_2w^2 + 2k_2) + wc_3(2ik_2 - wc_2)}{(iwc_2 + iwc_3 - m_2w^2 + 2k_2)(iwc_1 + iwc_2 - m_1w^2 + k_1 + 2k_2) + wc_2(wc_2 - 2ik_2) - k_2(2iwc_2 + 4k_2)} \quad (33)$$

where for the purposes of this formula k'_2 is being represented as k_2.

Due to the non-linear stiffness parameter as well as the complex nature of the equation, it is being left in this format for now. The equation is further discussed in Chapter 8 – Transmissibility Discussion.

6.4 Configuration 2B

6.4.1 Force Transmissibility of Configuration 2B

As before, F_1 applied to m_1 will be considered as a harmonic force with a loading frequency of ω. From this model, while considering x_0 = 0 for the force transmissibility response, the equations of motion can be determined as:

$$m_1\ddot{x_1} + c_1\dot{x_1} + c_2(\dot{x_1} - \dot{x_2}) + k_1x_1 + 2k'_2(x_1 - x_2) = F_1\cos(\omega t) \quad (34)$$

$$m_2\ddot{x_2} + c_2(\dot{x_2} - \dot{x_1}) + 2k'_2(x_2 - x_1) + k_3x_2 = 0 \quad (35)$$

$$F_0 = k_1x_1 + c_1\dot{x_1} + k_3x_2 \quad (36)$$

Performing Fourier Transformation on equation 34 gives:

$$F_1 = (-m_1\omega^2 + k_1 + 2k'_2 + i\omega c_1 + i\omega c_2)X_1 + (-2k'_2 - i\omega c_2)X_2 \quad (37)$$

Performing Fourier Transformation on equation 35 gives:

$$(-m_2\omega^2 + k_3 + 2k'_2 + i\omega c_2)X_2 = (-2k'_2 - i\omega c_2)X_1$$

Making X_1 the subject of the formula gives:

$$X_1 = \frac{(-m_2\omega^2 + k_3 + 2k'_2 + i\omega c_2)}{(-2k'_2 - i\omega c_2)}X_2 \quad (38)$$

Performing Fourier Transformation on equation 36 gives:

$$F_0 = (k_1 + i\omega c_1)X_1 + (k_3)X_2 \quad (39)$$

Substituting equation 38 into equation 37 gives:

$$F_1 = \frac{(-m_1\omega^2 + k_1 + 2k'_2 + i\omega c_1 + i\omega c_2)(-m_2\omega^2 + k_3 + 2k'_2 + i\omega c_2)}{(-2k'_2 - i\omega c_2)}X_2$$

$$+(-2k'_2 - i\omega c_2)X_2 \quad (40)$$

Substituting equation 38 into equation 39 gives:

$$F_0 = (k_1 + i\omega c_1)\frac{(-m_2\omega^2 + k_3 + 2k'_2 + i\omega c_2)}{(-2k'_2 - i\omega c_2)}X_2 + (k_3)X_2 \quad (41)$$

Solving for T_f using equations 40 and 41 and cancelling the common X_2, the force transmissibility equation can be shown as:

$$T_f = \frac{F_0}{F_1} =$$

$$\frac{(iwc_1 + k_1)(iwc_2 - m_2w^2 + k_3 + 2k_2) + k_3(iwc_2 + 2k_2)}{(iwc_2 - m_2w^2 + k_3 + 2k_2)(iwc_1 + iwc_2 - m_1w^2 + k_1 + 2k_2) + wc_2(wc_2 - 2ik_2) - k_2(2iwc_2 + 4k_2)} \quad (42)$$

where for the purposes of this formula k'_2 is being represented as k_2.

Due to the non-linear stiffness parameter as well as the complex nature of the equation, it is being left in this format for now. The equation is further discussed in Chapter 8 – Transmissibility Discussion.

6.4.2 Displacement Transmissibility of Configuration 2B

Determining the displacement transmissibility of the system, where the forces F_1 and F_0 are not considered, however, we do consider the displacements of the payload, NES mass and the base represented by x_1, x_2 and x_0 respectively. From this model the equations of motion can be determined as:

$$m_1\ddot{x_1} + c_1(\dot{x_1} - \dot{x_0}) + c_2(\dot{x_1} - \dot{x_2}) + k_1(x_1 - x_0) + 2k'_2(x_1 - x_2) = 0 \quad (43)$$

$$m_2\ddot{x_2} + c_2(\dot{x_2} - \dot{x_1}) + 2k'_2(x_2 - x_1) + k_3(x_2 - x_1) = 0 \quad (44)$$

Performing Fourier Transformation on equation 43 gives:

$$(-m_1\omega^2 + k_1 + 2k'_2 + i\omega c_1 + i\omega c_2)X_1 - (k_1 - i\omega c_1)X_0 - (2k'_2 + i\omega c_2)X_2 = 0$$

Making X_2 the subject of the formula gives:

$$X_2 = \frac{(-m_1\omega^2 + k_1 + 2k'_2 + i\omega c_1 + i\omega c_2)}{(2k'_2 + i\omega c_2)}X_1 - \frac{(k_1 - i\omega c_1)}{(2k'_2 + i\omega c_2)}X_0 \quad (45)$$

Performing Fourier Transformation on equation 44 gives:

$$(-m_2\omega^2 + k_3 + 2k'_2 + i\omega c_2)X_2 - (k_3)X_0 - (2k'_2 + i\omega c_2)X_1 = 0 \quad (46)$$

Substituting equation 45 into equation 46 gives:

$$\frac{(-m_2\omega^2 + k_3 + 2k'_2 + i\omega c_3 + i\omega c_2)(-m_1\omega^2 + k_1 + 2k'_2 + i\omega c_1 + i\omega c_2)}{(2k'_2 + i\omega c_2)} X_1$$

$$-\frac{(-m_2\omega^2 + k_3 + 2k'_2 + i\omega c_2)(k_1 - i\omega c_1)}{(2k'_2 + i\omega c_2)} X_0 - (k_3)X_0 - (2k'_2 + i\omega c_2)X_1 = 0$$

Solving for T_d, the force transmissibility equation can be shown as:

$$T_d = \frac{X_1}{X_0} =$$

$$\frac{(iwc_1 + k_1)(iwc_2 - m_2w^2 + k_3 + 2k_2) + k_3(iwc_2 + 2k_2)}{(iwc_2 - m_2w^2 + k_3 + 2k_2)(iwc_1 + iwc_2 - m_1w^2 + k_1 + 2k_2) + wc_2(wc_2 - 2ik_2) - k_2(2iwc_2 + 4k_2)} \quad (47)$$

where for the purposes of this formula k'_2 is being represented as k_2.

Due to the non-linear stiffness parameter as well as the complex nature of the equation, it is being left in this format for now. The equation is further discussed in Chapter 8 – Transmissibility Discussion.

6.5 Conclusion

The force transmissibility and displacement transmissibility equations for Configuration 2A are shown in Equation 28 and Equation 33 respectively, and for Configuration 2B are shown in Equation 42 and Equation 47 respectively.

Comparing the equations, it can be seen that the transmissibility equations for Configuration 2A are identical and that of Configuration 2B are also identical, meaning that these are linear systems. Further discussion and analysis can be found in Section 8.2.

7 LINEAR ISOLATOR INTEGRATED A SKYHOOK DAMPER AND A NES SYSTEM

7.1 Introduction

In this chapter a traditional linear isolator integrated a skyhook damper and a NES system will be considered and analysed. The objective is to decide on the setup to be analysed and determine the force transmissibility and displacement transmissibility equations which is further discussed in Section 8.3.

7.2 The setup

For this analysis, we will be considering a traditional linear isolator together with a skyhook damper and an NES system as shown in Figure 7-1. The traditional linear isolator is composed of a payload mass m_1 supported by a spring with stiffness k_1 and damping c_1.

The skyhook damper is composed of a mass m_2, which is connected to the payload mass m1 by damper c_2 and connected to the base by spring with stiffness k_2.

The NES system is formed of a central mass (m_3), two springs (each with stiffness k_3) orientated at 90-degrees from the direction of motion being considered and connected to the skyhook mass m_2 , as well as a damper connecting the NES mass m_3 to the skyhook mass m_2.

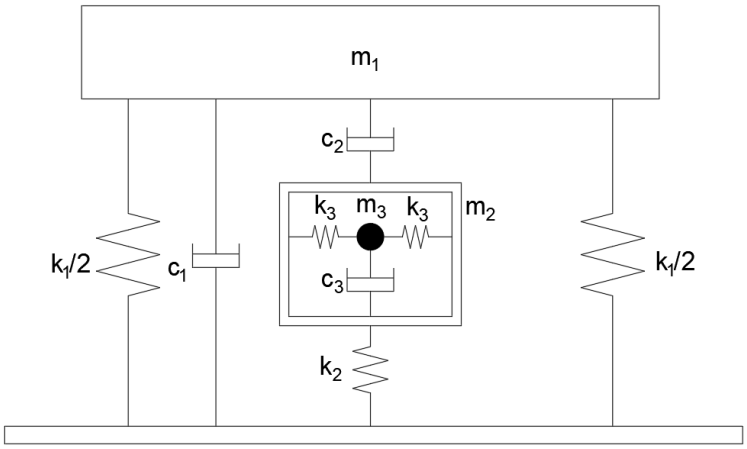


Figure 7-1: Setup of a linear isolator integrated a skyhook damper and NES system - Configuration 3

As before, Figure 7-2 shows that the force applied by the payload (m_1) and the force experienced as a result by the base is represented by F_1 and F_0 respectively when determining the force transmissibility. The displacement of the payload, skyhook damper mass and NES mass is represented by x_1, x_2 and x_3 respectively, and when determining the displacement transmissibility, the displacement of the base is considered as x_0.

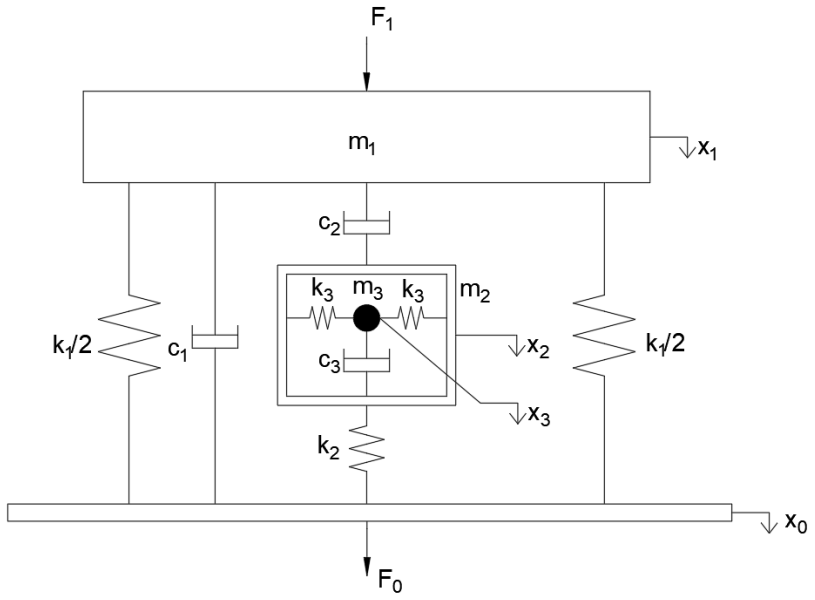


Figure 7-2: Three DOF model of a linear isolator integrated a skyhook damper and NES system - Configuration 3

This model can be adjusted to display the two k_3 non-linear springs as $2k'_3$ representing the effective linear stiffness in the direction of motion being considered. This simplifies the process of working with the models, and is visually shown as an arrow through the spring symbol as shown in Figure 7-3.

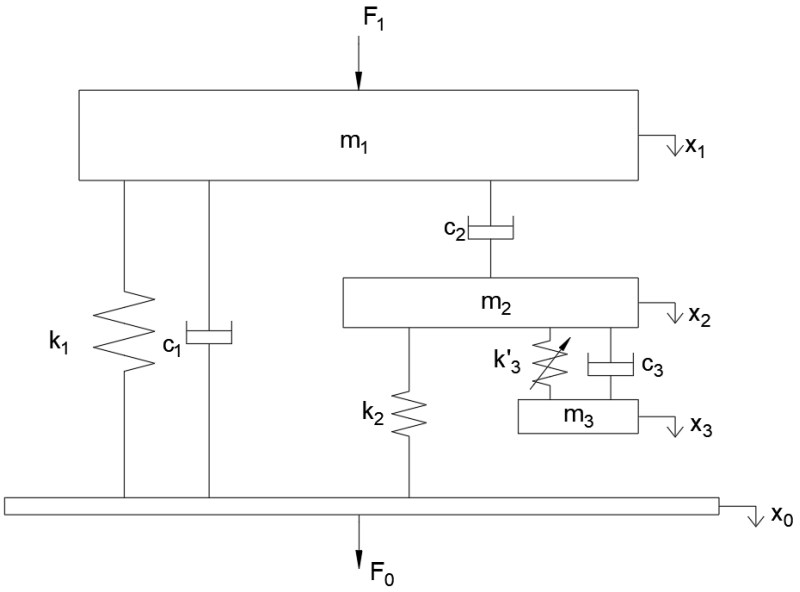


Figure 7-3: Configuration 3 shown with effective linear stiffness component

7.3 Force Transmissibility of Configuration 3

As before, F_1 applied to m_1 will be considered as a harmonic force with a loading frequency of ω. From this model, while considering x_0 = 0 for the force transmissibility response, the equations of motion can be determined as:

$$m_1\ddot{x_1} + c_1\dot{x_1} + c_2(\dot{x_1} - \dot{x_2}) + k_1x_1 = F_1\cos(\omega t) \quad (48)$$

$$m_2\ddot{x_2} + c_2(\dot{x_2} - \dot{x_1}) + c_3(\dot{x_2} - \dot{x_3}) + k_2x_2 + 2k'_3(x_2 - x_3) = 0 \quad (49)$$

$$m_3\ddot{x_3} + c_3(\dot{x_3} - \dot{x_2}) + 2k'_3(x_3 - x_2) = 0 \quad (50)$$

$$F_0 = k_1x_1 + c_1\dot{x_1} + k_2x_2 \quad (51)$$

Performing Fourier Transformation on equation 48 gives:

$$F_1 = (-m_1\omega^2 + k_1 + i\omega c_1 + i\omega c_2)X_1 + (-i\omega c_2)X_2 \quad (52)$$

Performing Fourier Transformation on equation 49 gives:

$$(-m_2\omega^2 + k_2 + 2k'_3 + i\omega c_2 + i\omega c_3)X_2 = (i\omega c_2)X_1 + (2k'_3 + i\omega c_3)X_3 \quad (53)$$

Performing Fourier Transformation on equation 50 gives:

$$(-m_3\omega^2 + 2k'_3 + i\omega c_3)X_3 = (2k'_3 + i\omega c_3)X_2$$

Making X_3 the subject of the formula gives:

$$X_3 = \frac{(2k'_3+i\omega c_3)}{(-m_3\omega^2+2k'_3+i\omega c_3)}X_2 \tag{54}$$

Performing Fourier Transformation on equation 51 gives:

$$F_0 = (k_1 + i\omega c_1)X_1 + (k_2)X_2 \tag{55}$$

Substituting equation 54 into equation 53 gives:

$$(-m_2\omega^2 + k_2 + 2k'_3 + i\omega c_2 + i\omega c_3)X_2 = (i\omega c_2)X_1 + \frac{(2k'_3+i\omega c_3)(2k'_3+i\omega c_3)}{(-m_3\omega^2+2k'_3+i\omega c_3)}X_2$$

Making X_2 the subject of the formula gives:

$$X_2 = \frac{i\omega c_2(-m_3\omega^2+2k'_3+i\omega c_3)}{[-m_2\omega^2+k_2+2k'_3+i\omega c_2+i\omega c_3][-m_3\omega^2+2k'_3+i\omega c_3]-[2k'_3+i\omega c_3]^2}X_1 \tag{56}$$

Substituting equation 56 into equation 52 gives:

$$F_1 = (-m_1\omega^2 + k_1 + i\omega c_1 + i\omega c_2)X_1 + \frac{\omega^2 {c_2}^2(-m_3\omega^2+2k'_3+i\omega c_3)}{[-m_2\omega^2+k_2+2k'_3+i\omega c_2+i\omega c_3][-m_3\omega^2+2k'_3+i\omega c_3]-[2k'_3+i\omega c_3]^2}X_1 \tag{57}$$

Substituting equation 56 into equation 55 gives:

$$F_0 = (k_1 + i\omega c_1)X_1 + \frac{i\omega c_2 k_2(-m_3\omega^2+2k'_3+i\omega c_3)}{[-m_2\omega^2+k_2+2k'_3+i\omega c_2+i\omega c_3][-m_3\omega^2+2k'_3+i\omega c_3]-[2k'_3+i\omega c_3]^2}X_1 \tag{58}$$

Solving for T_f using equations 57 and 58 and cancelling the common X_1, the force transmissibility equation can be shown as:

$$T_f = \frac{F_0}{F_1} =$$

$$\frac{iwc_1 + k_1 + \frac{k_2 iwc_2(iwc_3 + 2k_3 - m_3w^2)}{(iw(c_2+c_3) + k_2 + 2k_3 - m_2w^2)(iwc_3 + 2k_3 - m_3w^2) - (iwc_3 + 2k_3)^2}}{(iw(c_1+c_2) + k_1 - m_1w^2) + \frac{w^2{c_2}^2(iwc_3 + 2k_3 - m_3w^2)}{(iw(c_2+c_3) + k_2 + 2k_3 - m_2w^2)(iwc_3 + 2k_3 - m_3w^2) - (iwc_3 + 2k_3)^2}} \tag{59}$$

where for the purposes of this formula k'_3 is being represented as k_3.

Due to the non-linear stiffness parameter as well as the complex nature of the equation, it is being left in this format for now. The equation is further discussed in Chapter 8 – Transmissibility Discussion.

7.4 Displacement Transmissibility of Configuration 3

Determining the displacement transmissibility of the system, where the forces F_1 and F_0 are not considered, however, we do consider the displacements of the payload, skyhook damper mass, NES mass and the base represented by x_1, x_2, x_3 and x_0 respectively. From this model the equations of motion can be determined as:

$$m_1\ddot{x_1} + c_1(\dot{x_1} - \dot{x_0}) + c_2(\dot{x_1} - \dot{x_2}) + k_1(x_1 - x_0) = 0 \quad (60)$$

$$m_2\ddot{x_2} + c_2(\dot{x_2} - \dot{x_1}) + c_3(\dot{x_2} - \dot{x_3}) + k_2(x_2 - x_0) + 2k'_3(x_2 - x_3) = 0 \quad (61)$$

$$m_3\ddot{x_3} + c_3(\dot{x_3} - \dot{x_2}) + 2k'_3(x_3 - x_2) = 0 \quad (62)$$

Performing Fourier Transformation on equation 60 gives:

$$(-k_1 - i\omega c_1)X_0 = (m_1\omega^2 - k_1 - i\omega c_1 - i\omega c_2)X_1 + (i\omega c_2)X_2 \quad (63)$$

Performing Fourier Transformation on equation 61 gives:

$$(-i\omega c_2)X_1 = (k_2)X_0 + (m_2\omega^2 - k_2 - 2k'_3 - i\omega c_2 - i\omega c_3)X_2 + (2k'_3 + i\omega c_3)X_3 \quad (64)$$

Performing Fourier Transformation on equation 62 gives:

$$(-m_3\omega^2 + 2k'_3 + i\omega c_3)X_3 = (2k'_3 + i\omega c_3)X_2$$

Making X_3 the subject of the formula gives:

$$X_3 = \frac{(2k'_3 + i\omega c_3)}{(-m_3\omega^2 + 2k'_3 + i\omega c_3)}X_2 \quad (65)$$

Substituting equation 65 into equation 64 gives:

$$(-i\omega c_2)X_1 = (k_2)X_0 + (m_2\omega^2 - k_2 - 2k'_3 - i\omega c_2 - i\omega c_3)X_2$$

$$+\frac{(2k'_3 + i\omega c_3)^2}{(-m_3\omega^2 + 2k'_3 + i\omega c_3)}X_2$$

Making:

$$A = (m_2\omega^2 - k_2 - 2k'_3 - i\omega c_2 - i\omega c_3)$$

$$B = \frac{(2k'_3 + i\omega c_3)^2}{(-m_3\omega^2 + 2k'_3 + i\omega c_3)}$$

$$C = (m_1\omega^2 - k_1 - i\omega c_1 - i\omega c_2)$$

And making X_2 the subject of the formula, gives:

$$X_2 = \frac{-i\omega c_2}{A+B}X_1 - \frac{k_2}{A+B}X_0 \tag{66}$$

Substituting equation 66 into equation 60 gives:

$$(-k_1 - i\omega c_1)X_0 = CX_1 + \frac{\omega^2 {c_2}^2}{A+B}X_1 - \frac{i\omega c_2 k_2}{A+B}X_0$$

Solving for T_d, the force transmissibility equation can be shown as:

$$T_d = \frac{X_1}{X_0} =$$

$$\frac{-iwc_1 - k_1 + \dfrac{iwc_2k_2}{m_2w^2 - iwc_2 - iwc_3 - k_2 - 2k_3 + \dfrac{(iwc_3 + 2k_3)^2}{-m_3w^2 + iwc_3 + 2k_3}}}{m_1w^2 - iwc_1 - iwc_2 - k_1 - \dfrac{(iwc_2)^2}{m_2w^2 - iwc_2 - iwc_3 - k_2 - 2k_3 + \dfrac{(iwc_3 + 2k_3)^2}{-m_3w^2 + iwc_3 + 2k_3}}} \tag{67}$$

where for the purposes of this formula k'_3 is being represented as k_3.

Due to the non-linear stiffness parameter as well as the complex nature of the equation, it is being left in this format for now. The equation is further discussed in Chapter 8 – Transmissibility Discussion.

7.5 Conclusion

The force transmissibility and displacement transmissibility equations are shown in Equation 59 and Equation 67 respectively.

Comparing the equations, it can be seen that the transmissibility equations are not identical, meaning that the system is a non-linear problem. Further discussion and analysis can be found in Section 8.3.

8 TRANSMISSIBILITY DISCUSSION

8.1 Traditional Linear Isolator

Comparing the force and displacement transmissibility equations (equations 8 and 12 respectively), it can be seen that they are identical. This means that the system in question is a linear one.

The transmissibility equations for a range of damping ratios are plotted on Figure 8-1, the consistency in patterns demonstrates the strong relationship between damping ratio and transmissibility for this system.

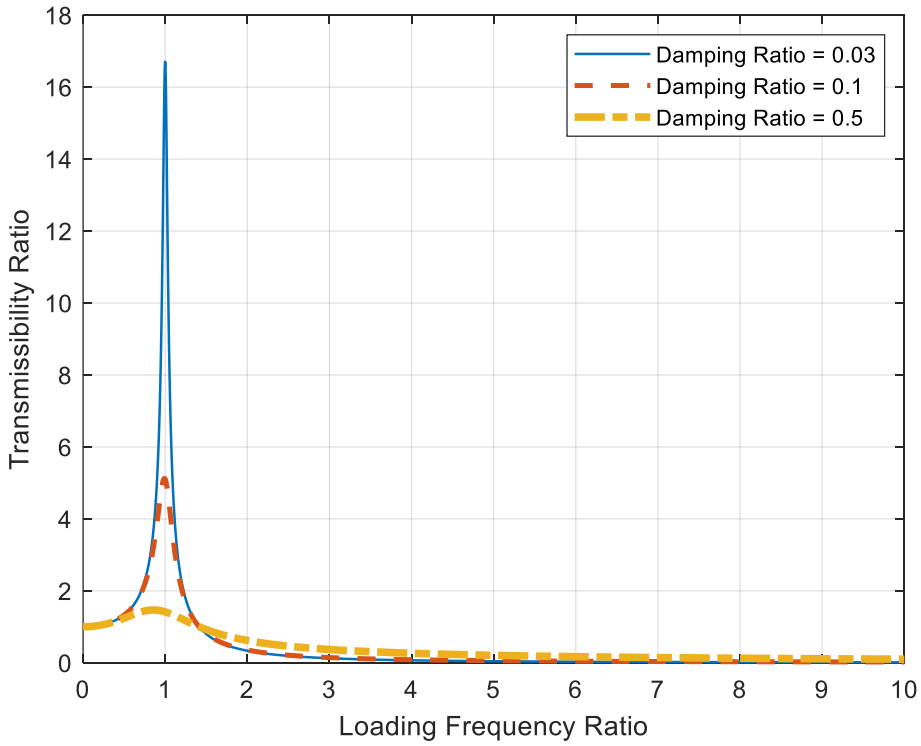


Figure 8-1: Traditional linear isolator transmissibility plotted against frequency ratio for various damping ratios

Figure 8-1 shows the peak transmissibility ratio is at a loading frequency ratio of 1, which makes sense as this is the point where the loading frequency is equal to the first natural frequency of the system.

As expected, Figure 8-1 shows that the systems with higher damping ratios have a lower peak transmissibility at a loading frequency ratio of 1, all three graphs

converge at a loading frequency of $\sqrt{2}$ (or 1.41), and after this point systems with a higher damping have a slightly higher transmissibility ratio than those with lower damping.

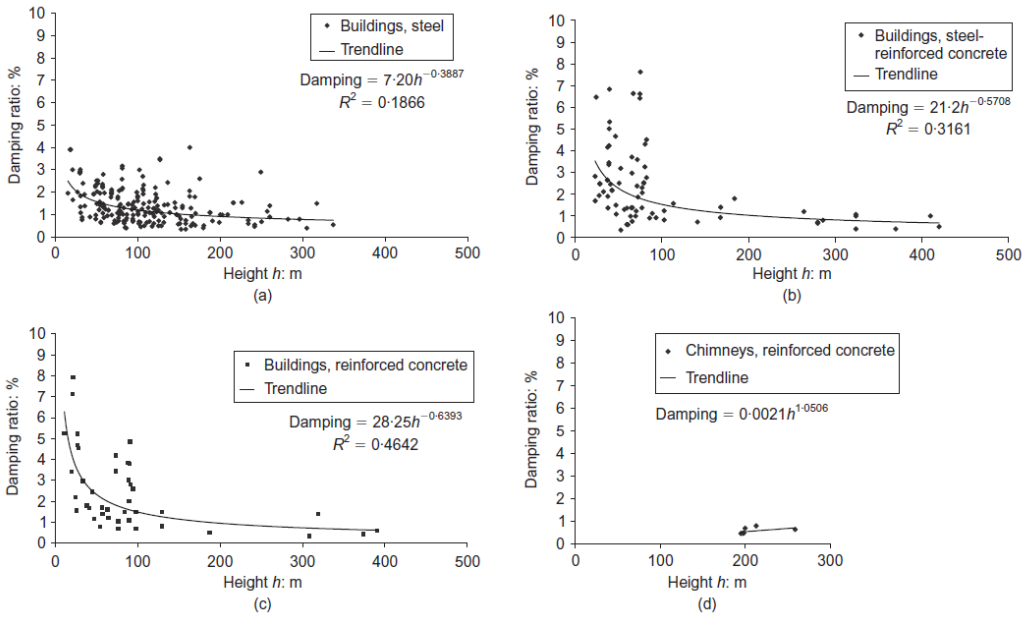


Figure 8-2: Damping ratio values for various heights of (a) steel buildings, (b) steel reinforced concrete buildings, (c) reinforced concrete buildings and (d) reinforced concrete chimneys (Smith, Merello and Willford, 2010)

In practice it is common to use a damping ratio of 0.03, from Figure 8-2 it is clear that for a structure less than 25m tall that it is realistic and achievable. Considering this, it is evident that the traditional linear isolator is able to successfully isolate vibrations at higher loading frequency ratios, however, at a loading frequency ratio of 1, the transmissibility ratio is equal to approximately 16.7 (Figure 8-1).

Practically speaking, for the case of the force transmissibility, this means that if the loading frequency is equal to the first natural frequency of the system, the force experienced by the base would be 16.7 times higher than the force acting on the payload. Similarly for the displacement transmissibility, this means that the displacement of the payload would be 16.7 times larger than that experienced by the base, in the event of an earthquake for example. This demonstrates the importance of vibration control in a structure.

8.2 Linear isolator integrated NES

Comparing the transmissibility equations, it is found that the force and displacement transmissibility equations are identical for both Configuration 2A (equations 28 and 33 respectively) and 2B (equations 42 and 47 respectively). As per the definition of identical force and displacement transmissibility equations, this means that both configurations are linear in nature.

However, the non-linear stiffness component of the setup is represented as an effective stiffness variable which is a function of the relative displacement between the payload and the NES mass. This means that in order to accurately plot out the relationship between the transmissibility ratio and the loading frequency ratio, one would need an accurate representation of the displacement of these masses for a reasonable period of time such that stability is achieved before each loading frequency ratio can be plotted. This is very difficult to achieve when only working with the transmissibility ratios and first principles, it would take extended periods of time to complete and would not be conducive to repetition in the case that parameters need to be adjusted for optimisation purposes.

In order to find the relative displacement of the NES mass at all times such that the effective linear stiffness can be known at all times and the system response can be correctly represented, a MATLAB code has been developed which simulates the system's response calculated using the 4^{th} order Runge-Kutta numerical analysis method.

The system is 'modelled' by assuming reasonable parameters for all relevant masses, stiffnesses and damping components as well as the applied loads. The result is a set of data describing the displacements, velocities and accelerations of all masses throughout the period of time specified, which can then be plotted on a graph.

Once the system's measurable outputs reach stability, the maximum amplitude of displacement and velocity readings are saved, and the transmissibility manually calculated as per the relationship of input vs output amplitudes. This calculation is then looped for various loading frequencies in constant small steps, and when all

results are compiled, a graph is plotted of transmissibility ratio versus loading frequency ratios.

Due to the non-linear unpredictable nature of the system, variables must be manually adjusted in order to perform a parametric study.

In order to display the transmissibility ratio graph and have something to compare against, an example setup is used with the following assumed fixed parameters (these parameters are chosen as they form part of the basic system (i.e. machine or structure) to which the NES is integrated):

Payload mass $m_1 = 3000\ kg$

Stiffness $k_1 = 400\ kN/m$

The damping ratio (ξ) is set at 0.03. While the typical damping formula is generally only applicable to single degree of freedom systems, it is used for this analysis as an approximation and can be determined as:

Damping $c_1 = 2\xi\sqrt{k_1 m_1} = 2.08\ kN.s/m$

Damping $c_2 = 2\xi\sqrt{k_2 m_2}$

Variables which are open for optimisation are: k_2, k_3, m_2, c_3, L_0 and x_i, where c_3 and k_3 are only applicable to Configurations 2A and 2B respectively.

8.2.1 Configuration 2A

Performing a parametric study of the variables open for optimisation, Figure 8-3 to Figure 8-7 shows the relationships between parameter value and peak force transmissibility when the loading frequency is set to the first natural frequency. The graphs focus on the point at which the peak force transmissibility is at it's lowest.

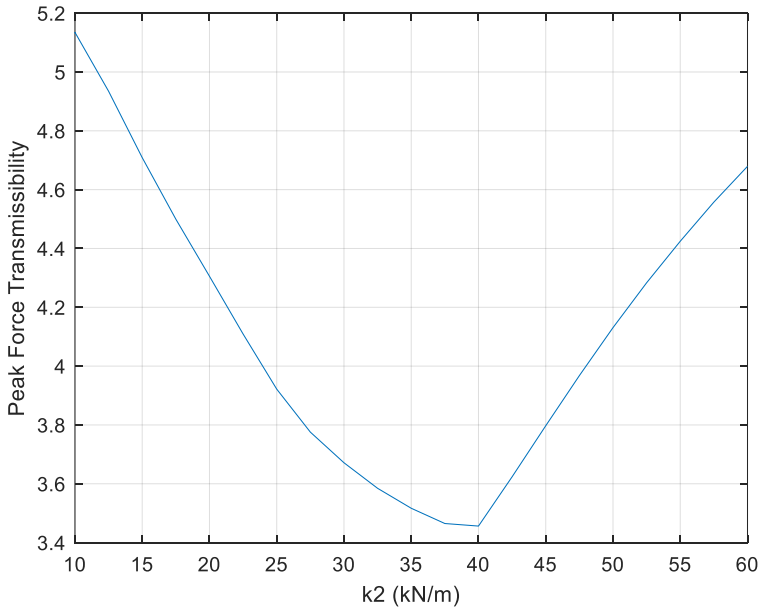


Figure 8-3: Peak force transmissibility for varying values of k_2 in Configuration 2A

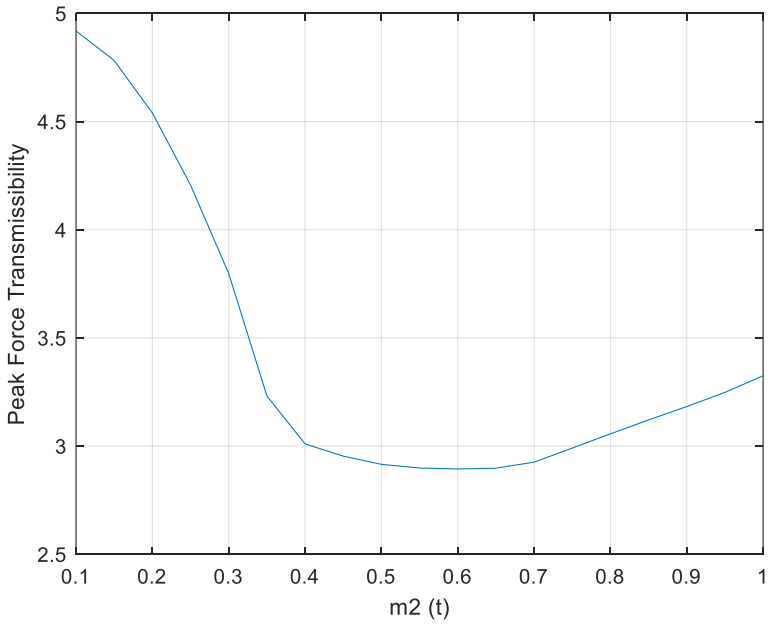


Figure 8-4: Peak force transmissibility for varying values of m_2 in Configuration 2A

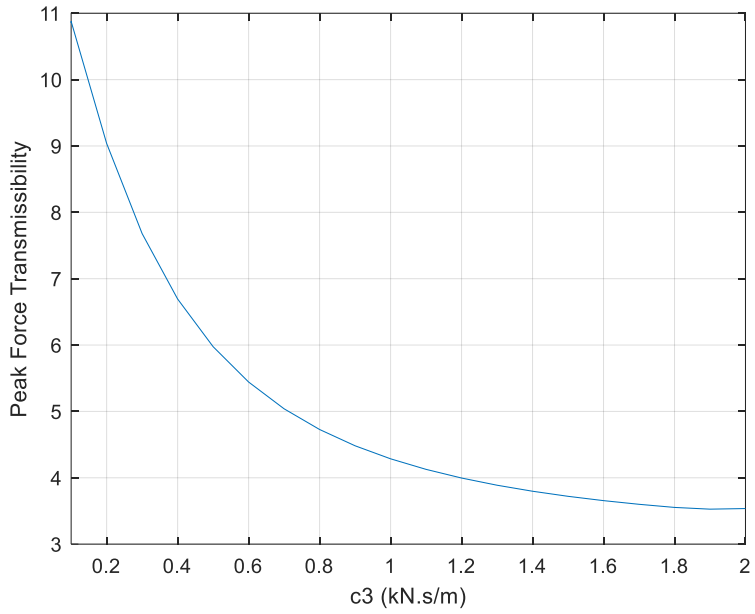


Figure 8-5: Peak force transmissibility for varying values of c_3 in Configuration 2A

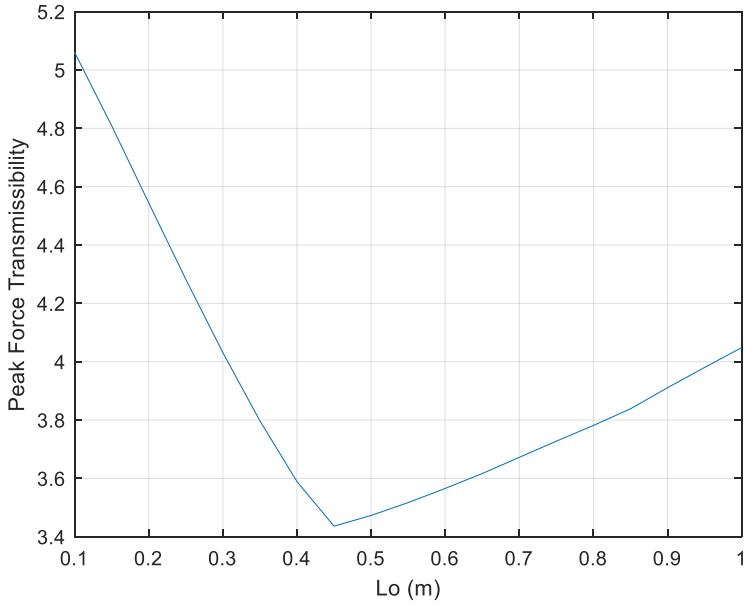


Figure 8-6: Peak force transmissibility for varying values of L_0 in Configuration 2A

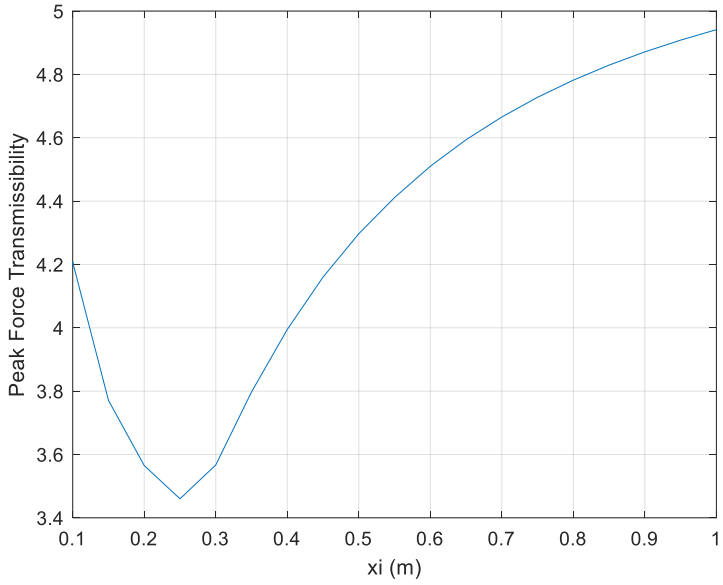


Figure 8-7: Peak force transmissibility for varying values of x_i in Configuration 2A

The graphs shown in Figure 8-3 to Figure 8-7 focus on the point at which the peak force transmissibility is at it's lowest and provides an indication as to which variable values could result in the most optimum solution. Given this, the parameters are manually adjusted on a repetitive basis until the optimised solution of Configuration 2A is determined as:

NES mass $m_2 = 300\ kg$

Stiffness $k_2 = 45\ kN/m$

Damping $c_3 = 1.4\ kN.s/m$

Original NES spring length $L_0 = 0.35\ m$

Stretched NES spring length $x_i = 0.35\ m$

Investigating the sensitivity of force transmissibility to parameter adjustments, Table 8-1 outlines the percentage change in force transmissibility for a -20%, -10%, +10% and +20% adjustment in the variables to be optimised.

Table 8-1: Evaluation of force transmissibility sensitivity to change in parameters

	Change in Force Transmissibility			
Parameter	-20% adjustment	-10% adjustment	+10% adjustment	+20% adjustment
k_2	31.4%	5.5%	8.3%	17.8%
m_2	25.5%	10.6%	-3.7%	1.3%
c_3	7.9%	3.4%	0.5%	3.2%
L_0	11.8%	5.5%	-2.9%	0.8%
x_i	2.9%	-3.2%	5.0%	9.5%

The force transmissibility is most sensitive to small changes of parameters k_2 and m_2, whereby in some instances the percentage change in transmissibility is larger than that of the parameter change.

Increasing m_2 by 10% produces a lower transmissibility, however, the peak moves up to a loading frequency ratio of 1.3 which is undesirable. From the graph in Figure 8-8 it is evident that a smaller mass m_2 of 0.2t produces a higher peak transmissibility of 5.77, however, the transmissibility drops down quicker after a loading frequency ratio of 1. While a slightly higher m_2 of 0.33t may produce a lower transmissibility peak, increasing the mass further to 0.4t increases the transmissibility peak overall while also moving the peak to an even higher loading frequency ratio, as shown in the graph in Figure 8-8.

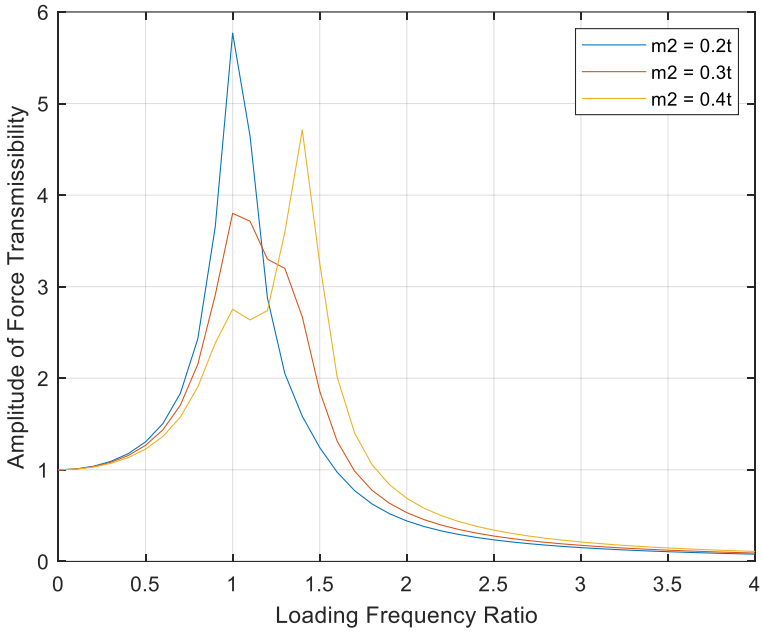


Figure 8-8: Configuration 2A transmissibility graphs for various m_2 values

When considering c_3 in Figure 8-9, a lower damping of 0.6kNs/m produces a higher peak transmissibility at a loading frequency ratio of 1 with a second lower peak at a loading frequency ratio of 1.4. One can observe that as the damping is increased, the second peak moves closer to the peak at a loading frequency ratio of 1 until it takes over as the higher peak. Interestingly, all variants of damping converge to the same point at a transmissibility of 1.0.

Similarly for original spring length L_0 in Figure 8-10, lower lengths produce a higher transmissibility peak at a loading frequency ratio of 1 with a second lower peak following, which gets closer and higher with an increased length.

For the spring stretch length x_i in Figure 8-11, an opposite trend is noticed whereby higher lengths produce a higher transmissibility peak at a loading frequency ratio of 1 with a second lower peak following at a higher loading frequency ratio, and as the length is decreased the second peak gets closer to the first peak and increases in amplitude until it takes over from the first peak.

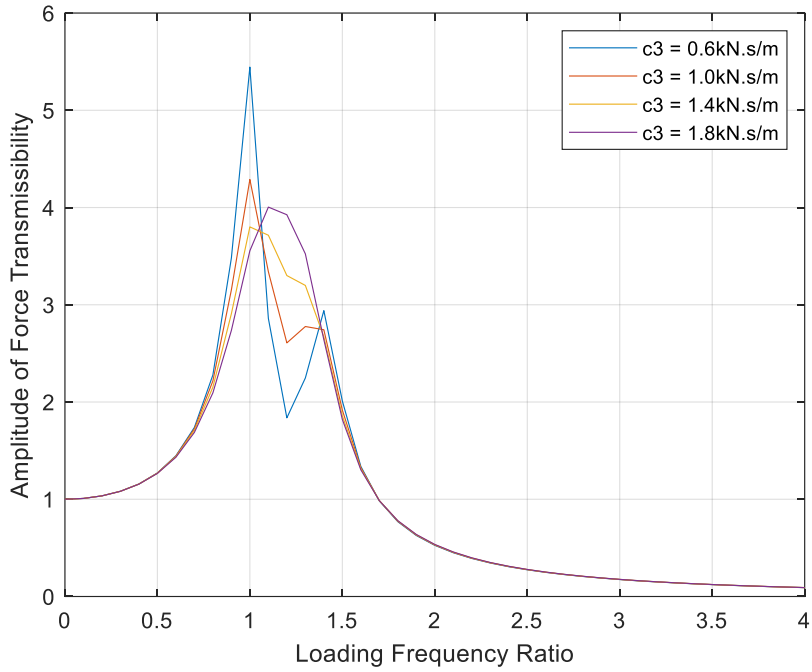


Figure 8-9: Configuration 2A transmissibility graphs for various c_3 values

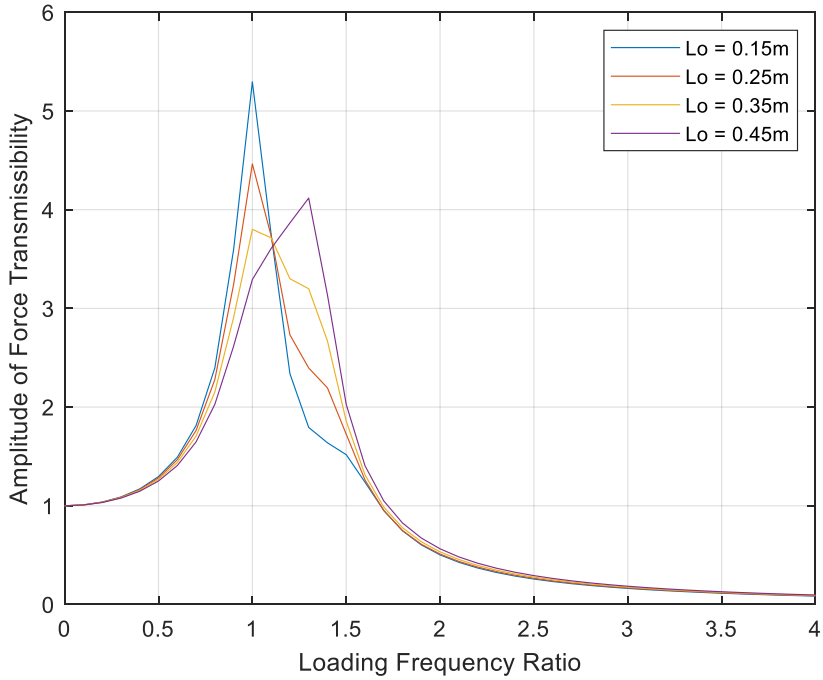


Figure 8-10: Configuration 2A transmissibility graphs for various L_0 values

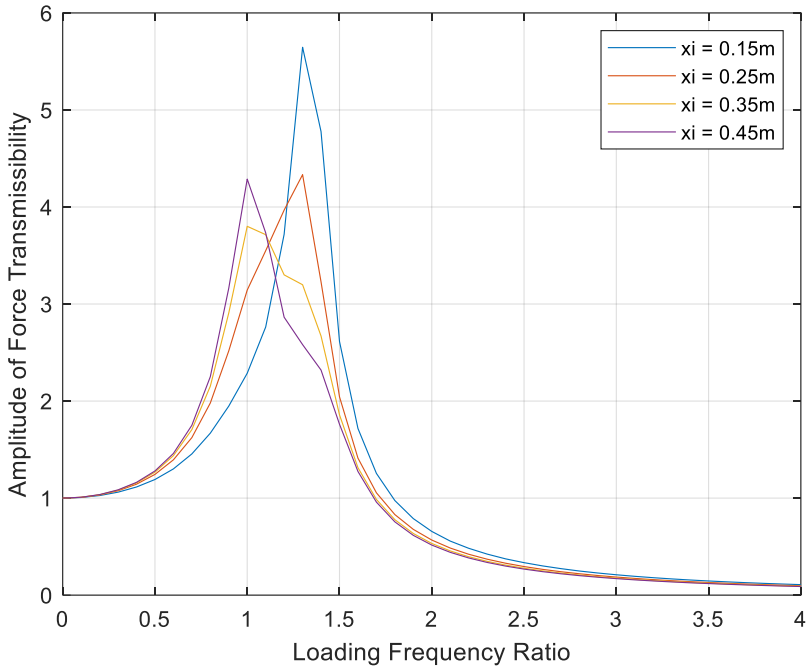


Figure 8-11: Configuration 2A transmissibility graphs for various x_i values

The peak force transmissibility ratio of the optimised solution plotted in Figure 8-12 is found to be 3.80 at a loading frequency ratio of one.

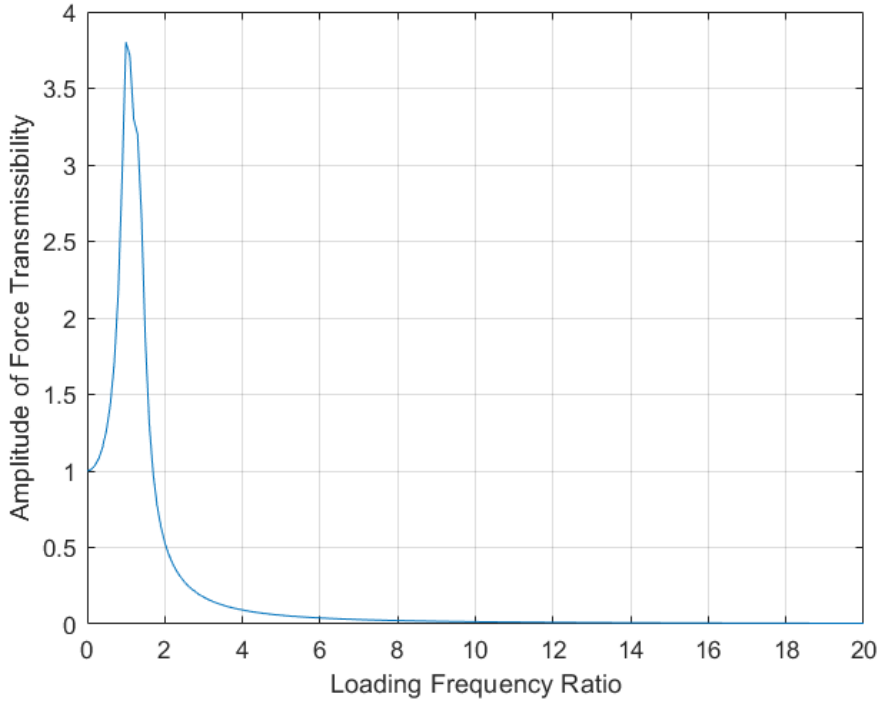


Figure 8-12: Optimised transmissibility graph of Configuration 2A

While this peak transmissibility is a very promising result, the transmissibility only drops to below 1 at a loading frequency ratio of 1.68, which is larger than that of the traditional linear isolator working alone.

8.2.2 Configuration 2B

It is found that Configuration 2B is not as effective at providing low transmissibility ratios as Configuration 2A. The set of variables achieving the best results are:

NES mass $m_2 = 100\ kg$

Stiffness $k_2 = 45\ kN/m$

Stiffness $k_3 = 100\ kN/m$

Original NES spring length $L_0 = 0.55\ m$

Stretched NES spring length $x_i = 0.10\ m$

The peak force transmissibility ratio of the optimised solution is found to be 15.52 at a loading frequency ratio of one, as shown in Figure 8-13. This is not a large improvement over the linear isolator acting alone.

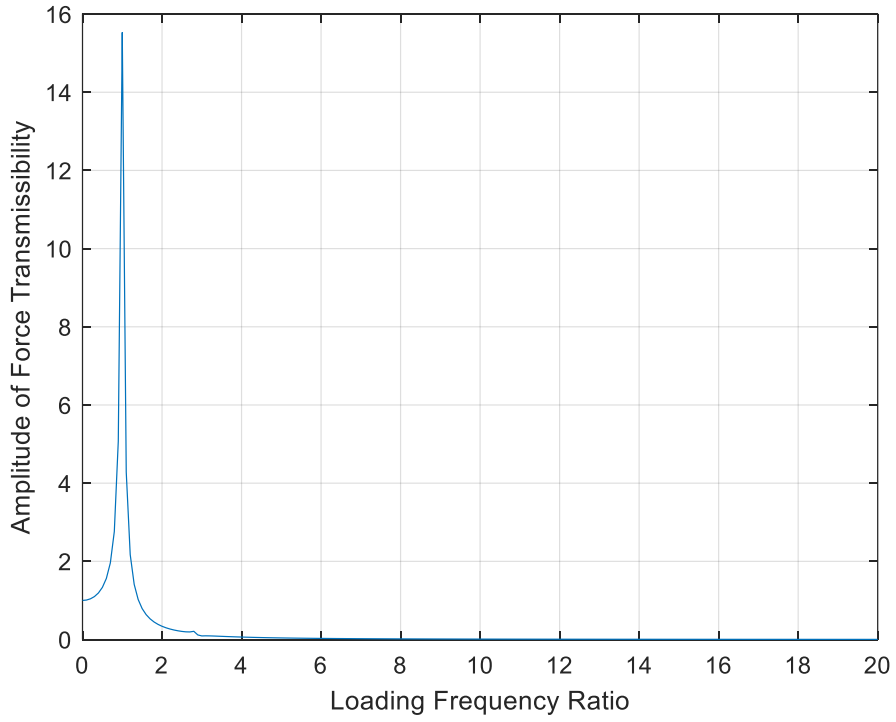


Figure 8-13: Optimised transmissibility graph of Configuration 2B

8.3 Linear isolator integrated skyhook damper and NES

Comparing the transmissibility equations, it can be seen that the force and displacement transmissibility equations differ from each other, meaning that this is a non-linear system.

As discussed for Configurations 2A and 2B, the transmissibility equations for Configuration 3 are a function of the effective linear stiffness variable k'_3 which is a function of the relative displacement between the NES mass m_3 and the skyhook damper mass m_2.

A similar approach is taken to determine the transmissibility relationship with the loading frequency ratio, however this time, the example parameters will be aligned with an example from a paper by Dr Kuinian Li (Li, 2020), where a system of a traditional linear isolator integrated with a skyhook damper showed positive transmissibility results with a peak transmissibility of only 4.585 at a loading frequency ratio of 0.885, as shown in Figure 8-14.

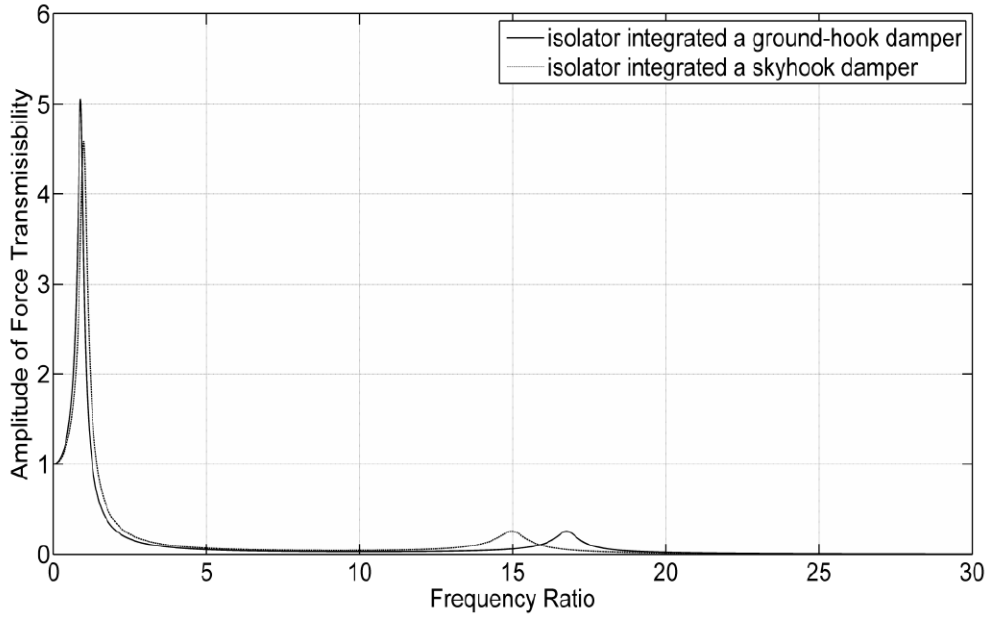


Figure 8-14: Force transmissibility graph of a linear isolated integrated a skyhook damper (Li, 2020)

For following input parameters were used for this example:

Mass ratio $\mu = \frac{m_2}{m_1} = 0.25$

Damping ratio $\xi = \frac{c_2}{2\sqrt{k_2 m_2}} = 0.03$

Damping ratio $\alpha = \frac{c_1}{c_2} = 0$, meaning $c_1 = 0$

Frequency ratio $v = \frac{\omega_2}{\omega_1} = 15$

Where $\omega_1 = \sqrt{\frac{k_1}{m_1}}$ and $\omega_2 = \sqrt{\frac{k_2}{m_2}}$

Manipulating the above equations, one can determine parameter values of:

$$v = \frac{\sqrt{\frac{k_2}{m_2}}}{\sqrt{\frac{k_1}{m_1}}}$$

$$k_2 = \frac{v^2 k_1 m_2}{m_1} = v^2 k_1 \, \mu = 56.25 \, k_1$$

Keeping the fixed parameters of the previous example of:

Payload mass $m_1 = 3000 \; kg$

Stiffness $k_1 = 400 \; kN/m$

The following parameters can therefore be matched to the reference example:

$k_2 = 22500 \; k$

$m_2 = 750 \; kg$

$c_1 = 0 \; kN.s/m$

Retaining a damping ratio (ξ) of 0.03 and using the typical dampening formula as an approximation once again, damping can be determined as:

Damping $c_2 = 2\xi\sqrt{k_1 m_1} = 7.79 \; kN.s/m$

Damping $c_3 = 2\xi\sqrt{k_3 m_3}$

Variables which are open for optimisation are: k_3, m_3, L_0 and x_i.

Performing a parametric study of the variables open for optimisation, Figure 8-15 to Figure 8-18 shows the relationships between parameter value and peak force transmissibility when the loading frequency is set to the first natural frequency.

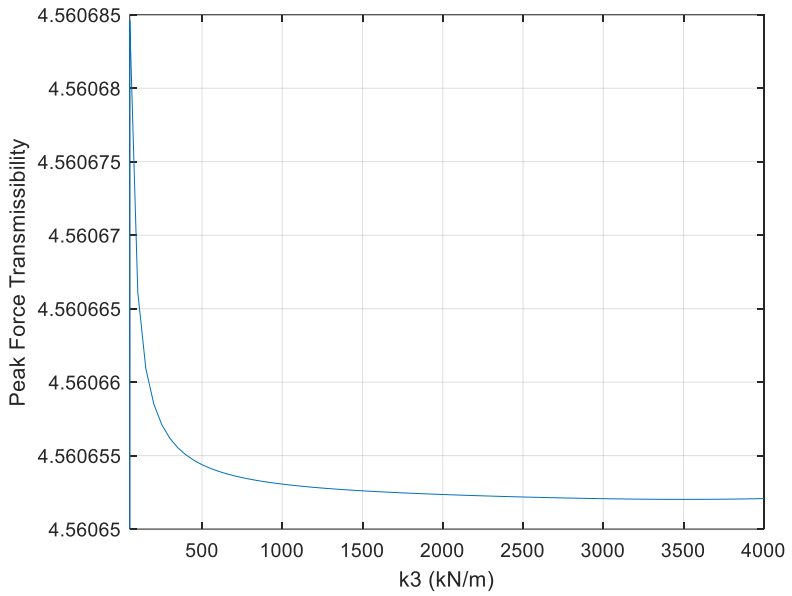


Figure 8-15: Peak force transmissibility for varying values of k_3 in Configuration 3

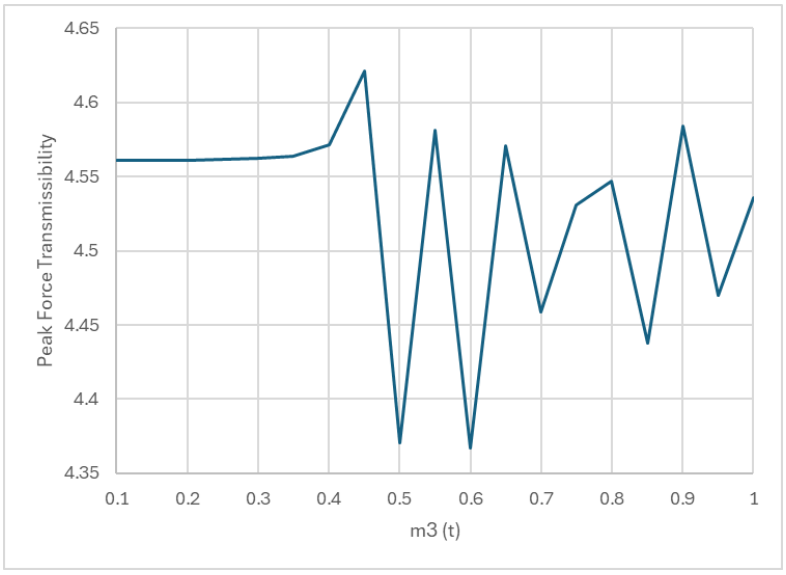


Figure 8-16: Peak force transmissibility for varying values of m_3 in Configuration 3

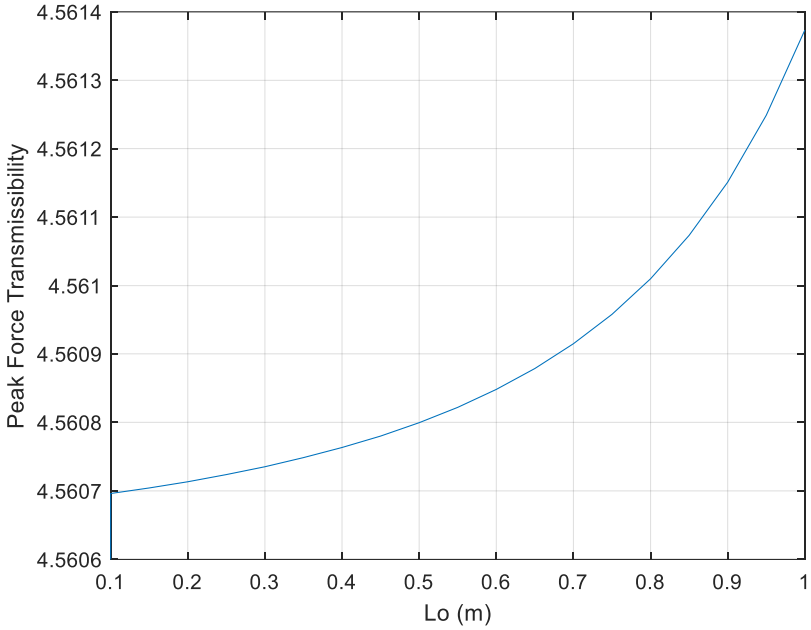


Figure 8-17: Peak force transmissibility for varying values of L_0 in Configuration 3

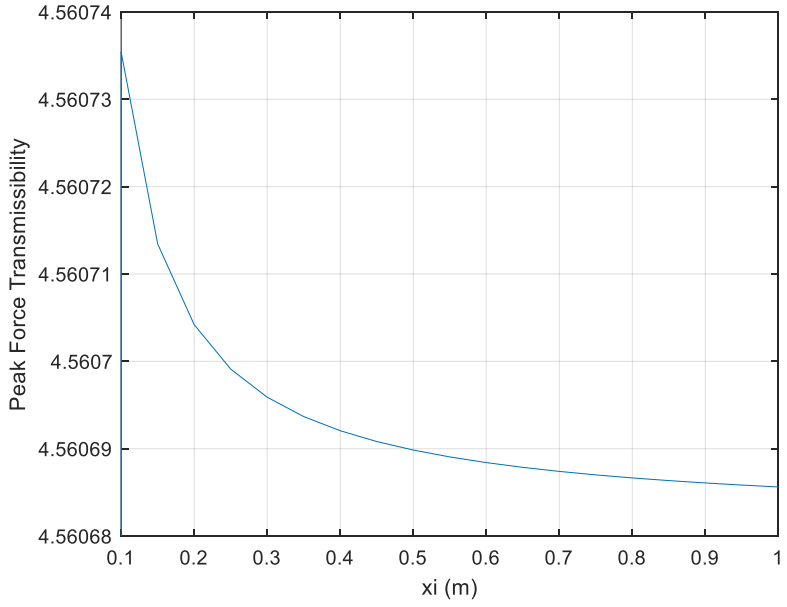


Figure 8-18: Peak force transmissibility for varying values of x_i in Configuration 3

The graphs shown in Figure 8-15 to Figure 8-18 plot out the variance of the peak force transmissibility of the system against a change in k_3, m_3, L_0 and x_i within a reasonable range for each parameter. While at first glance it seems that there is a large variance in transmissibility, however, once the y-axis scale is observed it is

clear that the peak force transmissibility has a low sensitivity to change in these parameter values, with a very low variance of between 4.56 and 4.57 for parameters k_3, L_0 and x_i. The sensitivity is slightly larger for parameter m_3 with a variance of peak force transmissibility between 4.35 and 4.65, however, the variance fluctuates greatly with change in mass with no trend observed.

Given the above, the parameters chosen for Configuration 3 are determined as:

NES mass $m_3 = 100\ kg$

Stiffness $k_3 = 80\ kN/m$

Original NES spring length $L_0 = 0.1\ m$

Stretched NES spring length $x_i = 0.3\ m$

Given the above parameters, the optimised solution has a peak transmissibility ratio of 4.56 (at a loading frequency ratio of 1) is shown on the graph plotted in Figure 8-19. This is only marginally better than the result from the reference paper (Li, 2020). There is a very small second peak at a frequency ratio of approximately 14.5 with a transmissibility amplitude of 0.077, however, this peak has a notably lower amplitude than that compared in the reference paper (Li, 2020).

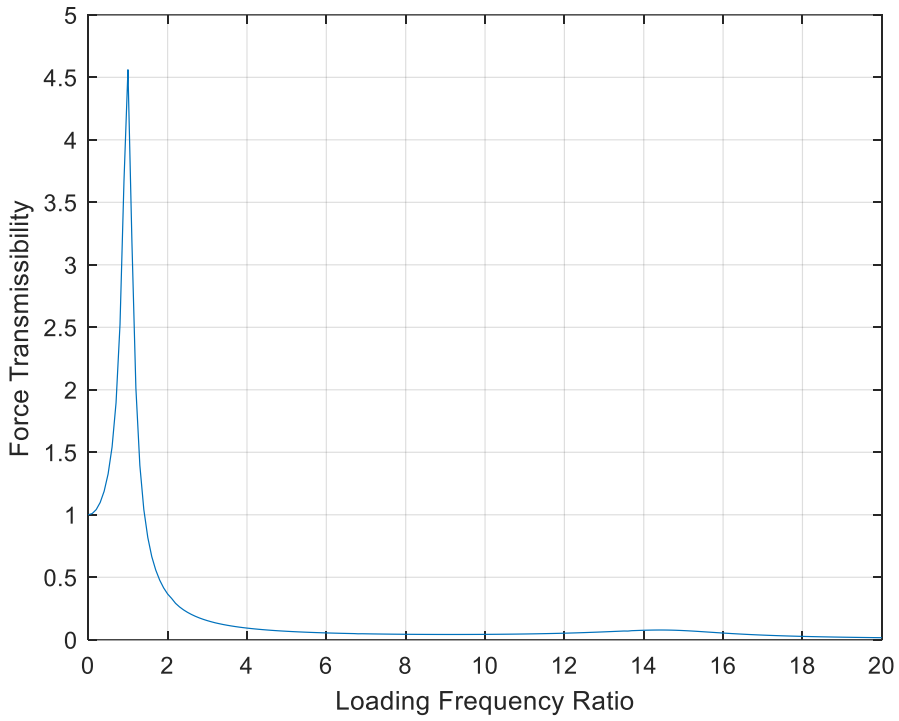


Figure 8-19: Optimised force transmissibility graph of Configuration 3 without c_1

When the same parameters are used but the damping c_1 is provided as:

$$c_1 = 2\xi m_1\sqrt{k_1/m_1} = 2.08\ kN.s/m$$

An immediate drop in transmissibility is observed to 3.65 at a loading frequency of 1 as shown in Figure 8-20, which is lower than the result achieved previously with no c_1. Once again, when investigating the sensitivity of the force transmissibility ratio to a change in parameters, little to no variance is noted.

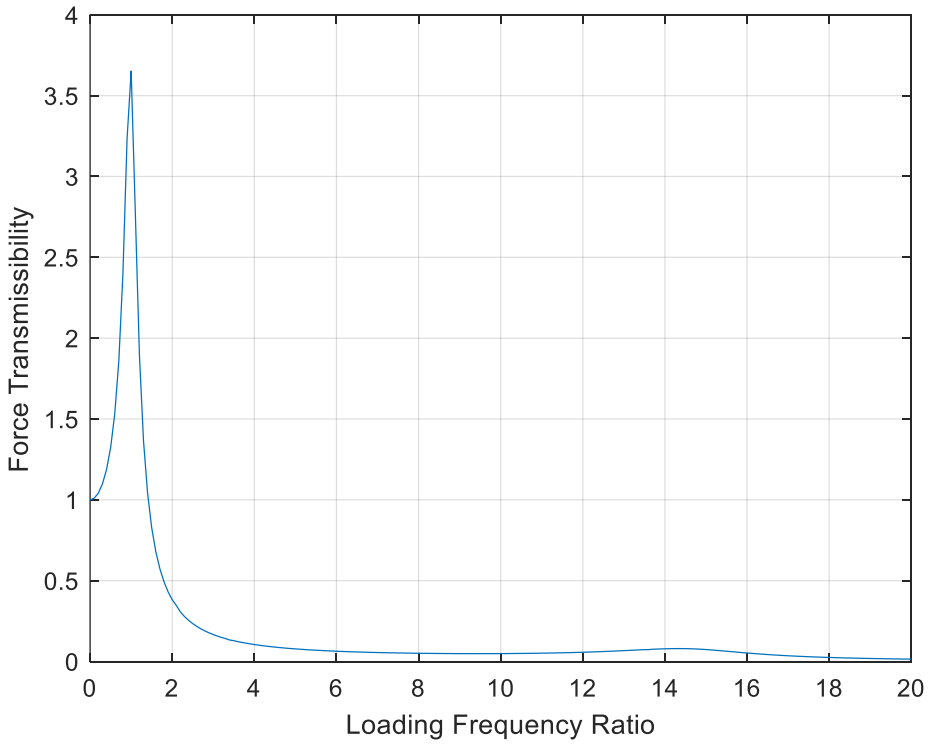


Figure 8-20: Optimised force transmissibility graph of Configuration 3 with c_1

8.4 Comparison of Transmissibility Results

Combining the graphs for the force transmissibility of a linear isolator (Configuration 1), linear isolator integrated a NES with damper to base (Configuration 2A), linear isolator integrated a NES with spring to base (Configuration 2B), as well as a linear isolator integrated a skyhook damper and NES without c_1 (Configuration 3).

From the graph plotted in Figure 8-21, it can be seen that Configuration 1 as a linear isolator has the highest transmissibility of the setups considered with an amplitude of 16.7, following which Configuration 2B as a linear isolator integrated a NES with a spring connected to the base with the amplitude of 15.52, which is still considered very close to the performance of the linear isolator working alone.

Configuration 3 as a linear isolated integrated a skyhook damper and NES has the next lowest peak transmissibility ratio with an amplitude of 4.56, and while this seems positive on face value, it should be noted that the amplitude of a setup of only a linear isolator and skyhook damper with identical parameter values achieved

an amplitude of 4.585 (Li, 2020). It is therefore considered that the addition of the NES system here has little to no benefit at all.

Configuration 2A as a linear isolator integrated a NES with a damper connected to the base achieved a force transmissibility peak amplitude of 3.80, however, while this is the lowest amplitude achieved the transmissibility ration after the peak tends to be marginally higher up until a loading frequency ratio of approximately 4.

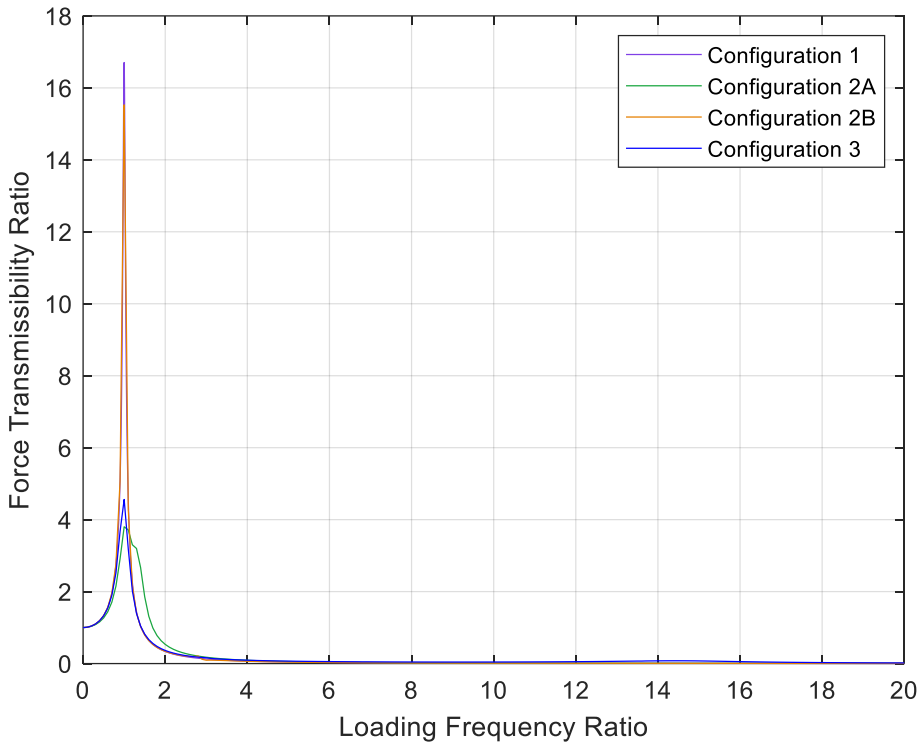


Figure 8-21: Optimised Configuration 1, 2A, 2B and 3 Transmissibility Results

Considering medium to high range loading frequency ratios of 10 and 20, the graphs plotted in Figure 8-22 and Figure 8-23 shows that only Configuration 2B achieves an approximate 5% lower transmissibility ratio compared to that of Configuration 1, the linear isolator. Configuration 2A and Configuration 3 achieve a transmissibility ratio of approximately 20% higher and 425% higher than Configuration 1 respectively.

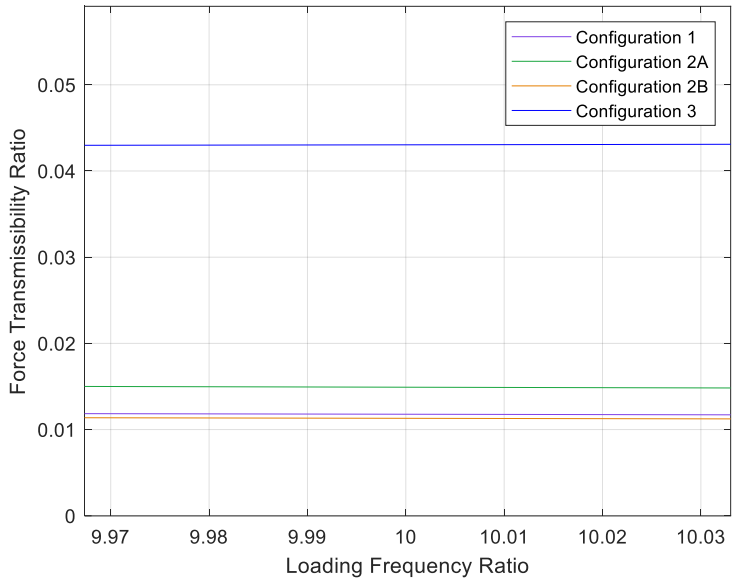


Figure 8-22: Optimised Configuration 1, 2A, 2B and 3 Transmissibility Results at Loading Frequency Ratio=10

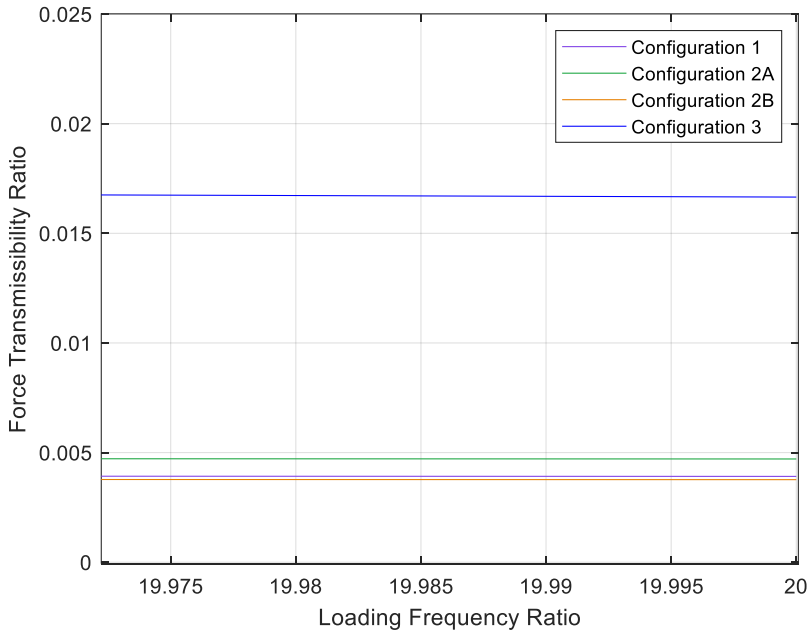


Figure 8-23: Optimised Configuration 1, 2A, 2B and 3 Transmissibility Results at Loading Frequency Ratio=20

9 APPLICATION TO EARTHQUAKES

The setups discussed in the above chapters can be tested for seismic applications by simply rotating the system by 90-degrees such that the direction of motion considered is switched to the horizontal direction.

Systems considered in this chapter include the traditional vibration isolator as a baseline case as well as Configuration 2A with a linear isolator integrated an NES system with a damper connected to the base. Configuration 2B is not considered as it showed ineffective when compared to the linear isolator alone, and Configuration 3 with the linear isolator integrated a skyhook damper and NES system is not considered as it showed little to no benefit in reduced outputs when compared to the optimised linear isolator integrated skyhook damper system from previous studies.

9.1 The applied loads

The horizontal acceleration data ($\ddot{x_g}$) of the El Centro Earthquake of 1940 (strongmotioncenter.org, 2024a) as well as the Northridge Earthquake of 1994 (strongmotioncenter.org, 2024b) are used as examples to investigate the behaviour of different structures and isolation systems. The data of the earthquakes can be seen in the graphs plotted in Figure 9-1 and Figure 9-2.

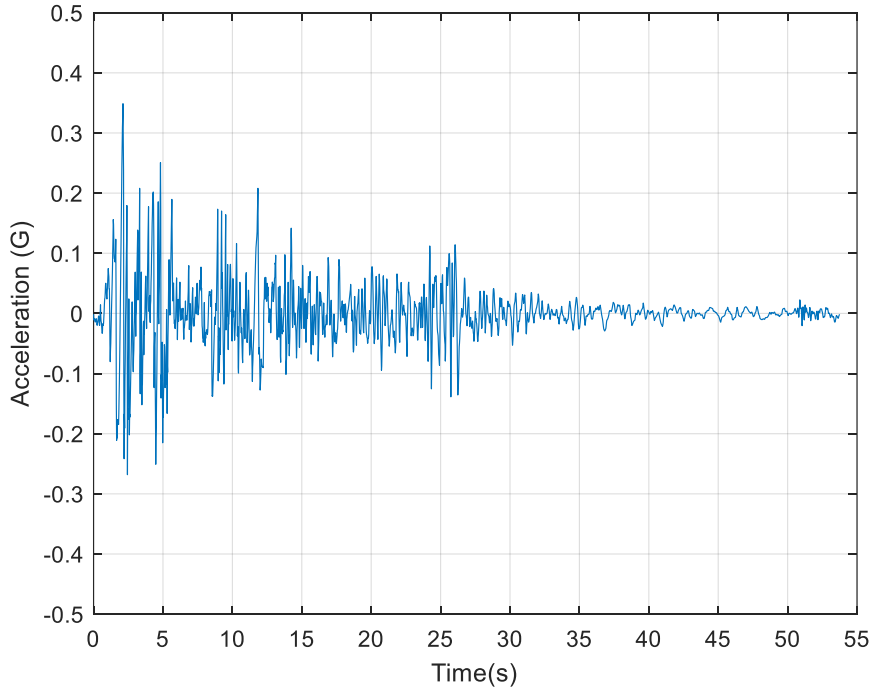


Figure 9-1: Measured acceleration of the El Centro Earthquake

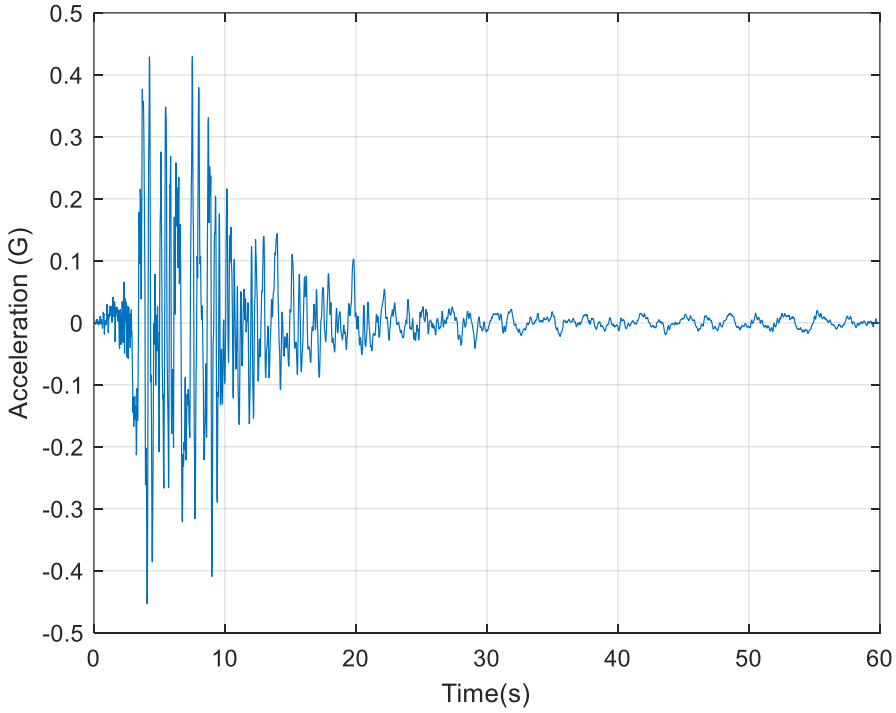


Figure 9-2: Measured acceleration of the Northridge Earthquake

9.2 SDOF Structure

9.2.1 Traditional Linear Isolator

Figure 9-3 shows a simple SDOF system.

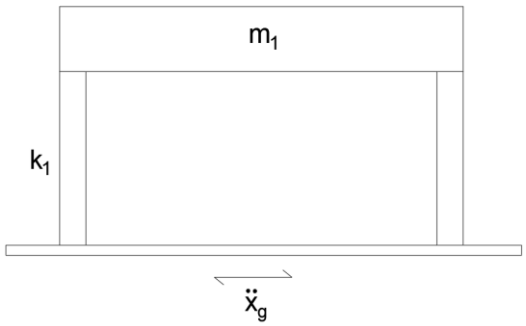


Figure 9-3: Setup of a SDOF structure with a linear isolator for application of seismic loading

This setup can also be shown as in Figure 9-4, where stiffness k_1 and damping c_1 form the system that supports mass m_1:

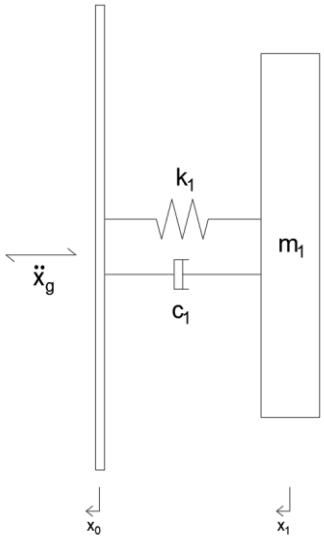


Figure 9-4: Setup of a SDOF structure with a linear isolator for application of seismic loading for analysis

It is assumed that this example is a long structure with parameters summed together to form a 2D representation of the structure.

The parameters used for this baseline example are:

$$m_1 = 1000\ t$$

$$k_1 = 3\ x\ 10^6\ \ kN/m$$

$$c_1 = 2\xi\sqrt{k_1 m_1} = 383.4\ kN.s/m$$

The displacement-time graph and base shear-time graph of the SDOF structure with only a linear isolator responding to the El Centro earthquake is shown in Figure 9-5 and Figure 9-6 respectively, where the first floor has a peak displacement of 5.02mm and peak base shear force of 13 071kN.

For that of the Northridge earthquake shown in Figure 9-7 and Figure 9-8 respectively, the first floor peak displacement is found to be 4.92mm with a peak shear force of 12 304kN.

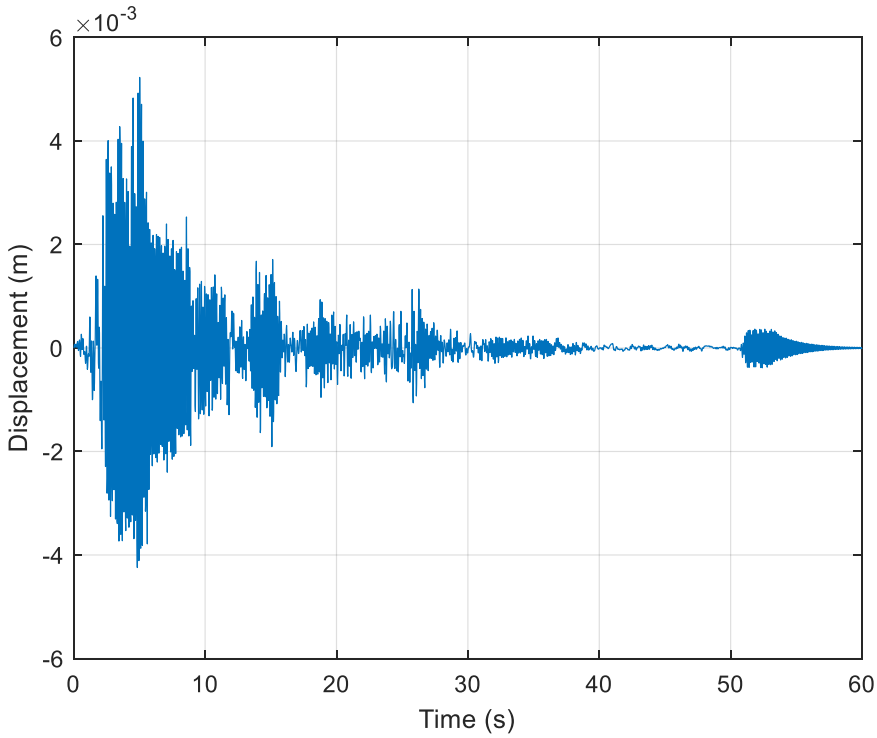


Figure 9-5: Displacement-Time graph of the response of a SDOF structure with a linear isolator to the El Centro Earthquake

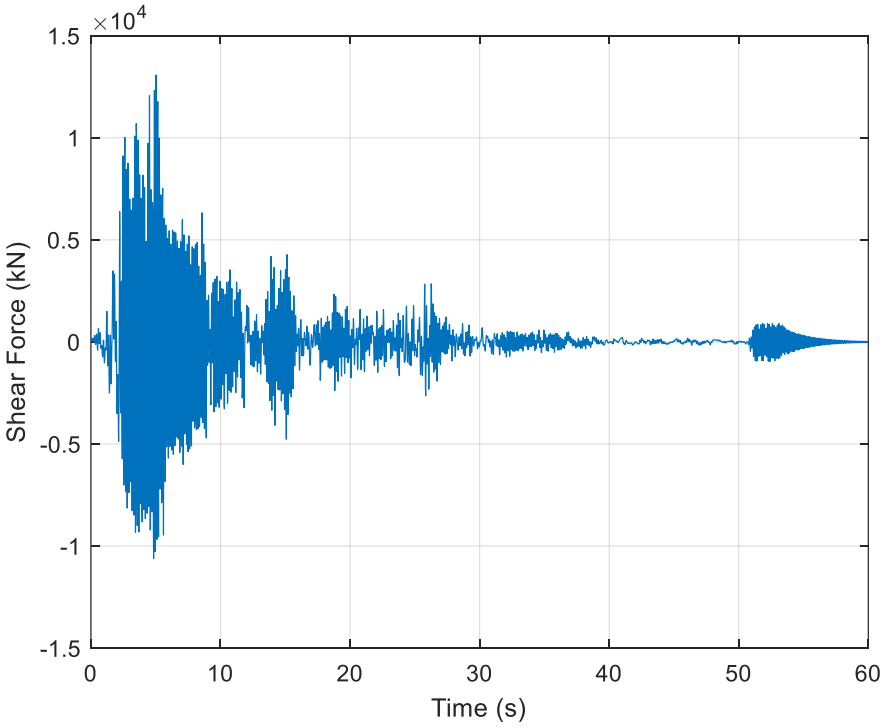


Figure 9-6: Base shear-Time graph of the response of a SDOF structure with a linear isolator to the El Centro Earthquake

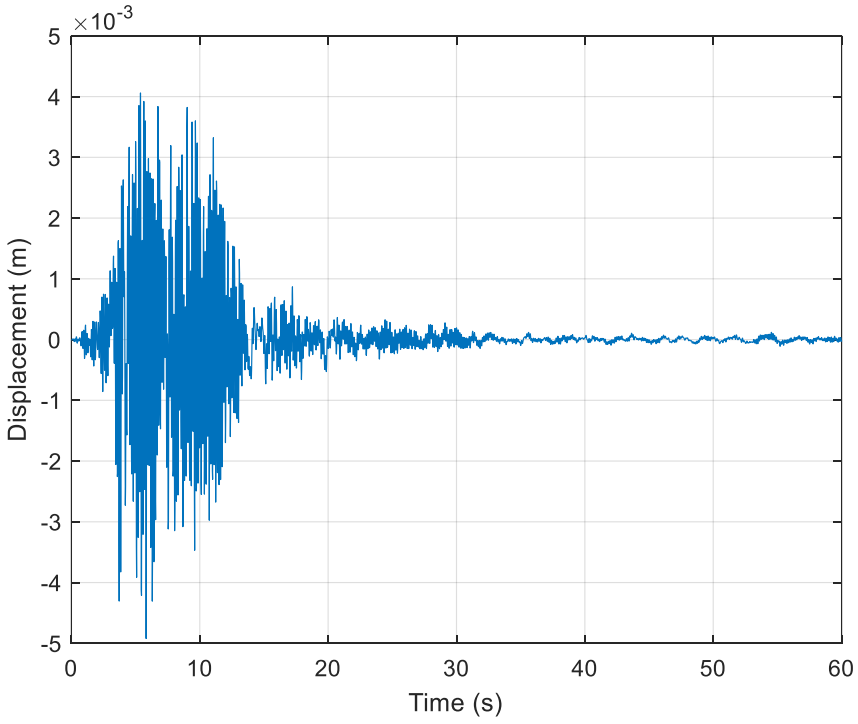


Figure 9-7: Displacement-Time graph of the response of a SDOF structure with a linear isolator to the Northridge Earthquake

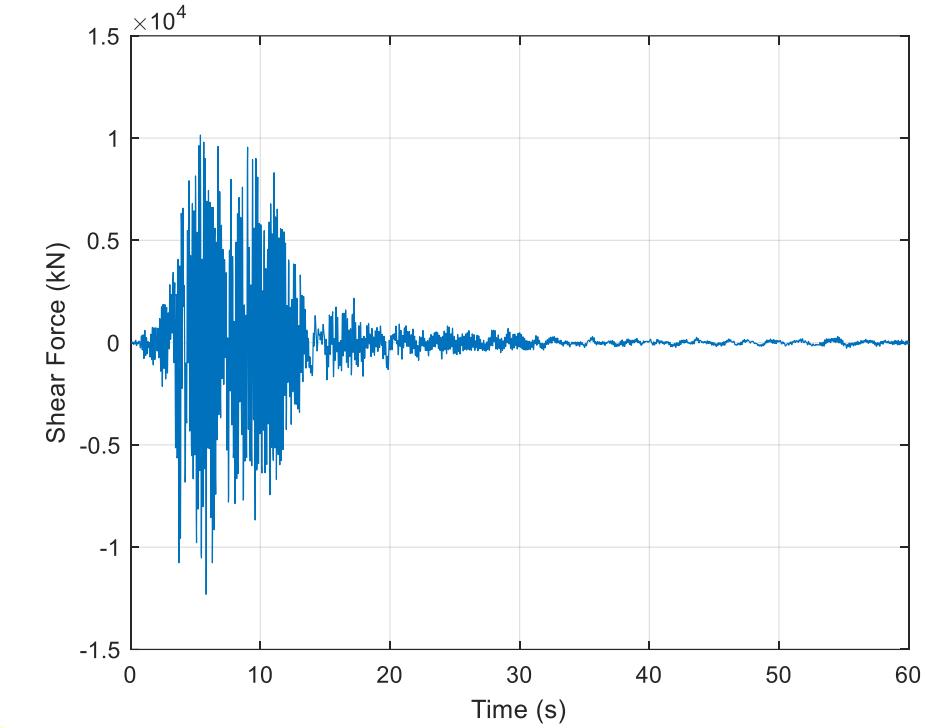


Figure 9-8: Base shear-Time graph of the response of a SDOF structure with a linear isolator to the Northridge Earthquake

9.2.2 Linear isolator integrated NES

Now the SDOF system is integrated with an NES as shown in Figure 9-9.

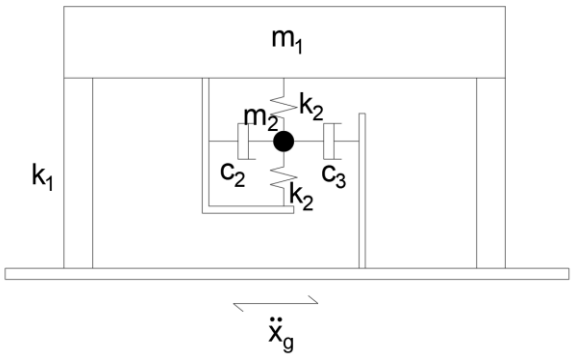


Figure 9-9: Setup of a SDOF structure with a linear isolator integrated NES for application of seismic loading

This setup can also be shown as in Figure 9-10, where stiffness k_1 and damping c_1 form the system that supports the first-floor mass m_1. NES mass m_2 is connected to the first floor by means of two springs (each with stiffness k_2) orientated at 90-degrees from the direction of motion being considered, as well as damper c_2, and is

connected to the base by damper c_3. The non-linear springs k_2 can also be shown as an effective linear stiffness $2k'_2$ in the direction of motion being considered, visually represented as an arrow through the spring symbol as shown in Figure 9-10.

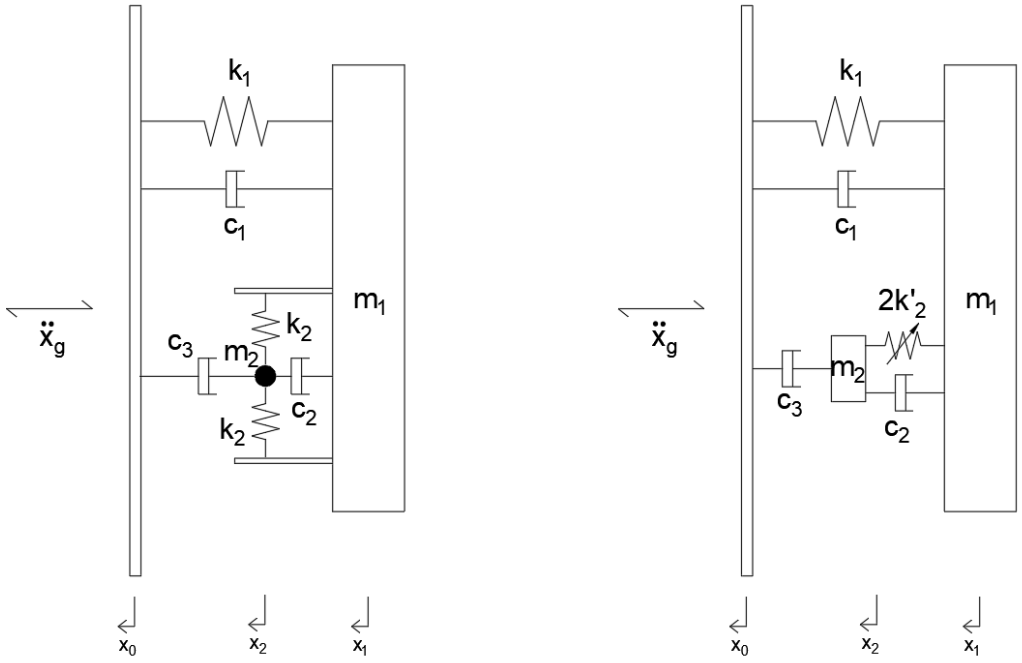


Figure 9-10: Setup of a SDOF structure with a linear isolator integrated NES for application of seismic loading for analysis

While the constant parameters remain the same for this example, the NES parameter values used are:

$$m_2 = 100\ t$$

$$k_2 = 0.3\ x\ 10^6\ \ kN/m$$

$$c_2 = \ c_3 = 2\xi\sqrt{k_2 m_2} = 38.3\ kN.s/m$$

These parameters are chosen to stay within the same mass, stiffness and damping ratios used during the transmissibility study.

The displacement-time graph of the SDOF structure with a linear isolator integrated NES responding to the El Centro earthquake is shown in Figure 9-11, where the

first floor has a peak displacement of 3.34mm and peak base shear of 8 372kN as shown in Figure 9-12. The NES mass has a peak displacement of 12.7mm.

The response to the Northridge earthquake results in a peak first floor displacement of 4.45mm and a peak base shear of 11 128kN as shown in Figure 8-14 and Figure 8-15 respectively. The NES mass has a peak displacement of 13.2mm.

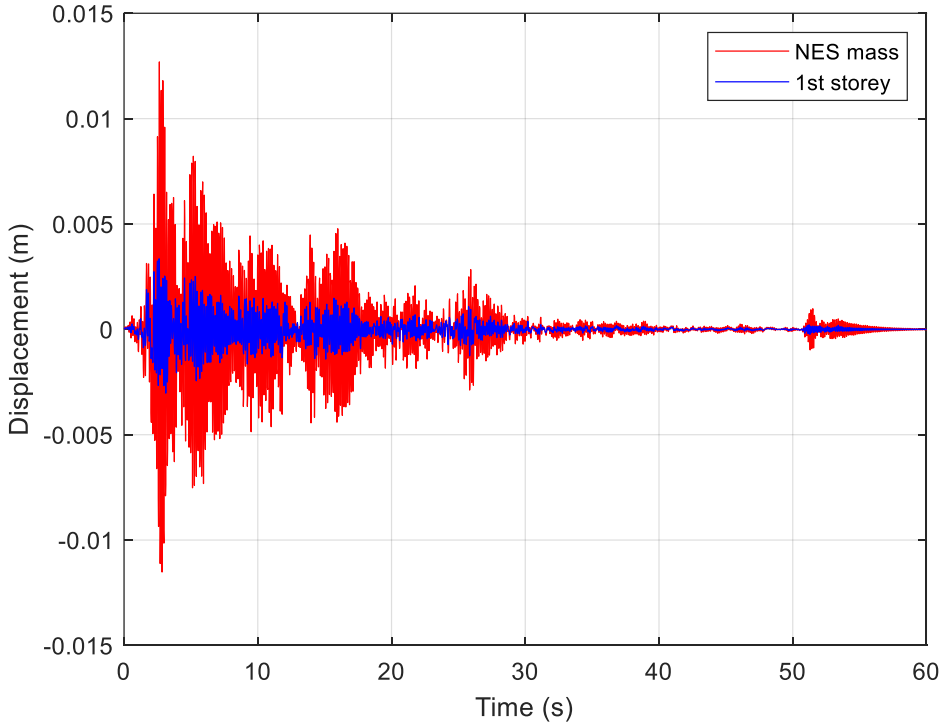


Figure 9-11: Displacement-Time graph of the response of a SDOF structure with a linear isolator integrated NES to the El Centro Earthquake

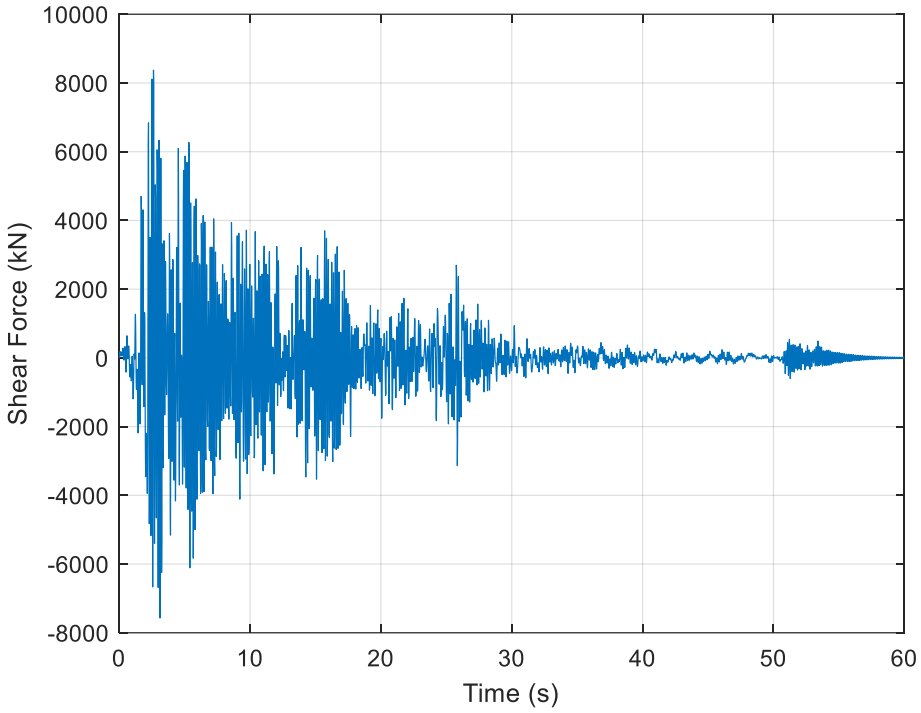


Figure 9-12: Base Shear-Time graph of the response of a SDOF structure with a linear isolator integrated NES to the El Centro Earthquake

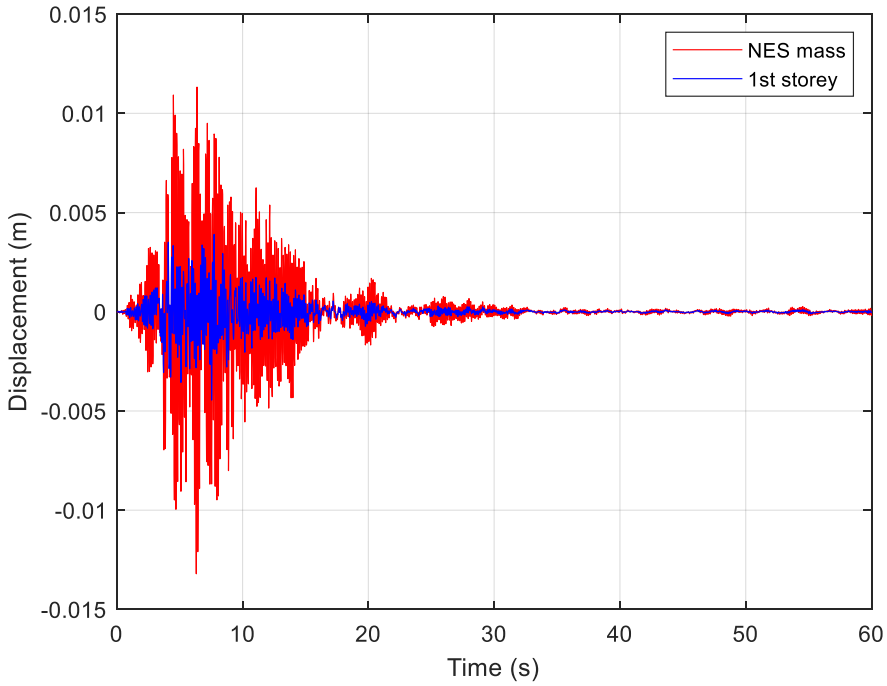


Figure 9-13: Displacement-Time graph of the response of a SDOF structure with a linear isolator integrated NES to the Northridge Earthquake

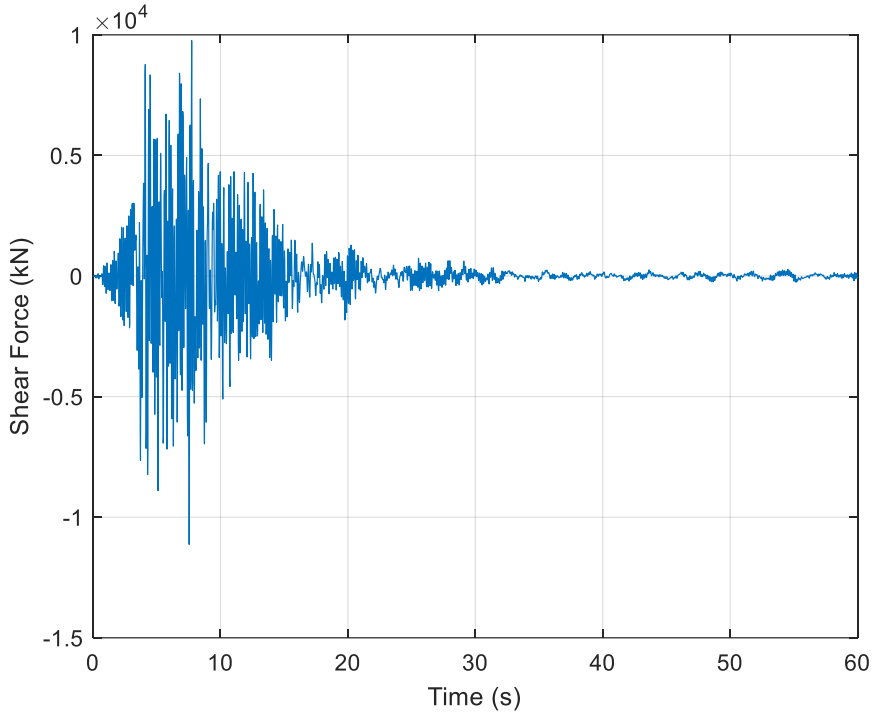


Figure 9-14: Base Shear-Time graph of the response of a SDOF structure with a linear isolator integrated NES to the Northridge Earthquake

9.3 MDOF Structure

9.3.1 Traditional Linear Isolator

Figure 9-15 shows the MDOF system t be considered.

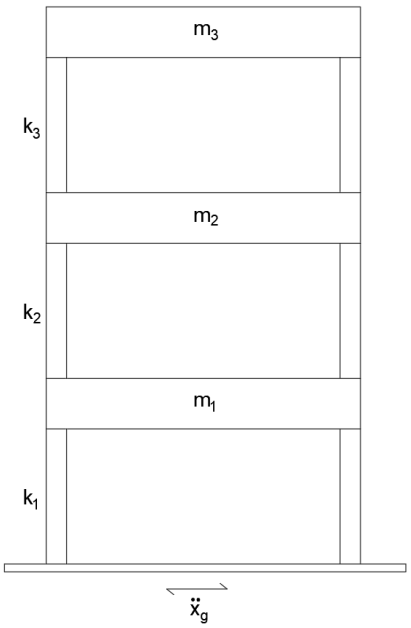


Figure 9-15: Setup of a MDOF structure with a linear isolator for application of seismic loading

This setup can also be shown as in Figure 9-16, where floors 1, 2 and 3 have mass m_1, m_2 and m_3 respectively. The support system for each floor has stiffness k_1, k_2 and k_3 respectively with damping c_1, c_2 and c_3 respectively.

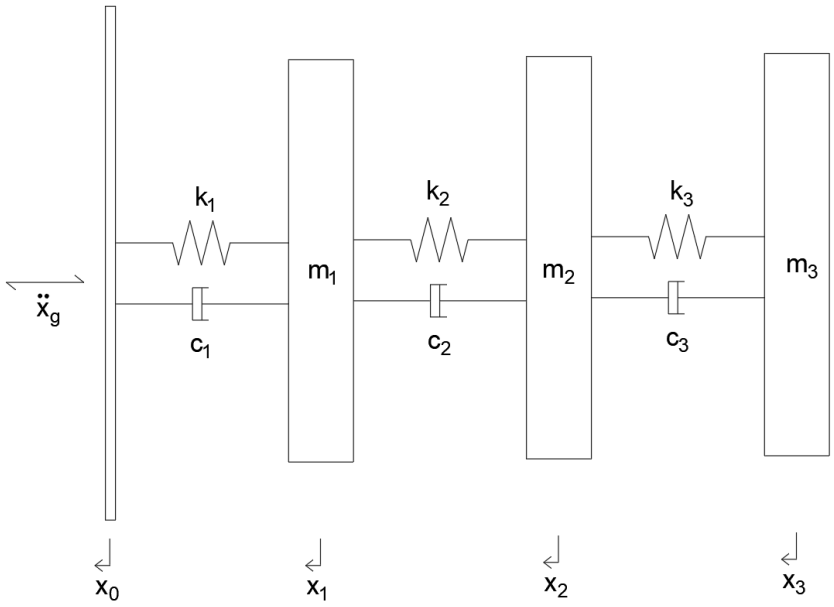


Figure 9-16: Setup of a MDOF structure with a linear isolator for application of seismic loading for analysis

The parameters used for MDOF example are matched to those in the SDOF example:

$$m_1 = m_2 = m_3 = 1000\ t$$

$$k_1 = k_2 = k_3 = 3\ x\ 10^6\ \ kN/m$$

$$c_1 = c_2 = c_3 = 2\xi\sqrt{k_1 m_1} = 383.4\ kN.s/m$$

The displacement-time graph and base shear-time graph of the MDOF structure with only a linear isolator responding to the El Centro earthquake is shown in Figure 9-17 and Figure 9-18 respectively. The first, second and third floors have a peak displacement of 19.7mm, 35.4mm and 44.1mm respectively. The first, second and third floors have a peak base shear of 26 201kN, 47 065kN and 59 057kN respectively.

For the Northridge earthquake, the same is shown in Figure 9-19 and Figure 9-20 respectively, where the first, second and third floors have a peak displacement of

16.1mm, 28.9mm and 35.8mm respectively. The first, second and third floors have a peak base shear of 20 988kN, 38 176kN and 48 411kN respectively.

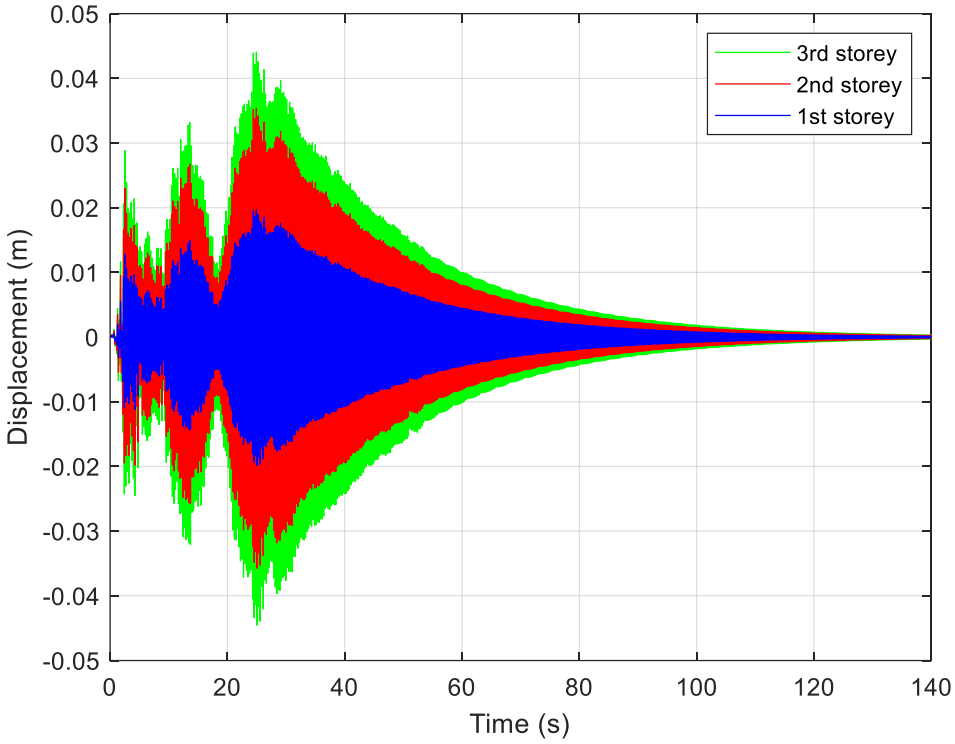


Figure 9-17: Displacement-Time graph of the response of a MDOF structure with a linear isolator to the El Centro Earthquake

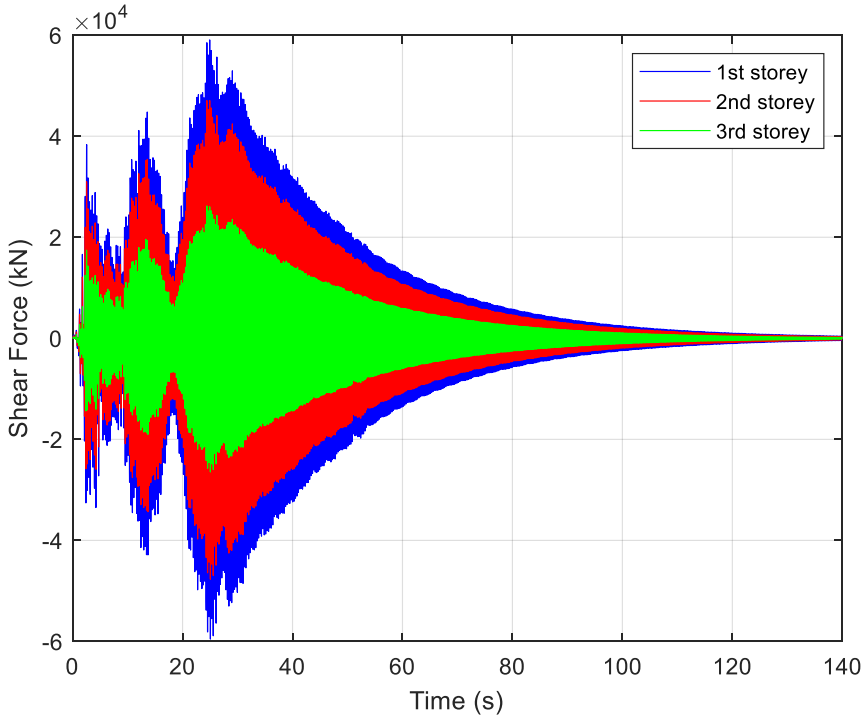


Figure 9-18: Base shear-Time graph of the response of a MDOF structure with a linear isolator to the El Centro Earthquake

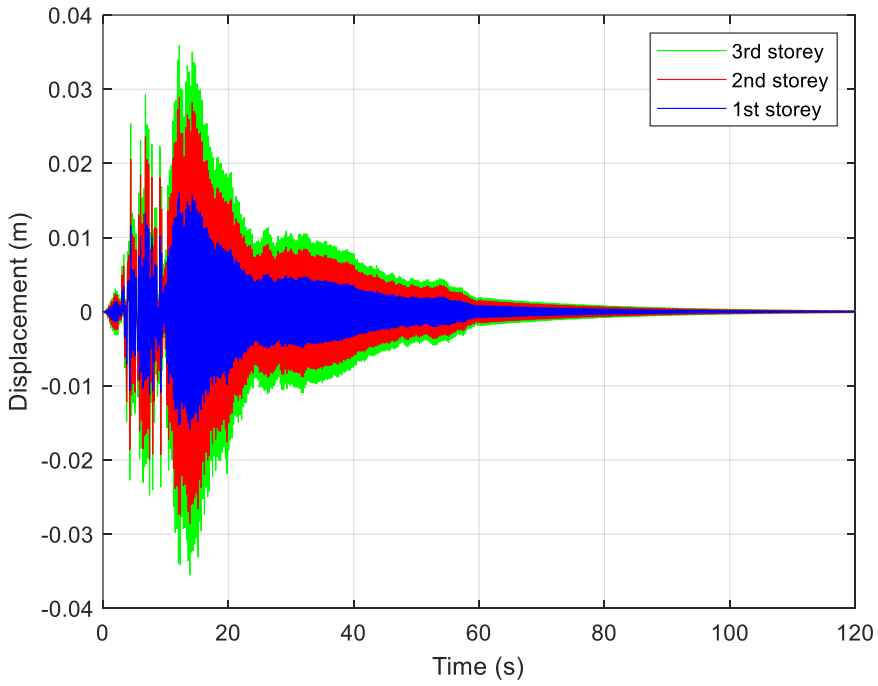


Figure 9-19: Displacement-Time graph of the response of a MDOF structure with a linear isolator to the Northridge Earthquake

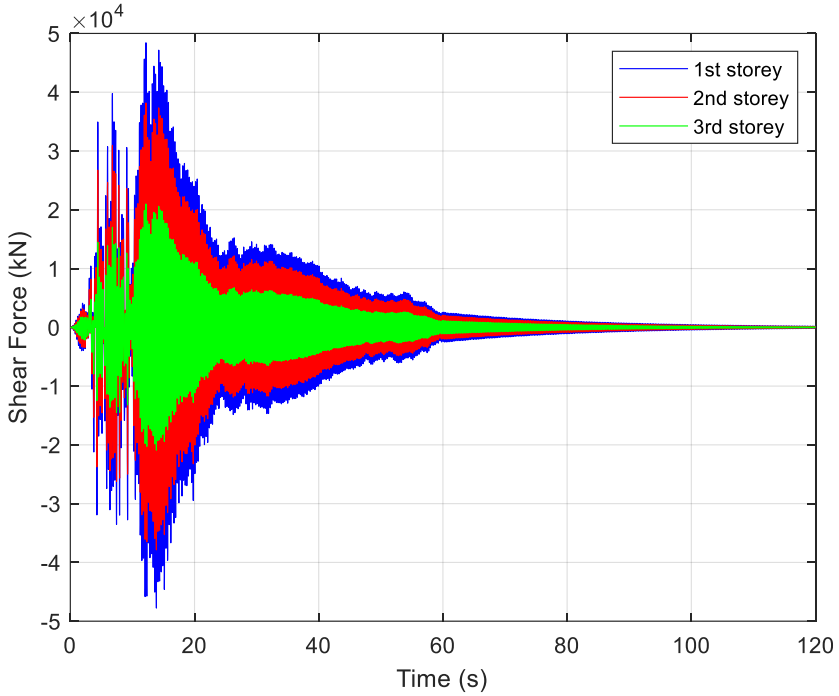


Figure 9-20: Base shear-Time graph of the response of a MDOF structure with a linear isolator to the Northridge Earthquake

9.3.2 Linear isolator integrated NES

Figure 9-21 shows the integration of a NES to the MDOF system being considered.

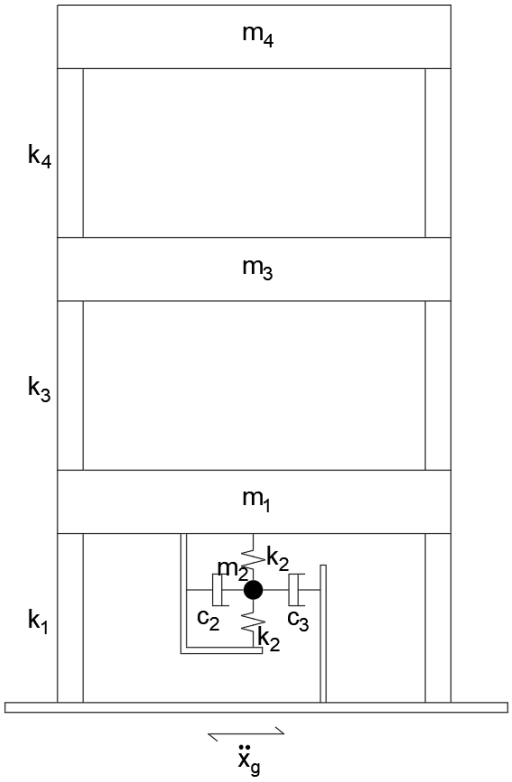


Figure 9-21: Setup of a MDOF structure with a linear isolator integrated NES for application of seismic loading

This setup can also be shown as in Figure 9-22, where floors 1, 2 and 3 have mass m_1, m_2 and m_3 respectively. The support system for each floor has stiffness k_1, k_3 and k_4 respectively with damping c_1, c_4 and c_5 respectively. As before, NES mass m_2 is connected to the first floor by means of two springs (each with stiffness k_2) orientated at 90-degrees from the direction of motion being considered, as well as damper c_2, and is connected to the base by damper c_3.

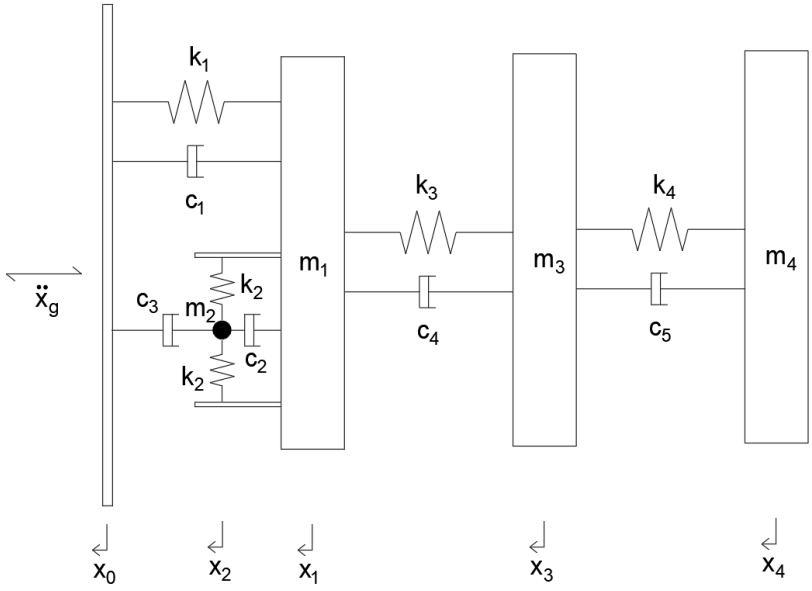


Figure 9-22: Setup of a MDOF structure with a linear isolator integrated NES for application of seismic loading for analysis

Alternatively, showing the non-linear springs k_2 as an effective linear stiffness $2k'_2$ in the direction of motion being considered, visually represented as an arrow through the spring symbol as shown in Figure 9-23.

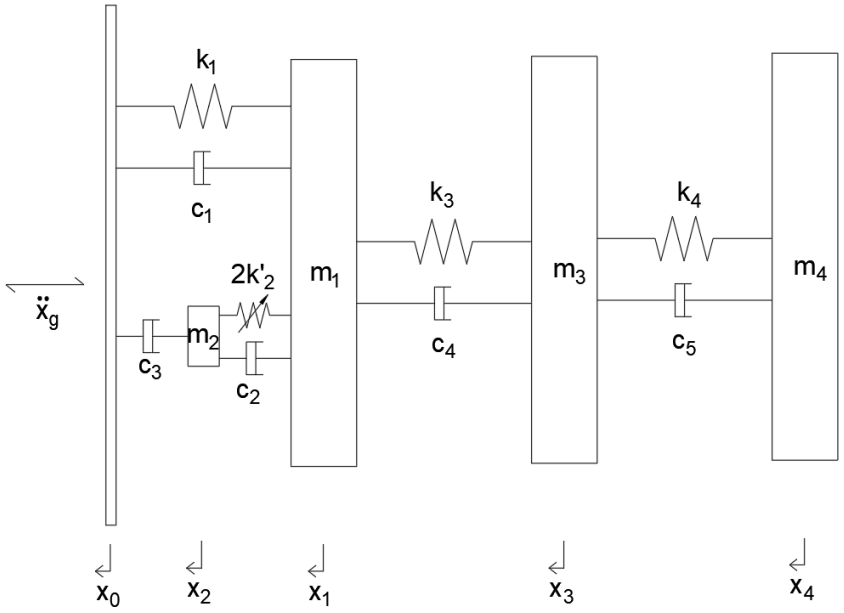


Figure 9-23: Setup of a MDOF structure with a linear isolator integrated NES for application of seismic loading for analysis with effective stiffness

As before, while the constant parameters remain the same for this example, the NES parameter values used are made to match that used in the SDOF example:

$$m_2 = 100\ t$$

$$k_2 = 0.3\ x\ 10^6\ \ kN/m$$

$$c_2 = \ c_3 = 2\xi\sqrt{k_2 m_2} = 38.3\ kN.s/m$$

The displacement-time graph of the MDOF structure with a linear isolator integrated NES responding to the El Centro earthquake is shown in Figure 9-24. The first, second and third floors have a peak displacement of 14.5mm, 25.7mm and 31.8mm respectively and the NES mass a peak displacement of 18.1mm. The base shear-time graph is shown in Figure 9-25 where the first, second and third floors have a peak base shear of 18 379kN, 33 463kN and 43 531kN respectively.

For the Northridge earthquake, the same is shown in Figure 9-26 and Figure 9-27 respectively, where the first, second and third floors have a peak displacement of 15.6mm, 27.6mm and 34.3mm respectively, with the NES mass a peak displacement of 19.2mm. The first, second and third floors have a peak base shear of 19 932kN, 36 133kN and 46 809kN respectively.

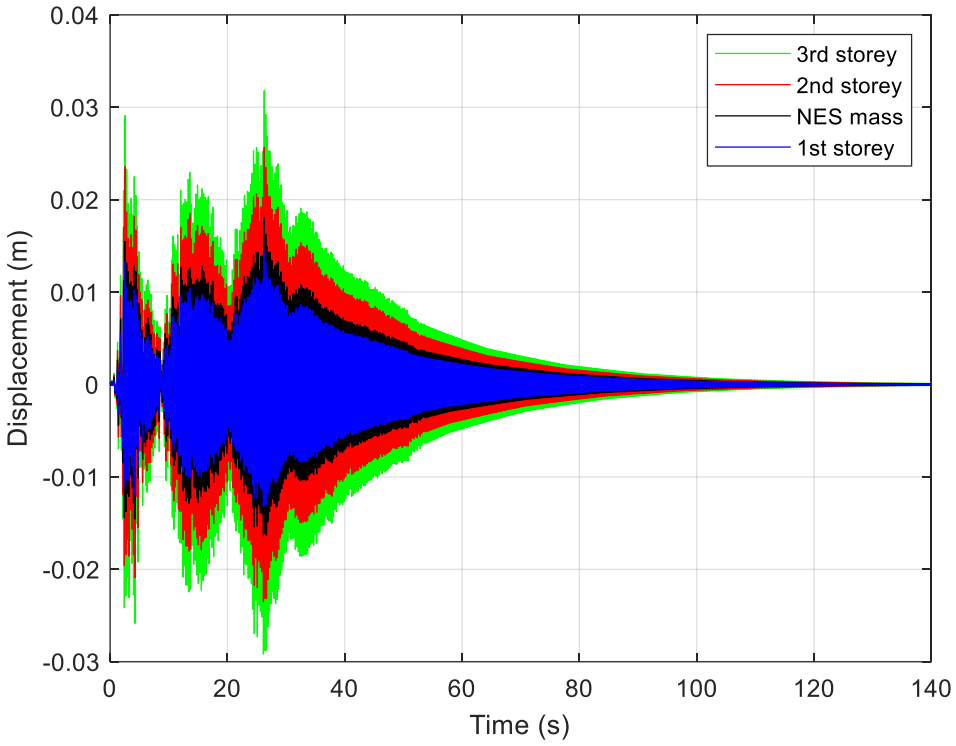


Figure 9-24: Displacement-Time graph of the response of a MDOF structure with a linear isolator integrated NES to the El Centro Earthquake

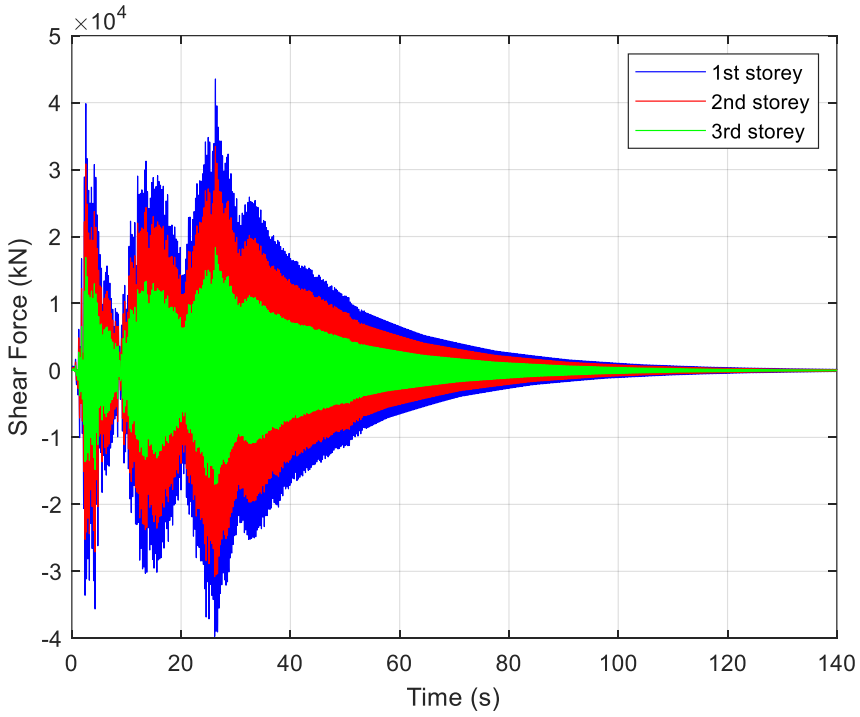


Figure 9-25: Base shear-Time graph of the response of a MDOF structure with a linear isolator integrated NES to the El Centro Earthquake

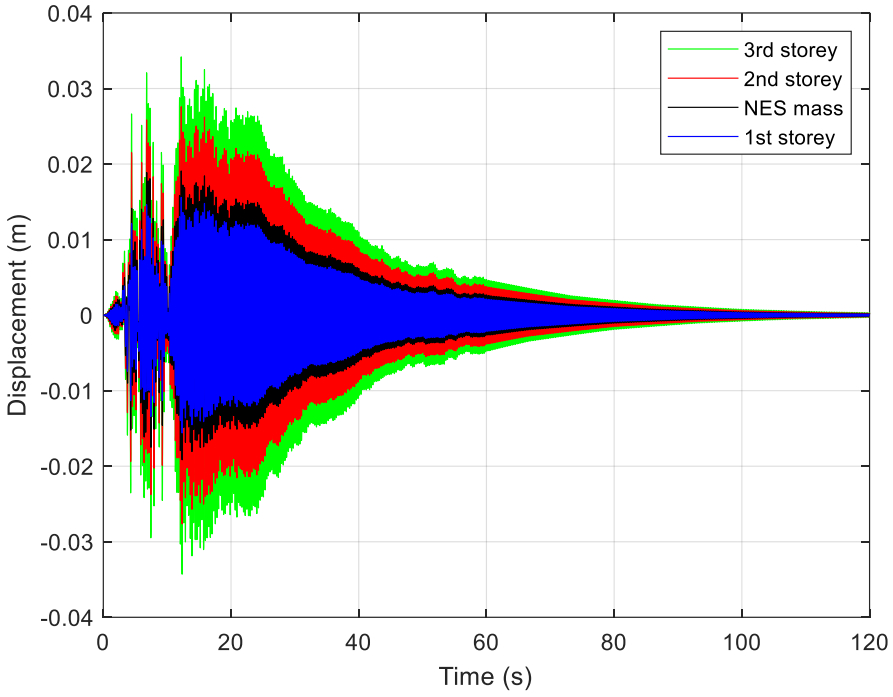


Figure 9-26: Displacement-Time graph of the response of a MDOF structure with a linear isolator integrated NES to the Northridge Earthquake

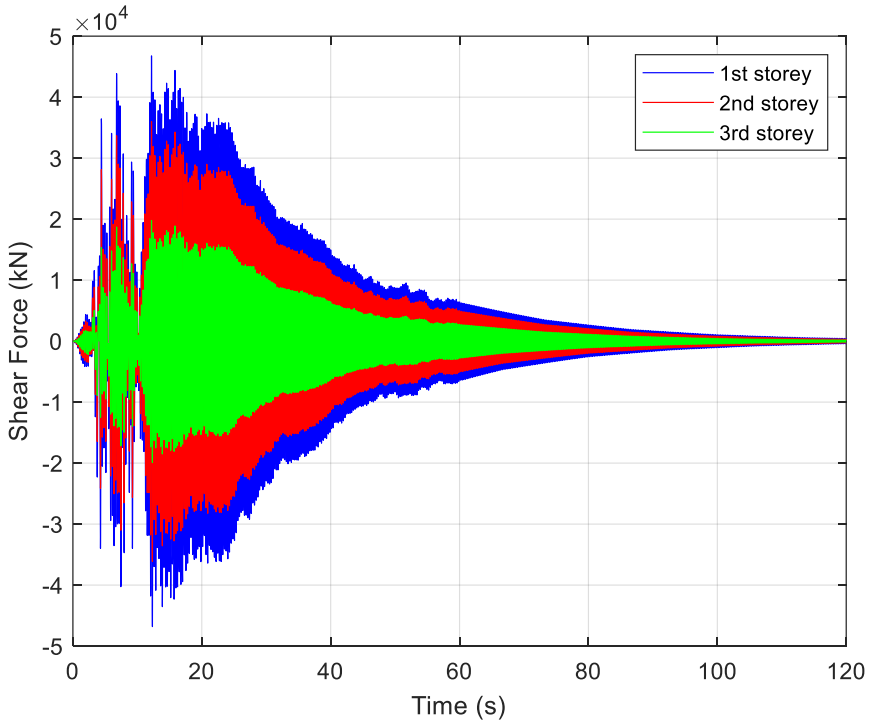


Figure 9-27: Base shear-Time graph of the response of a MDOF structure with a linear isolator integrated NES to the Northridge Earthquake

9.4 Earthquake behaviour discussion

Plotting the displacement-time graph and the base shear-time graph of the first floor of the SDOF system for a linear isolator only as well as a linear isolator integrated a NES system for both the El Centro earthquake and the Northridge earthquake.

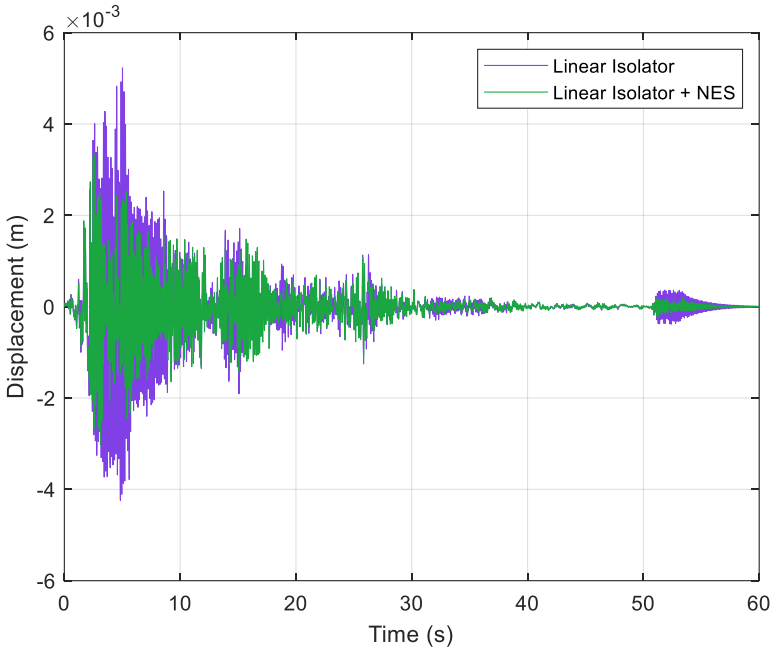


Figure 9-28: Displacement-Time graph of the response of a SDOF structure to the El Centro Earthquake

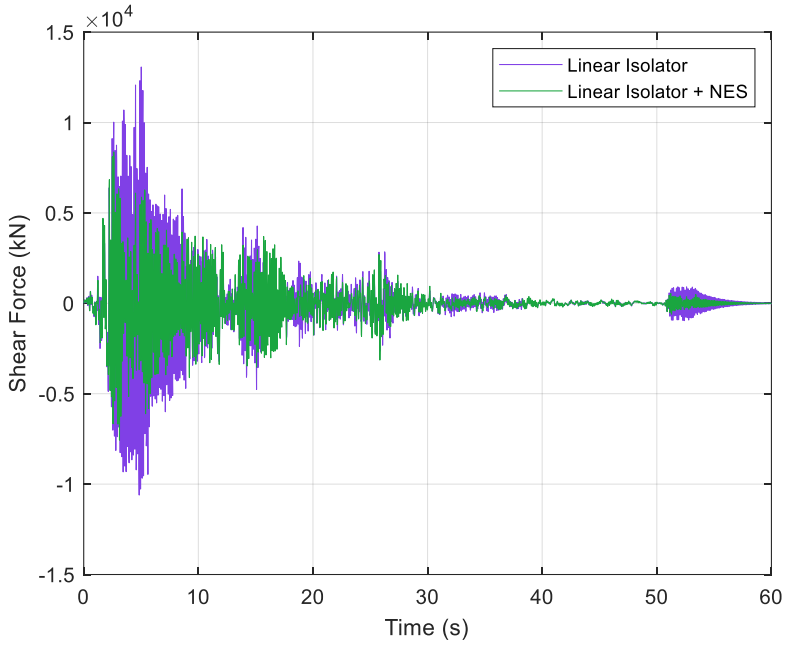


Figure 9-29: Base shear-Time graph of the response of a SDOF structure to the El Centro Earthquake

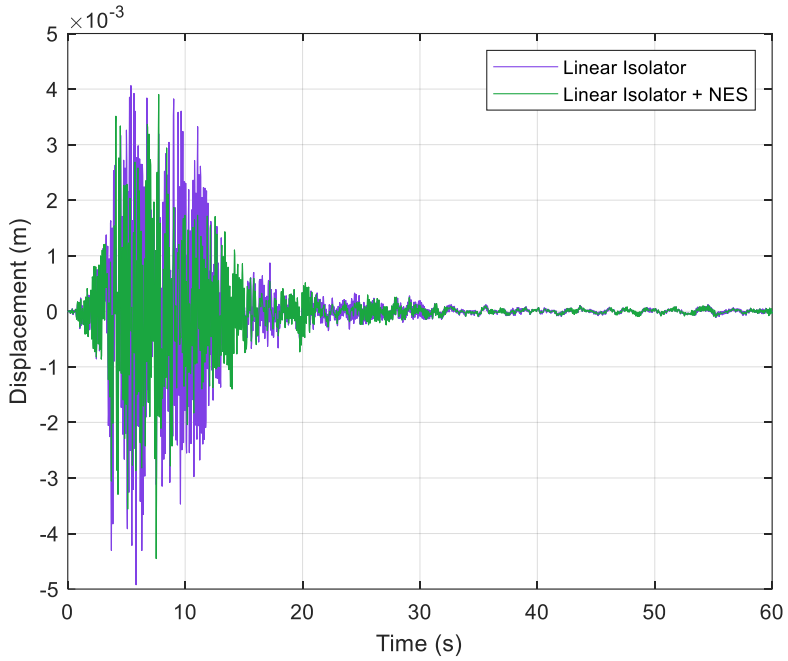


Figure 9-30: Displacement-Time graph of the response of a SDOF structure to the Northridge Earthquake

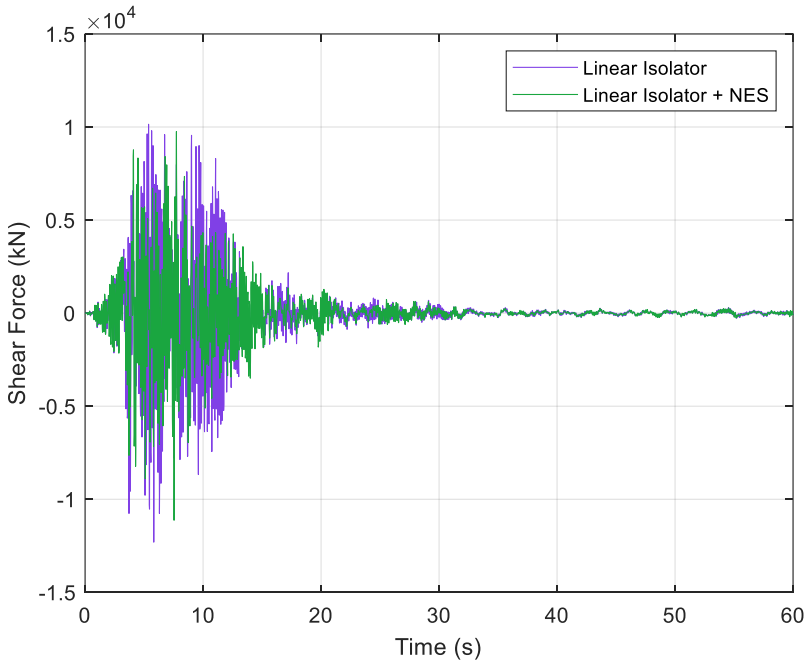


Figure 9-31: Base shear-Time graph of the response of a SDOF structure to the Northridge Earthquake

From the graphs shown in Figure 9-28 to Figure 9-31, a definite and large decrease in both displacement and shear readings can be seen for the SDOF structure with a linear isolator and integrated NES system for both the El Centro earthquake as well as the Northridge earthquake.

In order to get a feeling of the average effect of the integrated system on the SDOF structure, the absolute values of all shear experienced by the structure during the extent of the earthquakes is summed. It is found that the integrated system experiences approximately 25.9% less total shear during the El Centro Earthquake, and approximately 21.1% less total shear during the Northridge earthquake.

Plotting the displacement-time graph and the base shear-time graph of the third floors (as a representation of the behaviour of all three floors) of the MDOF system for a linear isolator only as well as a linear isolator integrated a NES system for both the El Centro earthquake and the Northridge earthquake.

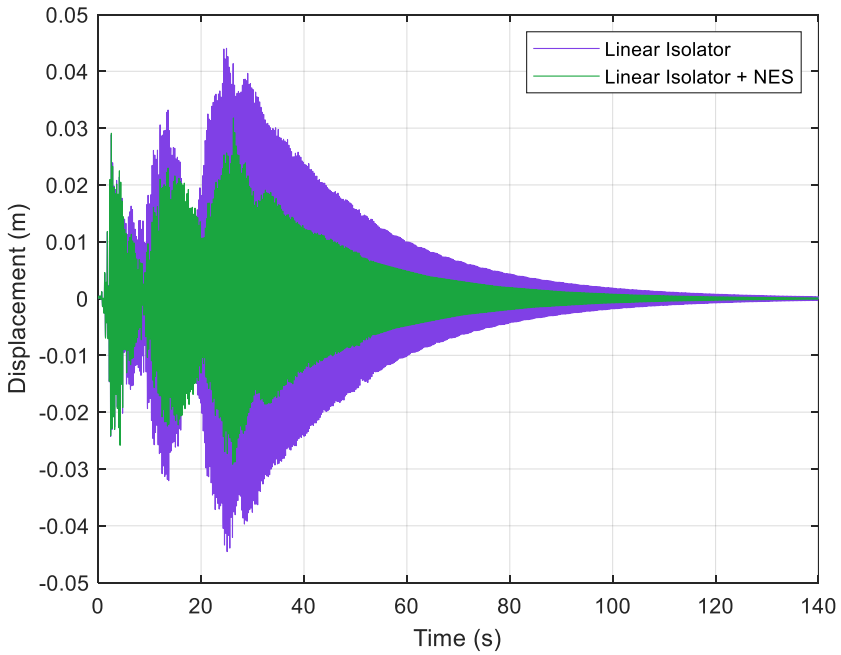


Figure 9-32: Displacement-Time graph of the response of a MDOF structure's third floor to the El Centro Earthquake

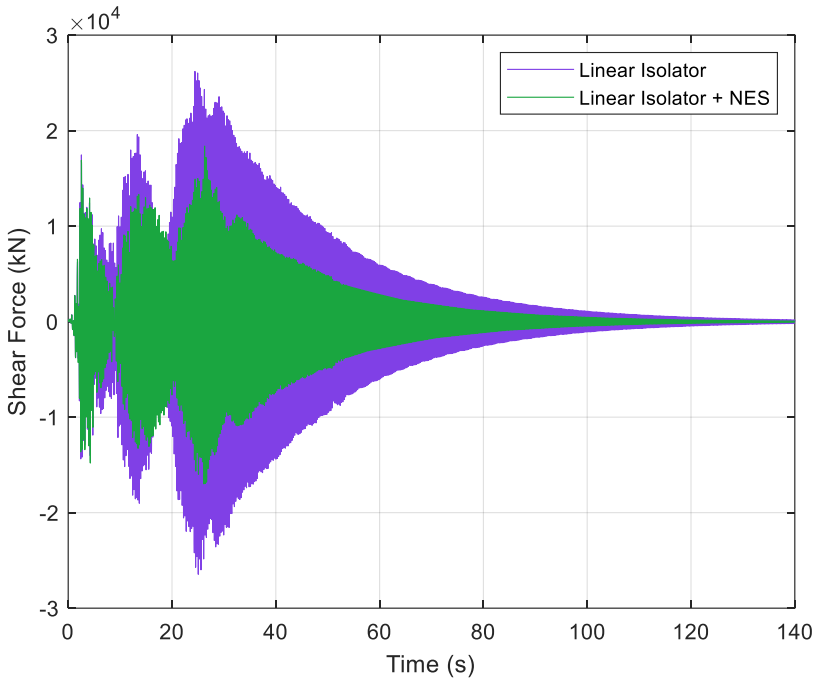


Figure 9-33: Shear-Time graph of the response of a MDOF structure's third floor to the El Centro Earthquake

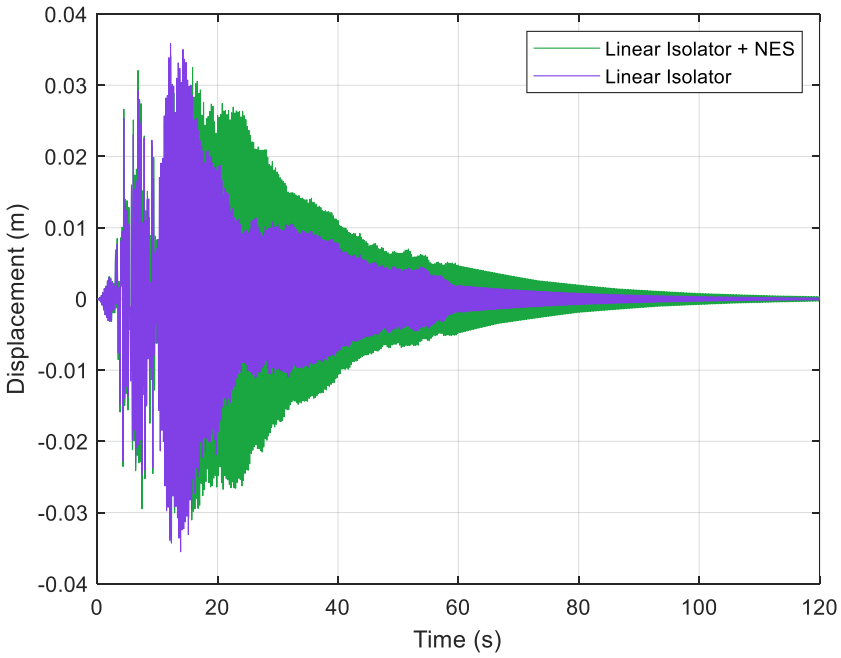


Figure 9-34: Displacement-Time graph of the response of a MDOF structure's third floor to the Northridge Earthquake

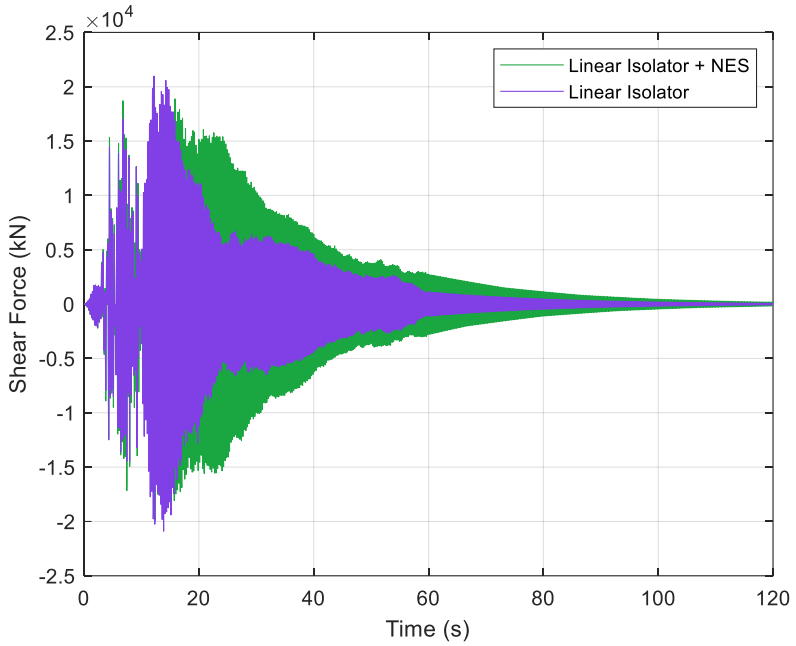


Figure 9-35: Shear-Time graph of the response of a MDOF structure's third floor to the Northridge Earthquake

As with the SDOF structure, a definite and large decrease in both displacement and shear readings can be seen for the MDOF structure with a linear isolator and integrated NES system for the El Centro earthquake (Figure 9-32 and Figure 9-33), however an increase in average amplitude is observed for the Northridge earthquake (Figure 9-34 and Figure 9-35).

In order to get a feeling of the average effect of the integrated system on the MDOF structure, the absolute values of all shear experienced by the structure's third floor during the extent of the earthquakes and until stabilisation is summed. It is found that the integrated system experiences approximately 41.8% less total shear during the El Centro Earthquake, and approximately 38.8% more total shear during the Northridge earthquake. While the average shear is more during the Northridge earthquake, it is noted that the peak shear is slightly decreased, as discussed below.

The peak amplitude results from the graphs shown in Figure 9-28 to Figure 9-35 is summarised in tabular format in Table 9-1 and Table 9-2.

Table 9-1: Summary of responses of SDOF and MDOF structures to the El Centro earthquake

SDOF Structure			
	Linear Isolator	Linear Isolator Integrated NES	% difference
Peak Floor 1 Displacement (mm)	5.02	3.34	-33.5%
Peak Floor 1 Base Shear (kN)	13071	8372	-35.9%
MDOF Structure			
	Linear Isolator	Linear Isolator Integrated NES	% difference
Peak Floor 1 Displacement (mm)	19.7	14.5	-26.4%
Peak Floor 2 Displacement (mm)	35.4	25.7	-27.4%
Peak Floor 3 Displacement (mm)	44.1	31.8	-27.9%
Peak Floor 1 Base Shear (kN)	26201	18379	-29.9%
Peak Floor 2 Base Shear (kN)	47065	33463	-28.9%
Peak Floor 3 Base Shear (kN)	59057	43531	-26.3%

Table 9-2: Summary of responses of SDOF and MDOF structures to the Northridge earthquake

SDOF Structure			
	Linear Isolator	Linear Isolator Integrated NES	% difference
Peak Floor 1 Displacement (mm)	4.92	4.45	-9.6%
Peak Floor 1 Base Shear (kN)	12304	11128	-9.6%
MDOF Structure			
	Linear Isolator	Linear Isolator Integrated NES	% difference
Peak Floor 1 Displacement (mm)	16.1	15.6	-3.1%
Peak Floor 2 Displacement (mm)	28.9	27.6	-4.5%
Peak Floor 3 Displacement (mm)	35.8	34.3	-4.2%
Peak Floor 1 Base Shear (kN)	20988	19932	-5.0%
Peak Floor 2 Base Shear (kN)	38176	36133	-5.4%
Peak Floor 3 Base Shear (kN)	48411	46809	-3.3%

The analysis shows that the introduction of the NES system to both the SDOF and MDOF structures results in a reduced peak floor displacement and base shear of between 26% and 36% for the El Centro earthquake and a reduction of between 3% and 10% for the Northridge earthquake.

When analysing the trends of Figure 9-32 and Figure 9-34, showing the displacements of the MDOF structure's floor three for the El Centro earthquake and Northridge earthquake respectively, it can be seen that once the major portion of the earthquake is over that the floor displacements stabilise faster in the structure with the NES system for the El Centro earthquake, however, stabilise slower in the structure with the NES system for the Northridge earthquake.

10 CONCLUSION

10.1 General discussion

A comprehensive analysis of the transmissibility and vibration control performance of various vibration isolation configurations are presented, specifically focusing on comparing the behaviour of traditional linear isolators to that of linear isolators integrating Non-linear Energy Sink (NES) systems and additional damping elements.

While the behaviour of traditional linear isolators are well-understood, there are limitations to it's effectiveness when considering loading frequencies close to the system's fundamental natural frequency. The transmissibility ratio at this point has shown to reach values as high as 16.70 when using what is considered a reasonable damping ratio of 0.03, demonstrating an extremely high amplification of forces and displacements which could result in severe human discomfort as well as structural damage.

When a NES system is integrated with a traditional linear isolator as done in Configuration 2A and it's parameters optimised to the system being analysed, the peak transmissibility at a loading frequency ratio of 1 is shown to decrease significantly to as low as 3.8. While this is a strong indicator for promising results, in some instances, the point at which transmissibility reduces back down to one may occur at a higher loading frequency ratio, and the transmissibility at higher loading frequency ratios may be higher in the integrated system due to the lower peak at the natural frequency, demonstrating that the addition of the NES system provides benefit in certain frequency ranges only. The advantages and disadvantages discussed above must be weighed against each other when determining which solution is better suited for the problem being considered. Integration with Configuration 2B where the NES is connected to the base with a spring, however, does not look promising as results are comparable to the linear isolator acting alone.

The addition of a NES to a linear isolator integrated skyhook damper system results in a system with non-linear behaviour. When adding the NES to an already

optimised solution, the benefit in reduced transmissibility seen is negligible. The very high stiffness parameters used in the already optimised solution results in the addition of the NES seeing very little benefit.

When considering a harmonic force as typically presented by vibrating equipment, Configuration 2A shows the most promising results with the lowest peak transmissibility. Only at higher frequency ratios of between 10 and 20 did Configuration 2B demonstrate slightly improved performance of 5% lower transmissibility when compared to the traditional linear isolator.

The traditional linear isolator (Configuration 1) and the linear isolator integrated NES in the form of Configuration 2A is used to investigate the effectiveness of the system on a Single Degree of Freedom (SDOF) and a Multi-Degree of Freedom (MDOF) structure under earthquake loading, specifically the El Centro and Northridge earthquakes, two prominent seismic events that is often referenced when performing studies of this nature.

When comparing the results from the two configurations, the El Centro earthquake results for Configuration 2A show that the SDOF structure has reduced peak floor level displacements and reduced base shears of approximately 33.5% and 35.9% respectively, and that the MDOF structure has an average reduced peak floor level displacements and reduced base shears of approximately 27.2% and 28.4% respectively. When considering the average results and not just the peak results, there is still a significant reduction in results for Configuration 2A of between 25.9% and 41.8%.

When comparing the results from the two configurations, the Northridge earthquake results for Configuration 2A show that the SDOF structure has reduced peak floor level displacements and reduced base shears of approximately 9.6% and 9.6% respectively, and that the MDOF structure has an average reduced peak floor level displacements and reduced base shears of approximately 3.9% and 4.6% respectively. When considering the average results and not just the peak results, there is a more significant reduction in results for Configuration 2A of approximately 21.1% for the SDOF structure, however, the MDOF structure shows an average increase in results of approximately 38.8%.

Analysing the results further shows that the NES integrated system provides the structures with faster stabilisation during the El Centro earthquake, reducing vibrations faster and more effectively, however, provides slower stabilisation during the Northridge earthquake, once again showing that the effectiveness of the system can vary depending on the specific seismic events. Further investigation can be done into the possibility of optimising parameters of the NES system to each structure applied to such that a reduction in results across the board could be achieved.

Overall, while the traditional linear isolator remains a competitive and useful solution for many applications in practice, integrating it with a NES system shows promising results where more refined vibration control solutions are required.

10.2 Limitations and recommendations for further study

As with all studies, there are certain limitations regarding the coverage of the topic which allows for possibilities for further study:

- Certain parameter values were assumed and regarded as fixed as a means to create a base case to compare against, further studies could investigate varying these parameters to investigate the effect thereof.
- The parameters and variables which are considered to be adjustable were only considered over a limited range, further studies could expand on the range of values considered.
- The harmonic loading cases considered only a single main mass to which the NES and dampers are connected – further studies could investigate the effect of adding additional components to emulate the effects of applied loads on the greater structure.
- The system configurations considered were relatively simple in nature, further studies could consider more complex configurations and compare results.
- Loading considered was limited to harmonic loading with a fixed loading frequency as well as the El Centro and Northridge earthquakes, further sties could expand on the loading types considered.

- Only a single variation of SDOF and MDOF structure was considered for the earthquake portion of this study, further studies could investigate different structural arrangements and the trend in results investigated.
- Only a typical Type 1 NES system was considered for integration in this study, further studies could investigate integrating not only different types of NES systems but also in varying combinations.
- The calculations in this study were limited to numerical simulation by using the Runge-Kutta analysis method, further studies could compare other simulation methods and compare results.
- Parameters or variables were optimised manually for this study, further studies could investigate automation of parameter optimisation or a more refined optimisation method such that it is a viable option for designers to use within the industry
- This study was limited to a desktop study, further studies could include physical experiments to test and verify results.

11 REFERENCES

AL-Shudeifat, M.A. (2014) ‘Highly efficient nonlinear energy sink’, *Nonlinear Dyn*, 76, pp. 1905–1920. doi:10.1007/s11071-014-1256-x.

Blake, R.E. (2002) ‘Basic Vibration Theory’, in Harris, C.M. and Piersol, A.G. (eds) *Harris’ Shock and Vibration Handbook*. 5th edn. McGraw-Hill.

Countervail (2019) *Vibration Isolation vs. Vibration Damoing: The What and Why*. Available at: https://countervailproducts.com/insights/blog/vibration-isolation-vs-vibration-damping-the-what-and-why#:~:text=While the terms are often,Vibration damping dissipates vibration energy. (Accessed: 14 April 2022).

Crede, C.E. and Ruzicka, J.E. (2002) ‘Theory of Vibration Isolation’, in Harris, C.M. and Piersol, A.G. (eds) *Harris’ Shock and Vibration Handbook*. 5th edn. McGraw-Hill.

Ding, H. and Chen, L.Q. (2020) ‘Designs, analysis, and applications of nonlinear energy sinks’, *Nonlinear Dynamics*, 100(4), pp. 3061–3107. doi:10.1007/S11071-020-05724-1.

Ewins, D.J. (2001) ‘Mode of Vibration’, *Encyclopedia of Vibration*, pp. 838–844. doi:10.1006/rwvb.2001.0062.

Harris, C.M. (2002) ‘Introduction To The Handbook’, in Harris, C.M. and Piersol, A.G. (eds) *Harris’ Shock and Vibration Handbook*. 5th edn. McGraw-Hill.

Lage, Y.E. *et al.* (2014) ‘Force transmissibility versus displacement transmissibility’, *Journal of Sound and Vibration*, 333(22), pp. 5708–5722. doi:10.1016/j.jsv.2014.05.038.

Li, K. (2020) ‘A Passive Vibration Isolator Integrated a Skyhook Damper or a Groundhook Damper’, *Journal of Vibration Testing and System Dynamics*, 4(4), pp. 363–376. doi:10.5890/jvtsd.2020.12.005.

Lim, A. (2018) *No What is Natural Frequency?, ThoughtCo.com*. Available at: https://www.thoughtco.com/natural-frequency-4570958 (Accessed: 14 April 2022).

Luo, J. *et al.* (2014) ‘Large-scale experimental evaluation and numerical simulation of a system of nonlinear energy sinks for seismic mitigation’, *Engineering Structures*, 77, pp. 34–48. doi:10.1016/j.engstruct.2014.07.020.

MathWorks (2021) *What Is MATLAB?* Available at: https://uk.mathworks.com/discovery/what-is-matlab.html (Accessed: 7 November 2021).

Qiu, Y. *et al.* (2021) ‘The analysis and design of nonlinear vibration isolators under both displacement and force excitations’, *Archive of Applied Mechanics*, 91(5), pp. 2159–2178. doi:10.1007/s00419-020-01875-0.

Racca, R.H. and Harris, C.M. (2002) ‘Shock and Vibration Isolators and Isolation Systems’, in Harris, C.M. and Piersol, A.G. (eds) *Harris’ Shock and Vibration Handbook*. 5th edn. McGraw-Hill.

Ruzicka, J.E. and Derby, T.F. (1971) *Influence of Damping in Vibration Isolation, Issue 7*. Edited by Technical Information Divison - Naval Research Laboratory. Washington, D.C.: Shock and Vibration Information Center. Available at: https://books.google.co.za/books?hl=en&lr=&id=krT34PziAz4C&oi=fnd&pg=PA1&dq=damping+vibrations+versus+isolating+vibrations&ots=54H63wbwN8&sig=tBhIVoVjU2xNJfjKGotv__1sWbs#v=onepage&q=damping vibrations versus isolating vibrations&f=false.

Sapsis, T.P. *et al.* (2012) ‘Effective Stiffening and Damping Enhancement of Structures With Strongly Nonlinear Local Attachments’, *Journal of Vibration and Acoustics*, 134(011016). doi:10.1115/1.4005005.

Smirnov, V. and Mondrus, V. (2016) ‘Comparison of Linear and Nonlinear Vibration Isolation System under Random Excitation’, in *Procedia Engineering*. Elsevier Ltd, pp. 673–678. doi:10.1016/j.proeng.2016.08.221.

Smith, R., Merello, R. and Willford, M. (2010) ‘Intrinsic and supplementary damping in tll buildings’, *Institution of Civil Engineers*, Structures(SB2), pp. 111–118. doi:10.1680/stbu.2010.163.2.111.

strongmotioncenter.org (2024a) *Strong-Motion Vitual Data Center (VDC) - El*

Centro 1940-05-19 04:36:41 UTC. Available at: https://www.strongmotioncenter.org/vdc/scripts/event.plx?evt=88 (Accessed: 11 March 2024).

strongmotioncenter.org (2024b) *Strong-Motion Vitual Data Center (VDC) - Northridge 1994-01-17 12:30:55 UTC*. Available at: https://www.strongmotioncenter.org/vdc/scripts/event.plx?evt=21 (Accessed: 11 March 2024).

Xue, J. *et al.* (2020) 'Vibration reduction evaluation of a linear system with a nonlinear energy sink under a harmonic and random excitation', *Applied Mathematics and Mechanics (English Edition)*, 41(1), pp. 1–14. doi:10.1007/s10483-020-2560-6.

Yang, B. (2001) 'Theory of Vibration - Fundamentals', *Encyclopedia of Vibration*, pp. 1290–1299. doi:10.1006/rwvb.2001.0112.

Zou, X. *et al.* (2014) 'Study on the auto-leveling adjustment vibrtion isolation system for the ultra-precision machine tool', *Proceedings of SPIE - The International Society for Optical Engineering*, 9281, 9281. doi:10.1117/12.2069463.